FLOW CHARACTERIZATION IN A VEGETATED MARSH ENVIRONMENT

by

Jenahvive Kelly Morgan

A dissertation submitted in partial fulfillment
of the requirements for the degree of
Doctor of Philosophy
(Environmental Engineering)
in the University of Michigan
2013

Doctoral Committee:

Associate Professor Aline J. Cotel, Chair
Associate Professor Avery H. Demond
Professor Nikolaos D. Katopodes
Professor Guy A.Meadows

Acknowledgements

The completion of this dissertation was possible due to the contributions of many people. I am grateful to each member of my dissertation committee, for the encouragement that they have showed me during my time at the University. Dr. Aline J. Cotel was an endless source of guidance during the last five years. Her patience and expertise aided me in this process. Thanks to Dr. Guy A. Meadows for his support in pursuing my professional career and for serving on my committee. Thanks also to Dr. Avery H. Demond for her enthusiasm and confidence in my abilities. I would also like to thank Dr. Nikolaos D. Katopodes, who has helped me with his guidance and encouragement as I navigated the academic environment.

Thanks to Nick Gutschow for designing the laser lens attachment, as well as the waterproof cases for the camera and laser on the mini-PIV device. A special thanks to Pratik Pradhan, Cheng Zhang, and Amy Mikus for their help in running laboratory experiments and collecting data. I would also like to thank Rick Burch, the technician of the Environmental and Water Resources program, for his help in creating experimental equipment that was essential in all of my work, and Nancy Osugi, for helping me navigate the logistics of running experiments in the department.

I am also extremely grateful to my husband, Jason Morgan, who has been a source of love, support, inspiration, and optimism from the beginning of pursuing a doctorate education, to the very end of this journey in academia. He has been there every step of the way and I will

never forget the adventures that we have had throughout this process as we made a home in Ann Arbor. I will always cherish our memories of the community that we found at the University.

Table of Contents

List of Figures

List of Tables

Abstract

Flow Characterization in a Vegetated Marsh Environment

by

Jenahvive Kelly Morgan

Chair: Aline J.Cotel

Marsh environments provide a multitude of beneficial functions in natural ecosystems, from flood storage, trapping of contaminated sediments, improved water quality, and creating protected habitat for aquatic species. However, marshes are at risk due to land development, lake level fluctuations related to climate change, misguided shoreline protection measures, etc. As a consequence, the need for artificial marshes has been growing. Thus far, artificial marshes have not performed as well as natural marshes, a potential culprit is the lack of understanding of the local hydrology and flow characteristics. This work focuses on quantifying these parameters in both field and laboratory experiments in order to fully assess the effect of vegetation on flow through a marsh. The field experiments were performed in the Huron River, MI where three different softstem bulrush colonies were investigated. Underwater Particle Image Velocimetry (PIV) was used for the first time in a natural marsh to determine flow structure for different stem densities. The data reveal a relationship between the reed density of the bulrush patches and the

wake turbulence downstream of the bulrush. The average spacing between reeds was found to dictate the size of eddies or flow structures observed in these environments.

To further the investigation of the effect of vegetation on flow, laboratory experiments were performed using arrays of vertically aligned cylinders, 0.64 cm in diameter, in a variety of flow configurations (alternating and random placement of rods), in a re-circulating water tunnel. Particle Image Velocimetry (PIV) was used to determine flow characteristics at different velocities from 2.5 to 15 cm/s. Different stem densities (50 to 400 stems/m^2) were tested depending on the geometry. Similarly to the field experiments, the spacing between rods controlled the eddy size.

In both the laboratory and field experiments, transverse vorticity (i.e. vorticity at a given downstream distance evaluated across the region of interest) was most revealing in terms of eddy size and strength. This parameter should be included in future design studies of artificial marshes to improve marsh performance when considering the important physical features of the flow in vegetated aquatic environments.

Chapter 1: Introduction

1.1 Motivation

Frequently found along the shorelines of streams, ponds, rivers and lakes, marshes represent a wide range of wetlands. A marsh is known for its prevalence of vegetation, including rushes and reeds. This type of wetland can be found in a variety of environments, including along the shores of the Great Lakes and are known as interdunal swale wetlands. Since the source of the water in these marshes is from the Great Lakes, their water levels also fluctuate with that of the lakes. Due to these variable characteristics in the ecosystem, these interdunal wetland marshes provide a habitat for many endangered and threatened species. Also, because of the fragility of the interdunal marshes and the development of the Great Lakes shoreline, which has greatly decreased the shoreline marsh habitat that is available, these marshes are threatened.

More than 50 percent of the wetlands in the United States have been lost over the past 200 years, with many of the remaining wetlands degraded due to decreasing water levels from the warming climate and the development of shorelines (EPA, 2005). The decrease in the amount of wetlands is significant, and will only continue unless more is known about how best to restore or create new marsh environments. Another influence of climate change is the formation of extreme weather events. Extreme weather adds extra challenges to the creation of artificial marshes, and requires that these new

environments can withstand varying weather conditions while they are successfully performing the functions of a marsh. These varying weather conditions are especially important due to the unique role that these marsh habitats serve in providing breeding grounds for many wildlife and fish species.

Some of the basic functions of a marsh are to control sediment, offer flood storage, and provide water quality maintenance (Ghisalberti and Nepf, 2002). The vegetation in marshes dampens waves and slows the speed of the current, therefore reducing erosion along shorelines (Cotel et al., 2008). Since a marsh also acts to store water, slowly releasing it to the surrounding environment, it assists in maintaining the base flow in streams. A very significant function of a marsh is its ability to act as a filter to remove pollutants through adsorption into its sediments, as well as uptake from its plant life (Crites et al., 2006). Many fish are also dependent on these marshes since they feed in them or on food that is produced within them (Palmer, 1988). In each of these functions, the flow structure and turbulence that is created downstream from the reeds in a marsh, influence the ability of the marsh to carry out these essential tasks. Therefore, the influence a marsh has on sediment control, flood storage, management of pollutants and the propensity of fish to breed is dependent on the marsh flow characteristics.

Since marsh environments provide many benefits in their role in the ecosystem, and wetlands themselves are becoming an endangered species due to land development, the need for artificial marshes has been growing. Many artificial marshes are designed and built to remove pollutants from wastewater (Crites et al., 2006). Usually these created marshes are constructed adjacent to a natural marsh, where the groundwater table is near the surface. This allows the marsh vegetation and basic hydrology to be

established. So far it has been found that artificial marshes are not able to function as well as natural marshes or even restored marshes (Cwikiel, 1998). The reason for the failure of artificial marshes has yet to be understood. It is significant that the restored marshes that have thrived are actually natural marshes that have been damaged or disturbed and then returned to their original state by restoring previously removed hydrology. Understanding this restored hydrology and typical flow characteristics in a marsh is crucial, due to the influence of the flow on the important functions of a marsh such as sediment transport, flood storage, water quality, etc. And yet, little has been discovered about the flow characteristics created by vegetation in a marsh environment.

1.2 Objectives

Aquatic vegetation in marsh environments, due to their cylindrical structure, create turbulence in the flow. This turbulence influences the response of the native fish species (Pavlov et al. 2000; Odeh et al. 2002), as well as contaminant and sediment transport. Therefore, it is important to understand the effect that vegetation in aquatic environments has on the flow characteristics of the surrounding environment, in an effort to provide information that can be applied to the creation and design of artificial marsh installations for environmental restoration projects. The evaluation of wake formation due to aquatic vegetation is necessary to understand the response of the environment to flow through a marsh. Therefore, this research aimed to examine turbulence downstream from both natural and simulated marsh environments. To achieve this goal, the following objectives were defined:

1. Construct an underwater Particle Image Velocimetry device and take the first underwater PIV data in a natural marsh environment to characterize the influence of reed density and growth pattern on the downstream flow structure (Chapter 4).
2. Examine and evaluate the marsh parameters that influence downstream flow structure (Chapters 4 – 5).
3. Determine the importance of reed/rod spacing on wake formation and the downstream eddy structure (Chapters 5) in controlled laboratory experiments.
4. Examine the influence of growth pattern on transverse vorticity, and whether the patterns in the vegetation are reflected in the wake patterns found downstream from the different marsh configurations (Chapter 4 – 5).

Chapter 2 provides a summary of previous work on flow past cylinders and marsh dynamics. Chapter 3 describes a comparison between turbulence measurement techniques. Chapter 5 examines the effects of flexibility on the downstream flow structure. Chapter 6 summarizes the conclusions from the field and laboratory experiments, and explores future research directions for the study of flow characteristics in marsh environments.

Chapter 2: Background

2.1 Flow Characteristics Downstream from Cylinders

In emphasizing the importance of obtaining flow structure information in a marsh environment, the characteristics of flow past cylinders are significant in their ability to be compared to the flow past reeds in a marsh. The characteristics of flow past cylinders have been extensively studied. The contributions by Gerrard (1966), Williamson (1985), Cimbala et al. (1988), Lam and Cheung (1988), Roshko (1993), Lin et al. (1995), Williamson (1996), and Sumner et al. (1999) have provided a summary of the distinct features of these flows. It has therefore been suggested that the hydrodynamics of flow past circular cylinders can be applied to aquatic plants with rodlike structures (Leonard & Luther, 1995; Anderson & Charters, 1982). This is useful in analyzing the complex flow in a marsh.

According to Williamson (1996), there are three shear layers in the bluff body wakes created by the flow past cylinders (Figures 2.1 and 2.2). These are the free shear layer, the boundary layer and the wake itself. As the wake is formed, alternate sides of the cylinder shed regions of concentrated vorticity of opposite rotation creating rows of positive and negative vortices. From the study performed by Gerrard (1966), it was suggested that the supply of vorticity to a vortex, created downstream from a cylinder, is

cut off by the forming vortex from the other side of the wake (with the opposite rotational sign). This creates a drawing of the shear layer over the wake centerline.

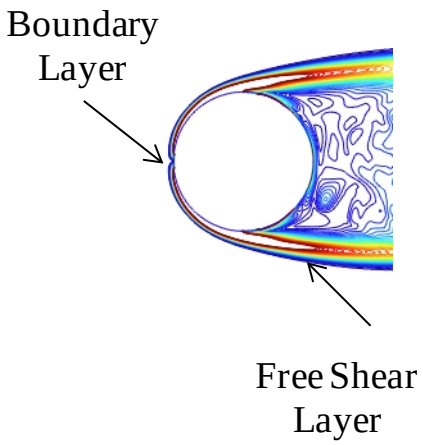

Figure 2.1: Two of the three shear layers of bluff body wakes identified.

Roshko (1993) argued that the contribution to the near wake dynamics by the free shear layer is enhanced as the distance between the separation point and the formation of the first vortex is increased. When the flow past a cylinder is at low Reynolds numbers (Re < 180) (Equation 2.1) then a steady wake is created with a region of recirculation located behind the cylinder. The Reynolds number measures the ratio of the inertial forces to viscous forces:

$$\mathrm{Re} = \frac{UL}{\nu} \qquad (2.1)$$

where U is the mean flow velocity , L the characteristic length scale such as a cylinder diameter, and ν the kinematic viscosity of the fluid.

At higher Reynolds numbers (Re > 180), an unsteady wake is created and forms a vortex street (Figure 2.3). The unsteady wake still possesses a region with mean recirculation. This region is identified in the unsteady wake by locating the downstream distance with the largest root mean square velocity fluctuations on the wake centerline. Also, as expected, the velocity fluctuations decreased as the downstream distance increased. Particle Image Velocimetry (PIV) measurements (Lin et al., 1995) revealed that the Karman vortices are the product of the amalgamation of the shear layer vortices in the near wake, before the Karman vortices are shed downstream from the cylinder.

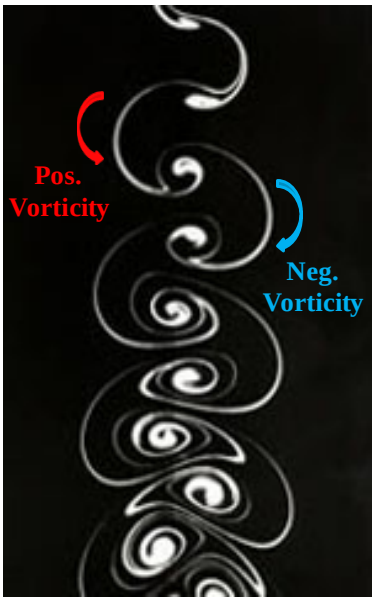

Figure 2.2: Diagram outlining positive and negative vorticity in the third shear layer, or the wake (Anderson, 1991).

Building from the examination of flow past a single cylinder to flow past multiple cylinders, Tanino and Nepf (2008) used emergent, rigid rods, or cylinders, in an array of over 100 cylinders in a laboratory experiment to analyze the effect of rod density on the drag coefficient. Here the drag coefficient decreased with increasing Reynolds number

and increased with increasing stem density. This experiment was conducted using a random configuration of rods, or cylinders, in the flume. Ayaz and Pedley (1999) and Stone and Shen (2002) found a similar increase in drag coefficient with an increasing rod density in square and staggered arrays, respectively. Still, previous work by Nepf (1999) found conflicting results with a decreasing drag coefficient with increasing rod density, but this trend occurred at higher Reynolds numbers. The Reynolds numbers referenced in these studies were calculated using the uniform flow velocity and the rod diameter as the characteristic length, and ranged from 200 to 10,000.

A study conducted by Lam and Cheung (1988) found that the spacing ratio, as well as the Reynolds number, had an influence on when discrete vortex shedding occurs for lower spacing ratios in cylinder arrays. A spacing ratio (SR) is defined as the distance between two neighboring cylinders divided by the diameter of the cylinders, regardless of the cylinder orientation perpendicular to the flow (side-by-side or staggered). The Strouhal number (Equation 2.2) also begins to converge for larger spacing ratios (SR $\geq$ 2.0) according to the measurements from Lam and Cheung (1988), as well as Sumner et al. (1999). Lam and Cheung (1988) examined a range of spacing ratios from 1.27 to 5.43, and Sumner et al. (1999) investigated spacing ratios from 0 to 2.0. The Strouhal number is a non-dimensional number that reflects the frequency with which vortices are being created downstream from the cylinder:

$$St = \frac{f_s L}{U} \tag{2.2}$$

where f_s is the shedding frequency of the vortices from the cylinder, and U and L are mean flow velocity and characteristic length scale or cylinder diameter, respectively.

A summary of these studies is presented in Table 2.1, with a comparison of the resulting Strouhal numbers in Figure 2.3. With the larger gaps in between the cylinders, two separate, alternate vortex streets were produced as separate wakes for each rod (Lam and Cheung, 1988). Usually, when vortices are simultaneously shed on both sides of the space in between two cylinders, the two vortex streets are shed in an alternating traditional formation. This is the predominant fluid behavior and leads to two parallel vortex streets in the near wake.

When two cylinders are placed either side-by-side, in tandem or staggered, the characteristics of the flow are dominated by the spacing ratio. For small spacing ratios, or spacing ratios less than 0.7, a combined wake of the two cylinders creates a single vortex street (Bearman & Wadcock, 1973). Whereas, at large spacing ratios, or spacing ratios greater than 2, two separate, alternate vortex streets are created and the Strouhal number converges to 0.2, or the value for a single cylinder (Spivack, 1946; Le Gal et al., 1990). The convergence of the Strouhal number to 0.2 for these different cylinder arrangements is also significant when examining the connection between reed/rod placement and the local biota. For example, typical Strouhal numbers for vortices created when fish and other aquatic creatures are swimming are in the range of 0.2 to 0.4 (Linden and Turner, 2001).

When intermediate spacing ratios are examined (Bearman & Wadcock, 1973; Kiya et al., 1980), for two cylinders, one side will create a wide, dominant wake, while the other will produce a smaller wake. These conditions will intermittently switch from one cylinder to another and can be controlled by the angle at which the flow is directed. There is an angle of incidence, below 30º, where the vortex shedding of one cylinder will

be suppressed by the other (Lam and Cheung, 1988). As long as there is no change in the angle of the flow, and the spacing ratio is above 2.0, then the initial vortex formation is discrete. Still, as the discrete wakes grow and move downstream, they will interact with one another. When two cylinders are placed in tandem arrangements, the upstream cylinder wake influences the downstream cylinder wake by combining with this wake and creating a wider wake downstream (Zdravkovich & Pridden, 1977; Kiya et al., 1980). This combining of vortex streams was shown to exist when two rods were producing wakes that were in close proximity with one another by Williamson (1985).

Table 2.1: Literature review of flow characteristics downstream from cylinders. Reynolds numbers were calculated using the rod diameter as the characteristic length.

Researchers	Methods	Technique	Re	SR	Results
Bearman & Wadcock (1973)	2 Side-by-Side Circular Cylinders	Flow Visualization in a Wind Tunnel	25000	0 - 6	For small spacing ratios, a combined wake of the two cylinders creates a single vortex street
Kiya et al. (1980)	2 Staggered Circular Cylinders	Constant Temp. Anemometry in a Wind Tunnel	1.58E+04	1 - 5.5	Upstream cylinder wake influencing the downstream cylinder wake and creating a wider wake
Lam & Cheung (1988)	3 Circular Cylinders in Equilateral Triangular Arrangements	Flow Visualization in a Water Tunnel	2.1E3 - 3.5E3	1.27 - 5.43	Convergence of Strouhal number to 0.2, independent wake formation, when SR > 2
Le Gal et al. (1990)	Side-by-Side Cylinder Arrangement	Flow Visualization in a Water Tunnel	110	0 - 6.5	For large spacing ratios, SR > 2.5, two separated alternate vortex streets are created as the wake is formed
Spivack (1946)	Side-by-Side Cylinder Arrangement	Constant Temp. Anemometry in a Wind Tunnel	5000 - 93000	0 - 5	Strouhal number converges to 0.2 for a single cylinder and this independent wake formation exists at larger SR
Sumner et al. (1999)	Side-by-Side Cylinder Arrangement, 2 to 3 Circular Cylinders of Equal Diameter	Flow Visualization in a Water Tunnel	500 - 3000	0.5 - 2.0	At large spacing ratios, the side-by-side circular cylinders form independent isolated bluff bodies
Williamson (1985)	Side-by-Side Cylinder Arrangement	Flow Visualization in a Water Tunnel	200	0 - 5	Vortex shedding that is in-phase in side-by-side cylinders creates a single, large wake
Zdravkovich & Pridden (1977)	Side-by-Side, Tandem, & Staggered Cylinder Arrangement	Force Balance from a Wind Tunnel	60000	1 - 5	Upstream cylinder wake combining and influencing the downstream cylinder wake
Current Study	Alternating Cylinder Arrangement	Flow Visualization in a Water Tunnel	700-1100	4 - 8	Rod spacing affects wake formation, or Strouhal number, as well as the downstream eddy structure
Current Study	Random Cylinder Arrangement	Flow Visualization in a Water Tunnel	200-1100	4 - 6.7	Growth pattern in the vegetation is reflected in a wake pattern found downstream from the marsh
Current Study	Field Reed Observation	Flow Visualization in a Natural Marsh Environment	200	1.5 - 2.1	The first underwater PIV data in a natural marsh environment were collected to characterize the influence of reed density and growth pattern on the downstream flow structure

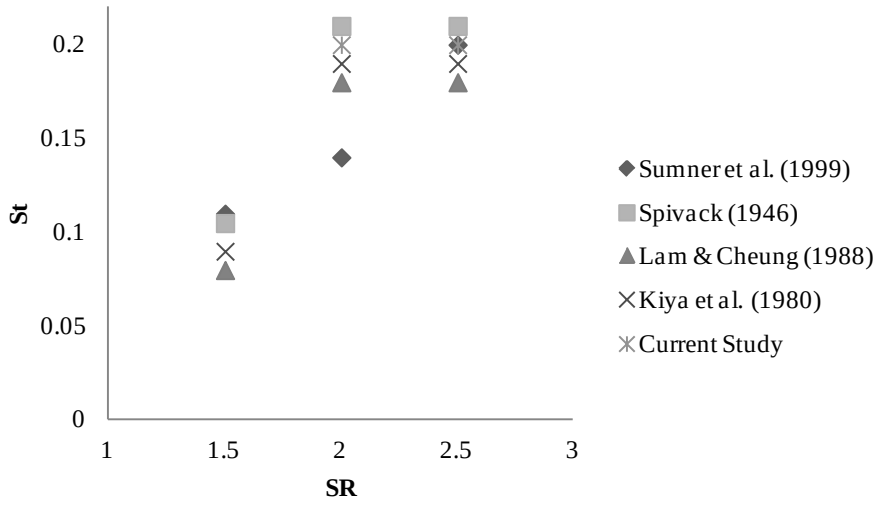

Figure 2.3: Literature comparison of Strouhal number results.

2.2 Flow in Marsh Environments

In addition to understanding flow past cylinders, it is also necessary to understand what has been discovered about basic flow through a marsh. Flow through vegetated environments has been analyzed in a multitude of ways. Some of these studies have been conducted in laboratory flumes with rods or live vegetation, while others have involved numerical modeling of the flow or field investigations. Most of what is presently known about flow in a vegetated environment has been conducted using a laboratory flume bed with simulated or live vegetation to represent vegetated channel flow (Peterson et al., 2004; Cui and Neary, 2008; Nepf, 1999; Lopez and Cowen, 2009). Previous experiments involving modeling the fluid dynamics of submerged vegetation in a laboratory flume focused on analyzing the mean flow within and above the canopy of the vegetation (Peterson et al., 2004). Flow reduction has been detected in seagrass beds and related to

the upstream flow and vegetation density of the beds, with greater flow reductions with increasing vegetation density. This reduction in the velocity of the flow within the vegetation is due to the frictional effects of the vegetation (Abdelrhman, 2003), which can affect the feeding of predators in this environment (Palmer, 1988). In some previous studies, PIV was utilized in a laboratory environment. Lopez and Cowen (2009) studied live, flexible, emergent plants, using PIV, to take an initial look at the velocity fields and turbulence fluctuations in a simulated vegetated marsh. However, this study was conducted in a laboratory setting and provided only a preliminary look at simulated marsh environments.

Several experiments have been performed on rigid, emergent vegetation in a laboratory. The efforts that have been made utilizing rods as a model for vegetation in a laboratory flume have provided useful information concerning vegetated marsh environments. If the vegetation is rigid there is more of a uniform velocity profile, except close to the bottom where the frictional properties of the bottom develop a region of velocity shear, i.e. a boundary layer. Nepf (1999) used emergent, rigid rods in a laboratory flume to simulate a marsh environment and to capture the physics of flow through this type of vegetation. It was found that turbulence intensity, defined in this study as the square root of the turbulent kinetic energy divided by the average velocity, increased with an introduction of sparse vegetation, but decreased as the vegetation density increased. Therefore, a dense vegetated marsh environment could decrease the turbulence seen in open channel flow if turbulence is defined solely on the turbulence intensity values from this study. Still, these values were acquired using point measurements, with no information on two-dimensional flow structures. While the

influence of stem density has been explored, what has yet to be understood is the influence of vegetation pattern and spacing on the downstream flow characteristics.

Field investigations have also been conducted on submerged vegetation. Rosman et al. (2007) examined the velocity profiles of kelp forests in an effort to capture the hydrodynamics within the vegetation. Again, it is found that currents are reduced by canopy coverage. The amount of the reduction in the current correlated to how much surface canopy coverage existed, and currents could be reduced to one fifth their original value of 5 cm/s. Other methods using numerical models were also used to assess both submerged and emergent vegetation and its effect on the velocity and stress profiles of mean flow (Velasco et al., 2008). Despite much recent progress in research examining how the interactions between submerged and emergent plants and the fluvial environment alter the flow regime, there are still many aspects that remain unexplored. For example, how the characteristics of the flow structures are affected by a vegetated environment.

2.3 Fish and Turbulence in Vegetated Environments

A strong connection can be made between turbulence in marsh environments and the local biota, or more specifically fish swimming in turbulent flows. Such flows are frequently found in natural environments, and turbulence can influence fish through its effect on food availability, energy spent on swimming and gamete dispersal. Turbulence also affects whether a fish chooses a specific area for its habitat (Cotel et al., 2006). This turbulence can be characterized either through physical features of the flow, such as eddies, or using statistical tools such as velocity fluctuations in the flow. When eddies

are used to identify turbulence: eddy diameter, vorticity and eddy circulation are all important parameters in quantifying turbulence. If turbulence is characterized through velocity fluctuations, then turbulence intensity and turbulent kinetic energy are typical parameters used in turbulence characterization. These parameters will be defined later in this chapter.

The turbulence encountered in natural systems is in the form of a continuum of eddies that causes temporal and spatial unsteadiness in the flow. A fish in such environments encounters eddies of different sizes and strengths and it is important to know how a wide variety of eddies affect a fish swimming in this environment. The interaction between the vegetation, acting as an obstruction to the flow, and the flow itself, creates additional turbulence and unsteadiness. A reed, modeled as a circular cylinder, when placed in a uniform flow creates a wake flow downstream from it, resulting in a vortex arrangement known as the Karman vortex street (Von Karman, 1937). As the downstream distance increases, the vortices grow in size, therefore increasing the width of the wake. Typical parameters that influence these vortices are the Reynolds number and the Strouhal number. Reynolds number plays an important part in vortex formation downstream from a cylinder, as described in Section 2.1. Understanding the frequency with which vortices are shed in a natural environment, as a function of Strouhal number, has been shown to be important in predicting fish-eddy interaction, according to Liao (2007). In this study conducted by Liao, it was observed that fish tend to utilize periodic and predictable flow conditions more efficiently for upstream migration. Understanding more about the influence of turbulence on biota is important when studying flow through a marsh.

2.4 Flow Structure Characterization Measurements: Eddy Diameter, Vorticity, and Eddy Circulation

Eddies can be identified in the flow through many methods. Curved or spiral streamlines, isovorticity and pressure minimums are all ways to identify the presence of an eddy or vortex in the flow (Jeong and Hussain, 1995; Drucker and Lauder, 1999; Epps and Techet, 2007). Spiral streamlines that reveal a circular motion similar to a whirlpool, identify an eddy in the flow and reveal vorticity. Vorticity, or the curl of the velocity vector, can also be used in and of itself to identify eddies on the basis of the presence of finite vorticity. Particle Image Velocimetry (PIV) captures vorticity by directly measuring the velocity and streamlines in the flow. This measurement of turbulence occurs through examining the displacement of neutrally buoyant particles that are illuminated by a two-dimensional laser sheet and captured by a camera. The displacement of particles is measured at a known time interval based on the time between images being captured. The size of an eddy can be measured from the vorticity information, obtained through PIV measurements, as the diameter of the rotating "disk," or coherent rotating structure shed from an obstruction, within the fluid (Drucker and Lauder, 1999). The identification of these coherent structures allows the water movements to be tracked and eddy diameter to be obtained.

Once the vorticity of the eddies is measured, it is important to calculate circulation to evaluate the impact of induced momentum caused by the eddies on fish swimming in such eddy-dominated flows (Cotel and Webb, 2011). Eddy circulation is the integration of vorticity over the surface area of the eddy:

$$\Gamma = \oint_A \omega \cdot dA \qquad (2.3)$$

From circulation, the momentum and forces related to a particular eddy can be determined. The Kutta- Joukowski theorem states that circulation can be related to force per unit length, through multiplying it by the density and velocity of the flow (Anderson, 1991). This methodology, based on the characterization of eddies, as opposed to point measurements of velocity, provides a more direct approach to calculating forces acting on fish due to the presence of turbulent eddies in the flow.

There are several factors that play a role in whether a fish will choose a particular water body as its habitat. These are access to food, avoidance of predation and the energy that is needed to swim in that environment. Cada and Odeh (2001), Nikora et al. (2003), Liao (2007) and Lupandin (2005) all propose that the size of eddies, when compared to the size of the fish, is significant when understanding how turbulence affects a fish swimming in a water body.

Cada and Odeh (2001) and Liao (2007) have found that certain eddies can significantly affect a fish swimming in a natural environment. Due to the wake created behind the vegetation in a marsh, vortices or eddies are created which can interact either positively or negatively with fish. The effect of scale is important when examining the stability challenges that are caused by the interaction of fish with unsteady water movements. Therefore, only eddies of certain sizes and strengths are of concern when evaluating their effect on fish (Tritico, 2009; Tritico and Cotel, 2010). A wide range of eddy sizes is found in the natural environment. For example, in the ocean, large gyres, such as the North Pacific Gyre, and other eddies very much larger than fish size are

certainly important in dispersal and migration, but it is likely that fish respond to them in the same way as they would to uniform flow. Cada and Odeh (2001) propose that the larger eddies, with sizes equivalent to the perimeter of the water body, would act as secondary currents and not create destabilizing effects on a fish swimming in this environment. In small streams, it is possible for the largest eddy size to be on the same order of magnitude as a typical salmonid body length.

As eddies become smaller, their frequency or occurrence increases. Cada and Odeh (2001) also suggest that eddies that will not have enough momentum to produce substantial torque on a fish body are those that are smaller in diameter than the fish length. The smallest eddy size is called the Kolmogorov eddy, defined to be of size λ_o, in the "inertial sub-range." The "inertial sub-range" is the range of eddy size where energy is passed from the larger eddy to the smaller eddy with no energy lost to viscous effects (Kolmogorov, 1941). The largest eddy, defined to be of size δ, is constricted by the boundaries of the water body. The decrease in the frequency of an eddy, with an increase in the size of the eddy, occurs on a logarithmic scale. Thus, fish encounter a multitude of small eddies in a natural environment, and even though the larger eddies are less common, they can have a significant impact.

It is predicted that eddies that have a diameter that is similar to the fish length could create destabilizing perturbations (Figure 2.4). Since marsh environments provide both spawning and nursery areas for fish, as well as serve as a habitat for the aquatic invertebrates that act as food for fish, even very small eddies can prove troublesome to the ability of young fish to swim and obtain food. The circulation, and therefore the momentum, of an eddy can also undermine a fish swimming in a natural environment if

the momentum of the eddy is larger, or of the same order of magnitude, than that of the fish (Tritico, 2009). This disruption in how a fish is swimming is then dependent on the speed of the flow, as well as the size and speed of the fish that is interacting with eddies created in a given aquatic environment.

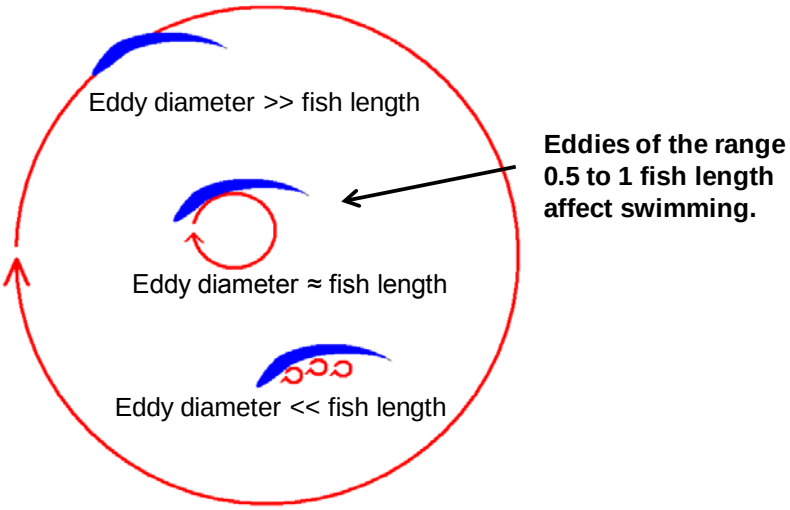

Figure 2.4: Range of eddy size compared to fish size (Cotel and Webb, 2011).

2.5 Velocity Fluctuation Measurements: Turbulence Intensity and Turbulent Kinetic Energy

As discussed earlier, turbulence in natural environments can be measured in a variety of ways. It can be assessed through eddy measurements, as previously discussed, or it can be analyzed through statistical turbulence parameters such as turbulence intensity and turbulent kinetic energy based on point measurements of velocity fluctuations (Cotel et al., 2008). Turbulence intensity is defined here as the ratio of the

standard deviation of the velocity of the flow (σ) over the temporal average velocity of the flow ($\bar{u}$):

$$TI = \frac{\sigma}{\bar{u}} \tag{2.4}$$

These velocity fluctuations, used to calculate TI, are measured in both the x (longitudinal or flow direction) and y (transverse or perpendicular to the flow) directions.

TI forms a non-dimensional measure of turbulence and is known to affect the response of a fish to the speed variations of the flow, with fish choosing lower TI locations (Cotel et al., 2006). Negative effects on fish swimming speed were also found to occur when the point measurements of turbulence increase (Pavlov et al. 2000; Odeh et al. 2002). In contrast to this, others have found no effect of turbulence intensity on fish swimming (Nikora et al., 2003), while some have described positive effects of turbulence on fish (Liao, 2007).

Turbulent kinetic energy, or TKE, is used to measure how turbulent fluctuations in the flow increase the kinetic energy. It provides another parameter, along with TI, to quantify turbulence in the flow.

$$TKE = \frac{1}{2}\left(\sigma_u^2 + \sigma_v^2\right) \tag{2.5}$$

TKE uses the standard deviation of the velocity fluctuations in the x (longitudinal), and y (transverse) directions (σ_u, σ_v) to calculate the turbulent fluctuations at a point. In a fluctuating velocity field, TKE represents the contributions of the turbulent fluctuations to the total kinetic energy of the flow. Larger values of TKE translate to an increase in

turbulence or overall energy levels, which have been found to correlate to a decrease in fish density once higher TKE levels were reached (Smith et al., 2006). Traditionally, in previous studies, velocity fluctuations, used to calculate TI and TKE, have been utilized as measurements of turbulence in field experiments. This use of TI and TKE to characterize turbulence was due to the difficulty of obtaining flow structure information in natural environments. However, there is a crucial need to understand flow characteristics in a marsh and their influence on how well a marsh is able to provide food and breeding grounds for fish, as well as sediment and contaminant control.

Thus far, no measurements of the flow structure within an actual marsh have been performed; Particle Image Velocimetry (PIV) now allows for this type of information to be obtained in natural vegetated environments. Acquisition of flow characteristics in a natural marsh environment, using PIV, provides flow structure based turbulence information in addition to velocity fluctuations that could also be captured by an Acoustic Doppler Velocimeter (ADV), which has been the most common way of analyzing marsh flows in the past. For these reasons, field experiments were performed to collect information about flow structures in a natural marsh, using PIV for the first time.

Chapter 3: Comparison of ADV and PIV Measurements

In an effort to provide a better means of comparison between the different turbulence measurement techniques, ADV measurements of velocity were compared at a sample point to PIV measurements. Typically, field measurements have focused on point measurements using an Acoustic Doppler Velocimeter (ADV) to characterize turbulence in the flow. However, with recent technological advances, it is now possible to perform PIV in a field setting. To allow for comparison between past, present and future data sets, it is important to understand and quantify the relationship between ADV and PIV measurements.

To investigate the difference between Acoustic Doppler Velocimeter (ADV) and Particle Image Velocimetry (PIV) when calculating statistical quantities such as Turbulence intensity and Turbulent Kinetic Energy, experiments were performed for both a single rod and uniform flow in a channel. Both methods of quantifying turbulence in the flow involved recording velocity measurements 11cm downstream from one rod placed in the center of the flume, and at the same location for the uniform flow case. These measurements were taken at Reynolds numbers of 700 and 1,100, (based on rod diameter), or 10 cm/s and 15 cm/s for the no rod case. The ADV data were taken at a sampling rate of 50Hz and over the same time period that the PIV data were recorded. Time separation for the PIV data was 8ms and 11ms for the Reynolds numbers of 700

and 1,100 respectively. The PIV data were analyzed at the same location as the ADV data, to obtain values for TI and TKE, 11cm downstream from rod and in the center of the flume, with a laser sheet 2 mm thick. Figure 3.1 shows a comparison between the PIV and the ADV data.

It was found that for the uniform flow case, there was a 10% difference in the PIV and ADV measurements, for both TI and TKE, at a velocity of 10cm/s. The difference increased to 30% for a velocity equal to 15cm/s. In the one rod case, for a Reynolds number of 700, the difference between PIV and ADV measurements for TI was 20%, and for TKE was 15%; for a Reynolds number of 1100, the difference in the PIV and ADV measurements changes to 14% for TI and 13% for TKE. Others have observed similar results, Mueller et al. (2007) found errors of the same magnitude, around 20%, in the comparison of ADV and PIV measurements of stream velocity profiles.

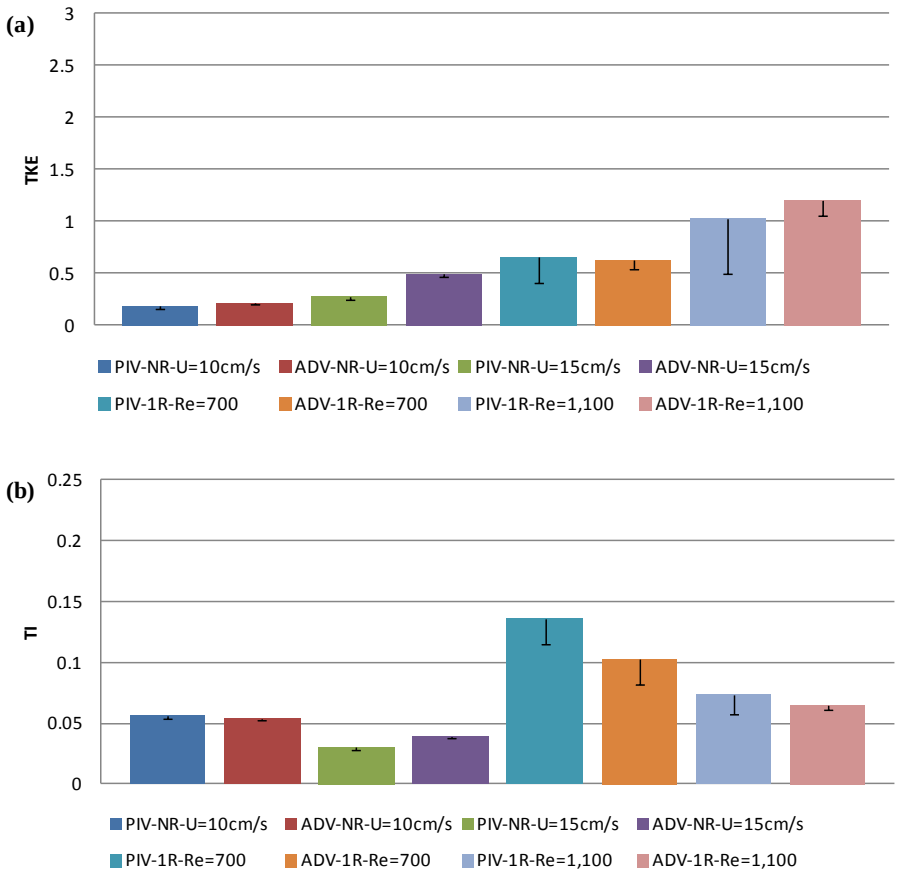

Figure 3.1: PIV comparison with ADV measurements of turbulent kinetic energy (a) and turbulence intensity (b) at Re = 700 and 1,100 using the rod diameter as the characteristic length, or 10 cm/s and 15 cm/s for the no rod case. These measurements were taken 11cm downstream from one rod and in the same location with uniform flow without a rod. A comparison of these results allows two methods of quantifying turbulence in the flow to be compared, despite the different measurement equipment involved in recording the data.

The difficulty in examining the differences in these two techniques in quantifying turbulence involves the requirement of each of these methods for a particular particle size. In the water tunnel, where the comparison of the two methods was conducted, experiments using the PIV system are primarily executed. PIV requires a very small particle size, on the order of 10 μm, to be able to quantify small changes in flow structure. At the same time, the ADV requires a particle size on the order of 20 μm to ensure a good signal-to-noise ratio and accurate measurement of the turbulence of the

flow (Sontek, 1997). Therefore, the two techniques have competing particle size requirements, and getting them to record measurements precisely under the same conditions, proved difficult. The difference in the turbulence quantities obtained by each technique is in some cases significantly different while in others is within the measurement errors of 20-30%. This discrepancy in the values, due to constraints of the equipment, explains the variations in the results, since the errors in many circumstances are under 20%. Further examination of the comparison of ADV and PIV techniques is conducted for the low-density alternating marsh configuration in the Appendix.

In addition to the difficulties in utilizing these two very different pieces of equipment to obtain similar measurements of turbulence in the flow, there are differences in the capabilities of each device. An ADV is very mobile and can easily be used in a variety of aquatic locations, while PIV is primarily a laboratory-based setup, requiring equipment that needs a constant energy supply, is expensive and is not waterproof. In addition to the benefit of mobility for an ADV, another benefit is that it is able to achieve a high temporal resolution. At the same time, PIV offers the user the ability to quantify turbulence in a two-dimensional image of the flow structure, capturing vorticity in eddy formations over space and time. This image can cover over a 1,000 cm^2 region, while an ADV's point measurements will only capture a 0.28 cm^2 region.

Both of these types of measurements of turbulence have been utilized when discovering the strong influence of turbulence on fish response (Pavlov et al., 2000; Tritico, 2009). Still, with the capabilities of Particle Image Velocimetry (PIV) to capture a large amount of information on turbulence in the flow, due to the two-dimensional image of the flow structure that is captured, more emphasis will be made in this study on

utilizing the ability of PIV to understand the physical characteristics of the flow structure in a marsh. In conducting this investigation, the connections can be made between the flow structures in a marsh and how those flow structures influence biota.

The turbulence caused by the flow through the vegetation, resulting in the presence of vortices or eddies in the flow, can impact the behavior of the fish swimming in this type of environment. This turbulence can also influence the basic functions of a marsh in controlling sediment and pollutants. For this reason, it is important to understand the impact that an artificially created marsh could have on modifying water movements and on creating changes in the flow structure due to turbulence. Choice of vegetation, the stem density of the plants and the arrangement of the plants (random or in a set pattern) all have an influence on turbulence downstream of a marsh. Understanding the interaction between turbulence and vegetation is important and can be achieved using *in situ* measurement techniques (PIV) of eddy-based parameters.

Chapter 4: Softstem Bulrush Field Experiments

4.1 Softstem Bulrush Characteristics

In examining the flow through a marsh, vegetation plays an important part in determining the downstream flow structure. A common example of a type of wetland vegetation is softstem bulrush. This wetland plant consists of reeds that resemble smooth cylinders. For this reason, softstem bulrush is an excellent plant to use for experiments characterizing cylindrical vegetation as an obstruction in the flow. Softstem bulrush, or Scirpus tabernaemontani (S. validus creber), is most commonly found in water depths of 0.15 to 0.3 m., but can grow in water up to depths of 1.5 m (Crites et al., 2006). These plants are found on the shorelines of the water bodies they inhabit, where the soil moisture is high. They grow tall, unbranched, with round stems that are around 0.64 cm in diameter. The reed-like stems are light green, smooth and flexible. Softstem bulrush has large air chambers that fill the stem and therefore may seem spongy when compressed. These plants are perennials that are able to withstand saline growing conditions, but overall have slow to moderate growth speeds. The growth of these plants requires little maintenance; they can grow in full sun or partial shade, and they are known for high levels of pollutant removal. The height of the stems of the bulrush grow between four to six feet tall, emergent from the water from which they are found. They prefer a pH between 4 and 9 and have a moderate nutrient load and siltation tolerance.

Softstem bulrush is able to grow in either fine, medium or coarse textured soils and have a high anaerobic tolerance (Crites et al., 2006). These plants are used in vegetated swales and also provide excellent lower shoreline zone stabilization. Waterfowl, shorebirds, muskrats and fish find food and valuable nesting cover within the environments where softstem bulrush is found, and the softstem bulrush offers shelter and habitat for young fish (Runkel and Roosa, 1999).

While the stems appear to be leafless, the stem bases are restrained by leaves which are mostly basal and modified into long, wide sheaths around the stems (Guard, 1995). Reddish brown scales of hanging inflorescence cover a cluster of spikelets which form the flowers of the bulrush. These flowers have many stalks and are found just below the top of the stem and look like a continuation of the tip (Tiner, 1987). Softstem bulrush can be found in ponds, streams, wooded wetlands, lakes and in the marshy ground around lakes. It is most often found in poorly drained soil, and if there is prolonged flooding or draining, their population can be reduced. Softstem bulrush grows from a long, shallow, linear rhizome system. The roots of these plants form a mat of new shoots rising from the roots that have spread either below the surface of the soil or under water. Softstem bulrush seeds can remain dormant for years, but when the plants do grow they form colonies. Softstem bulrush is found to be highly productive and flourish for a wide range of wastewater organic matter and nutrient loading rates within constructed wetlands. Small industries and communities are finding constructed wetlands to be a cost-effective, natural wastewater treatment technology utilizing these plants, which have shown to enhance the removal of pathogens and nitrogen. Softstem

bulrush has been commonly utilized around the world in wetland wastewater treatment systems (Crites et al., 2006).

4.2 Softstem Bulrush Reed Spacing and Pattern

Three different colonies of bulrush on the shorelines of the Huron River, Ann Arbor Michigan were examined on May 17, 2012. These softstem bulrush patches were chosen due to the three different stem densities represented in each colony. These reed densities were 140, 240 and 388 reeds/m^2. The reed density for each patch was calculated from counting all of the reeds in a 0.5 m^2 area. Each softstem bulrush patch density was then found by extrapolating the figure for 0.5 m^2 to 1 m^2, resulting in the three patch densities recorded for each of the chosen bulrush colonies. These densities are representative of average vegetation densities found in marsh environments studies (Augustin et al., 2009). An analysis of reed spacing for softstem bulrush was performed on these three colonies in the Huron River (Figure 4.1). The change in the spacing ratio, or the distance to the nearest neighbor divided by the reed diameter, was compared to the change in reed density, or the amount of reeds in a meter squared area, for each of the colonies. Here a decrease in the spacing ratio occurs as the reed density is increased. The average reed spacing is non-dimensionalized by the average diameter of the reeds, equal to 0.64 cm. It is observed that the bulrush non-dimensional reed spacing decreases by 10% from 140 reeds/m^2 to 264 reeds/m^2, and by 25% from 264 reeds/m^2 to 388 reeds/m^2. This relationship between reed spacing, or the spacing ratio (SR), of the natural bulrush reeds as found in natural marsh environments and the change in the reed density (RD) is modeled by a polynomial curve fit equation.

$$SR = -1 \times 10^{-5} RD^2 + 0.00431RD + 1.7947 \qquad (4.1)$$

This equation can be used to understand the change in spacing that occurs in the natural growth pattern and placement of bulrush reeds as the density of bulrush plants increases. Still, the main observation of the analysis of the softstem bulrush reed spacing is that the spacing ratio is near 2.0, or a distance of two reed diameters, over the change in reed densities.

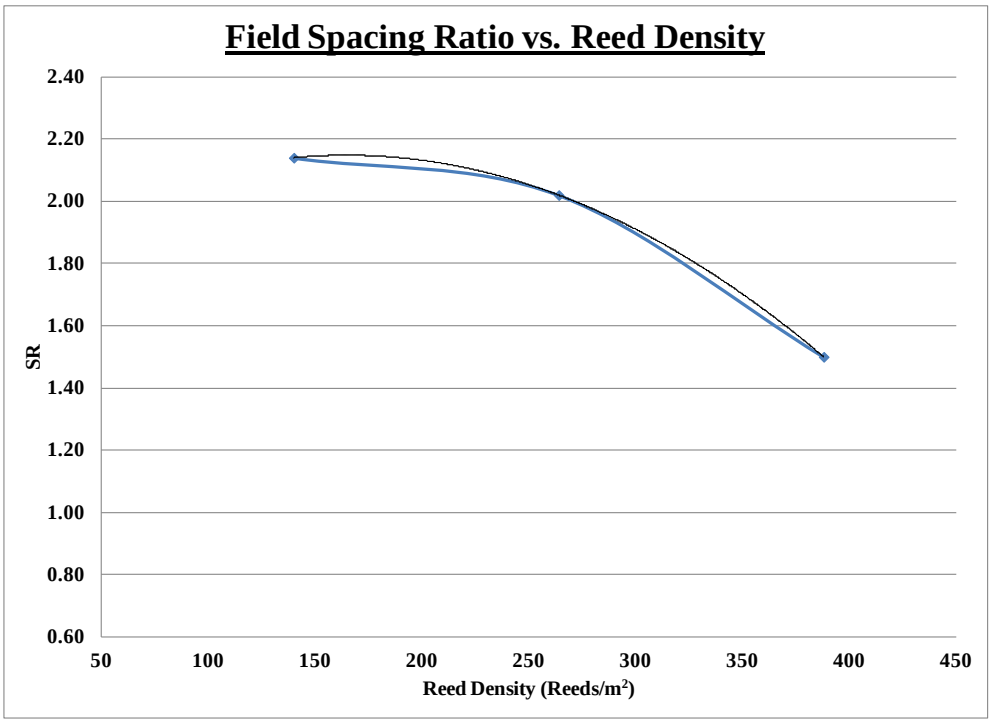

Figure 4.1: Spacing ratio measured in the marsh environments with different reed densities.

Figure 4.2 outlines the preliminary results of a growth pattern study of softstem bulrush on the Huron River, Ann Arbor, MI. This figure is the culmination of field research recording the coordinates for a 6 m^2 area of softstem bulrush. The distance from stem to stem, for all of the stems in this area, was measured and recorded to translate the

softstem bulrush growth pattern into a Cartesian grid system. An initial examination of the reed placement in this aerial coordinate map, using the basic methods suggested by Davis and Goetz (1990), of aerial analysis through looking at the percent of vegetated cover with evidence of a linear growth pattern, reveals that 68% of the vegetated area has evidence of a linear trajectory over a 0.2 m^2 area. In these regions, highlighted in yellow, the growth of consecutive reeds follows at an angle that can be measured and therefore is deemed to be a linear. Areas that are lacking this trajectory are then labeled non-linear, and in Figure 4.2, only consist of 32% of the vegetated cover in this aerial coordinate map. These areas of linear growth are most likely due to the formation of the softstem bulrush roots into a long, linear rhizome system (Crites et al., 2006). The result of this linear growth is the consistent spacing between softstem bulrush reeds in a marsh, due the regularity in spacing between the reeds along the root system. Some variation in the reed spacing occurs, as is seen in Figure 4.1 with the change in reed density, but this change in reed spacing only fluctuates around 20%. Therefore, a consistent growth pattern is observed with an average reed spacing of two diameters between the softstem bulrush reeds.

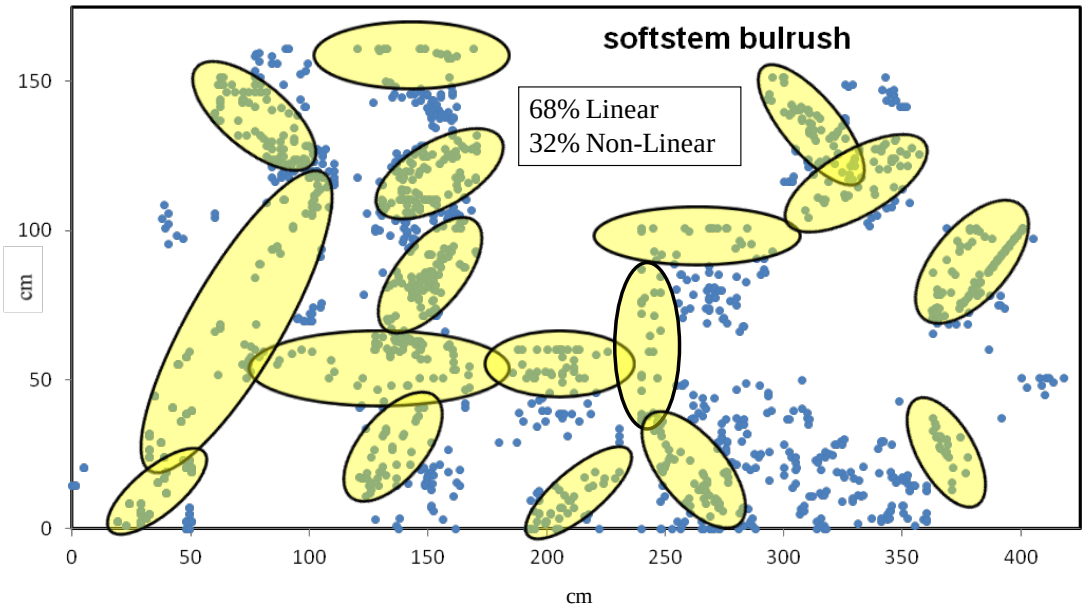

Figure 4.2: Aerial coordinate map of the growth pattern of softstem bulrush with pattern analysis. These colonies of softstem bulrush were located at 42º18'27.65" N 83º45'18.5" W on the Huron River, Ann Arbor, MI.

.

4.3 Field Experimental Procedure

A miniature submersible Particle Image Velocimetry (Mini-PIV) system was developed to quantify turbulence and flow characteristics in natural environments. The application of this type of equipment extends beyond marsh environments to the investigation of natural flow for stream restoration projects evaluation, as well as unsteady flow in a variety of coastal environments. The mini-PIV system is a portable, submersible and miniature version of the full scale PIV system used in the laboratory. The waterproof casing protected the laser and camera, and was lightweight enough to make data collection in natural environments achievable. Other experiments involving submersible PIV systems have looked at the ocean and its bottom boundary layer (Bertuccioli et al., 1999; Nimmo-Smith et al., 2002), while others have investigated

vortex formation in jelly fish swimming (Dabiri et al., 2005), but limited work has been done in developing systems that are easily transportable and can be used in a variety of applications (Tritico et al., 2007).

This mini-PIV system consists of a Laser Glow Technologies Hercules Series Green Laser, Class IIIb - 532 nm continuous laser exceeding 750 mW sustained output and producing a circular beam 2 mm in diameter (Figures 4.3 and 4.4). The beam is directed through two cylindrical lenses to create the laser light sheet required to illuminate particles. The laser is also continuously running once it is turned on through the waterproof laser case and attached by a metal arm to a Casio EX-F1 Exilim six megapixel digital camera which captures the transport of the particles downstream from the bulrush colonies. This camera captures up to 60 frames per second at full resolution, with a 1/1.8-inch high-speed CMOS Type CCD. The laser and camera were connected using a rigid arm that put the camera above the laser sheet capturing images below, so the laser sheet was parallel to the lens of the camera. Both the camera and the laser have separate waterproof cases as part of the submersible mini-PIV system. These waterproof housings do not communicate with each other. The camera case is connected to a laptop through a waterproof USB cable, and the laptop controls the functions of the camera while the images can be viewed real time on the laptop screen. The ability to collect PIV data using minimal pieces of equipment allowed increased accessibility to natural environments for the mini-PIV device.

Seeding for the mini-PIV system consisted of natural occurring particles in the water column. No corrections for light refraction at the water surface are necessary since the camera lens is underwater. The thickness of the laser light sheet was approximately

1mm. The average water depth and the average velocity of the water in the marsh where the experiments were conducted were 27 cm and 3.2 cm/s respectively. This average velocity is captured using an ADV (Figure 4.5) and provided a check for the PIV data while on site in the field. The average Reynolds number for these experiments was 200, based on the reed diameter and average flow velocity. The laser was placed 2 cm downstream from the bulrush patches, and 10 cm from the bottom of the river. The entire submersible mini-PIV system spans an area of 0.23 m^2, and is placed downstream, with the operator downstream, to guarantee that the region of interest is protected from flow disturbances.

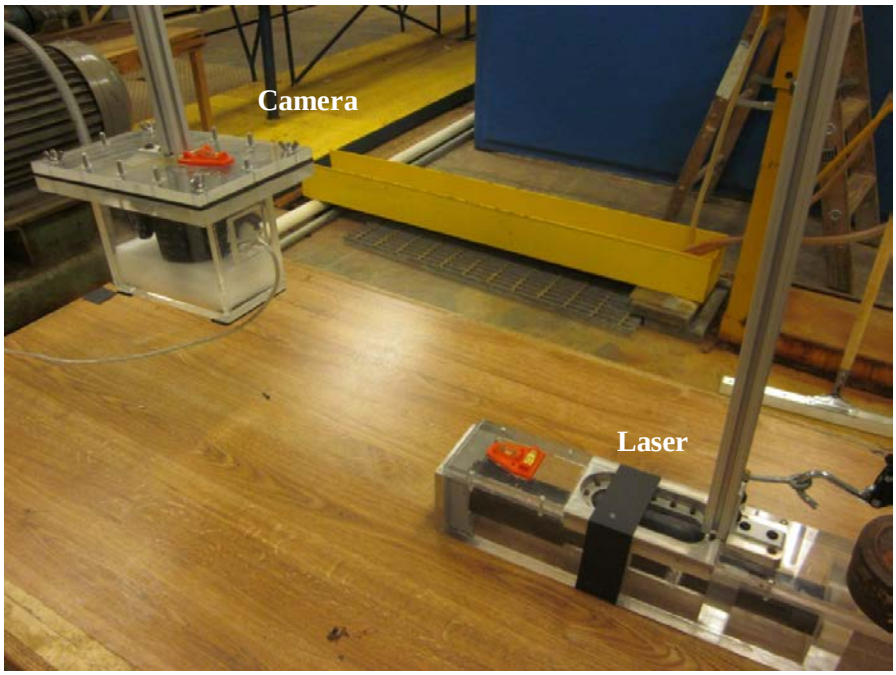

Figure 4.3: Image of the mini-PIV equipment in the Hydraulics Lab at the University of Michigan, Ann Arbor, MI.

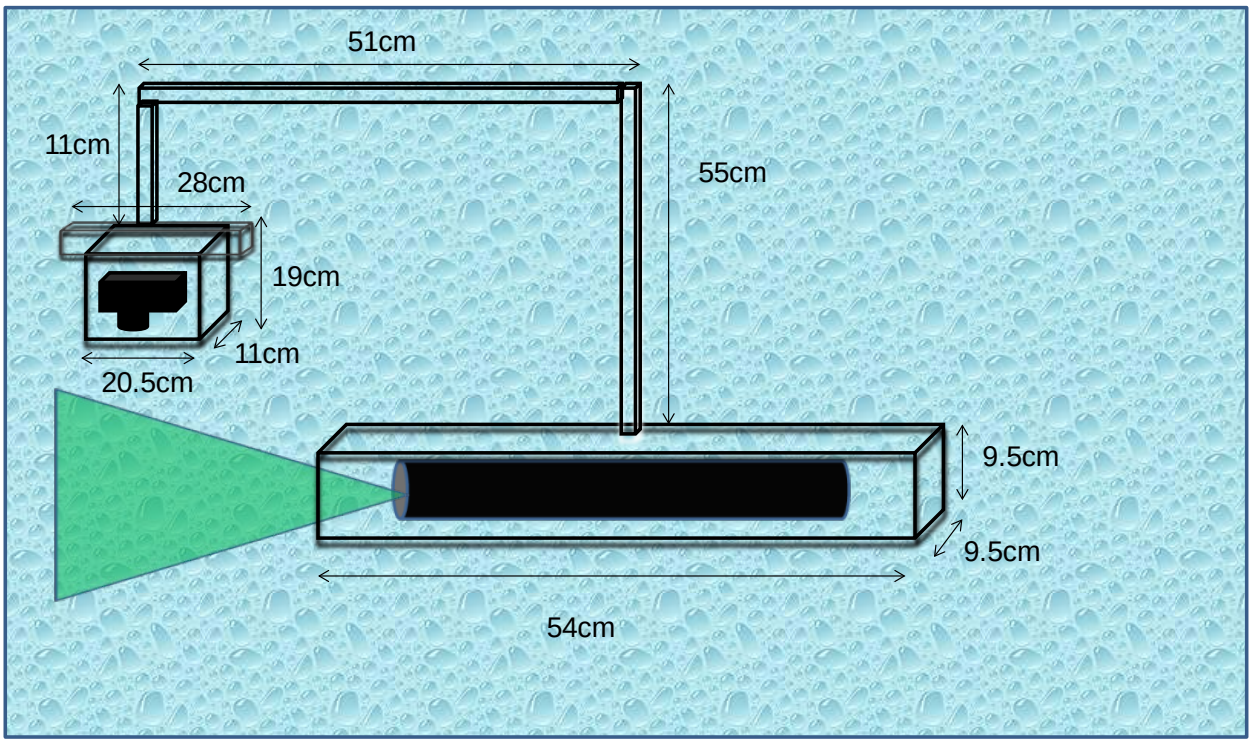

Figure 4.4: Schematic of the mini-PIV equipment.

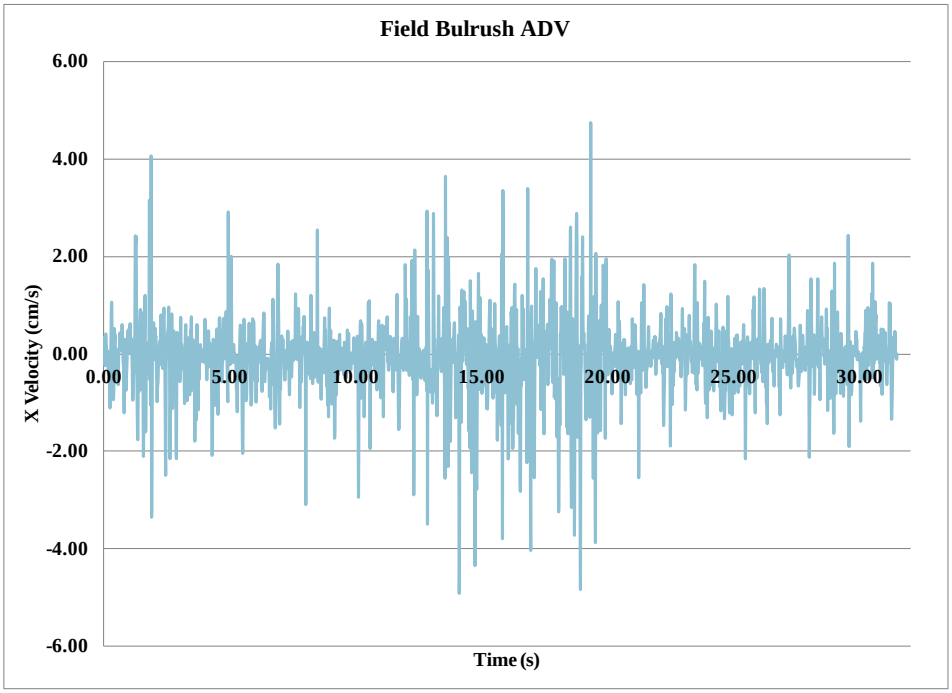

Figure 4.5: Sample field bulrush ADV measurements, from the colony with a reed density of 264 reeds/m^2, taken 2cm downstream from the marsh where the PIV measurements were made.

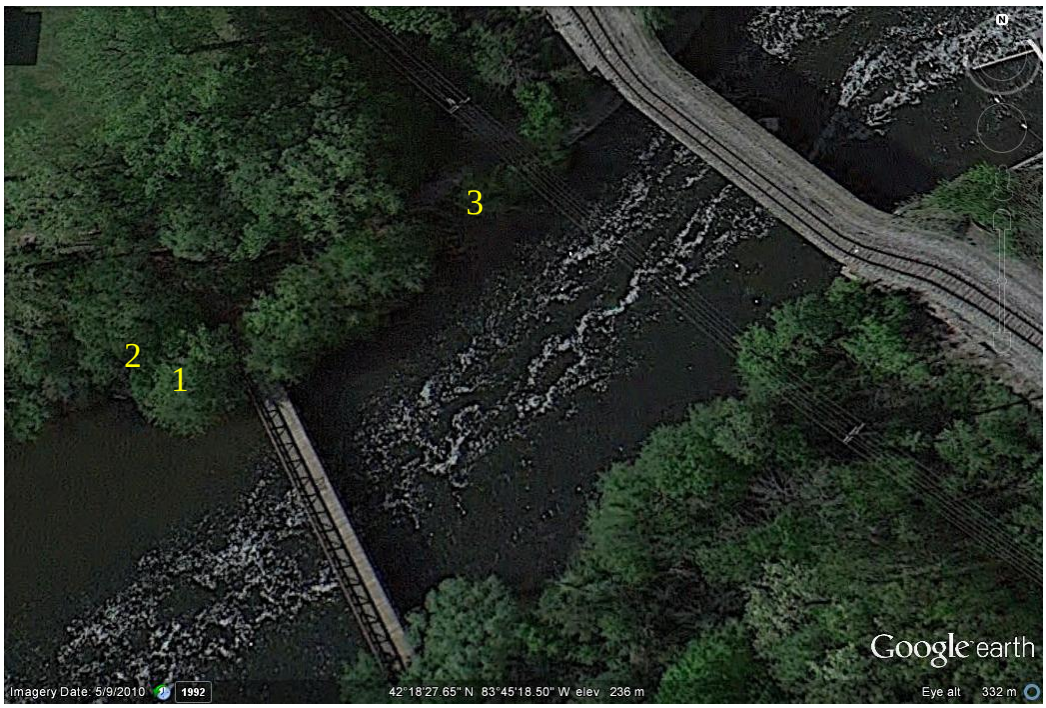

Figure 4.6: Map of the area where the bulrush patches were examined, located at 42º18'27.65" N 83º45'18.5" W. The reed density of softstem bulrush patch 1 was 140 reeds/m^2, 2 was 264 reeds/m^2, and 3 was 388 reeds/m^2.

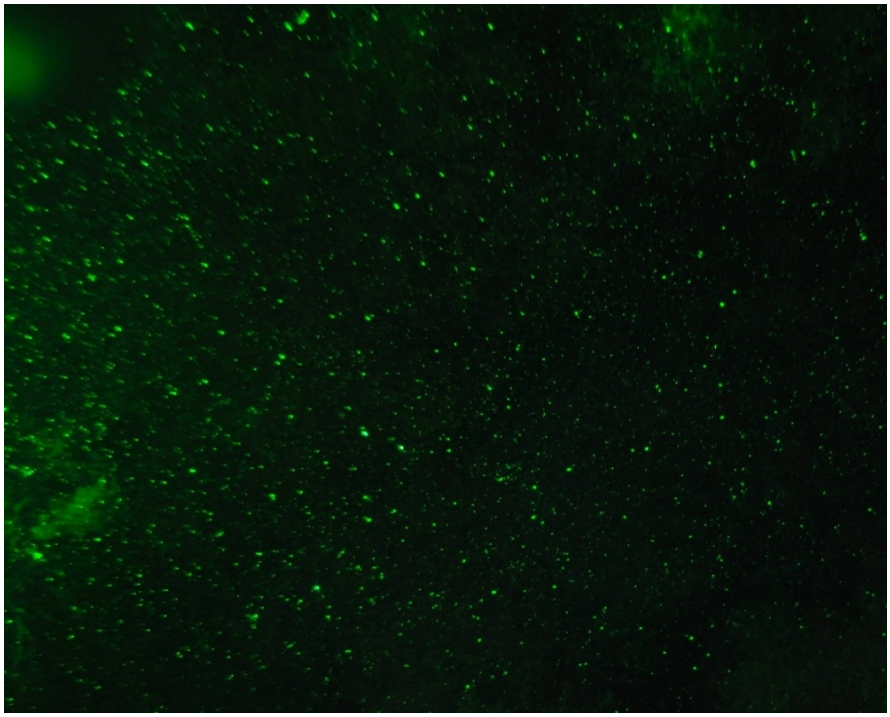

Figure 4.7: Laser image downstream from one of the softstem bulrush colonies on the shoreline of the Huron River, MI. This image contains only naturally occurring particles.

Once the laser was placed where flow downstream of the bulrush patch could be captured, the laser would be fired creating a laser sheet 16 cm by 11 cm. In the marsh area of the Huron River (Figure 4.6), where the softstem bulrush patches were found, there was significant sediment. Figure 4.7 shows typical natural seeding conditions for these experiments. To capture the flow through the marsh, a continuous set of images was collected at 60 frames per second while the laser was firing for five seconds. 150 pairs of images were collected. A time separation of 1/60s, or 0.017s, was used to avoid particle streaking. The processing of the image pairs was performed with PIVlab, an open source MATLAB-based PIV image processing software. With PIVlab, vorticity, eddy size, and eddy circulation are characterized based on the original laser images, as described in Section 2.4. The identification of eddies involved using the method described by Drucker and Lauder (1999) and eddy centers were identified based on the local maximum and minimum of vorticity. Using concentric circles around the eddy center, the circulation about the center was calculated until the maximum circulation was reached. The size of the eddy was determined by the diameter with the maximum circulation, and the vorticity of the eddy was based on the average vorticity within that area.

Images were collected once the sun was setting and the contrast of the ambient light to the laser light was enough to capture the movement of the particles downstream of the bulrush. In addition, low ambient light helped avoid background objects being illuminated. If some of the background objects became illuminated due to the laser sheet intersecting a rock or other natural element, masking of the object in question was performed on the image before post processing was conducted. Masking involves

replacing the section of the image with the illuminated object by a dark cover, rendering that region of the image invisible to the processing software. Removing illuminated background regions is important to avoid errors in the cross-correlation analysis that could miscalculate the magnitude of the velocity and vorticity present in the test area.

Each time a set of images was taken, a test shot was obtained to calculate image magnification i.e. pixels per centimeter, linking image information to real physical scales in the field. From these experiments, the image magnification for the bulrush field data was 65.5 pixels/cm. This is utilized along with the time separation to calculate particle displacement within the image during processing. MATLAB was used to adjust the contrast of the images to illuminate the moving particles, in most cases, increasing the contrast uniformly for each of the images from the same experimental run. Once the images were sorted into pairs, PIVlab used a cross-correlation analysis to determine the particle displacement for each image pair.

4.4 Flow Structures Results in a Natural Marsh Environment

Utilizing the newly constructed Mini-PIV device, the first measurements of flow structure in a natural marsh were obtained. Figures 4.8, 4.10 and 4.12 are images of the bulrush patches examined with the direction of the flow outlined with a blue arrow. In addition to this, a purple box is used to show the placement of the camera. Vorticity was averaged over 20 pairs of images within PIVlab for each of the three reed densities. Figures 4.9, 4.11 and 4.13 outline the results of these calculations from the images collected in the field. Based on this analysis, average eddy size, vorticity and eddy

circulation were calculated at 16 diameters downstream from the bulrush patches and are shown in Figures 4.15, 4.16 and 4.17. 16 diameters downstream was chosen as the representative distance for typical flow conditions downstream of natural marshes, as the flow is well established at that location.

Reed Density of 140 reeds/m^2

Figure 4.8: Softstem bulrush patch #1 with a reed density of 140 stems per m^2. Water is flowing through this patch of bulrush from top to bottom. The image captured was downstream of the reeds and is marked with the purple box. The black arrow signifies the X direction and the white arrow the Y direction, relating to the axes on the vorticity map in Figure 4.9.

Figure 4.9 outlines the vorticity for a reed density of 140 reeds/m^2. In the middle region of the vorticity map, from 12 to 20 diameters downstream of the reeds, the vorticity range was less than half of the value of the preceding region (from 0 to 12 diameters), which is 0.7 s^{-1} to -0.7 s^{-1} with an error of 10%. Merging of the middle region eddies results in an increase in vorticity at 20 diameters downstream from the reed colony, and is outlined by the circles in Figure 4.9. This region saw the largest amount of vorticity, i.e a peak vorticity ranging from 2.5 s^{-1} to -2.5 s^{-1}. The average eddy size remains relatively consistent at 0.7 cm in diameter throughout the region of interest. This eddy size is slightly larger than the average reed diameter, found to be approximately 0.64 cm, since in the lower density patches the eddies may have room to slightly grow in size. The size of the eddies in the field is most probably determined by the spacing between reeds, with the eddy size being half of the wake width or reed spacing of 1.28 cm (Figure 4.1). In the region from 12 to 20 diameters, based on the average eddy size and vorticity, an average eddy circulation from 0.3 cm^2/s to -0.3 cm^2/s was found.

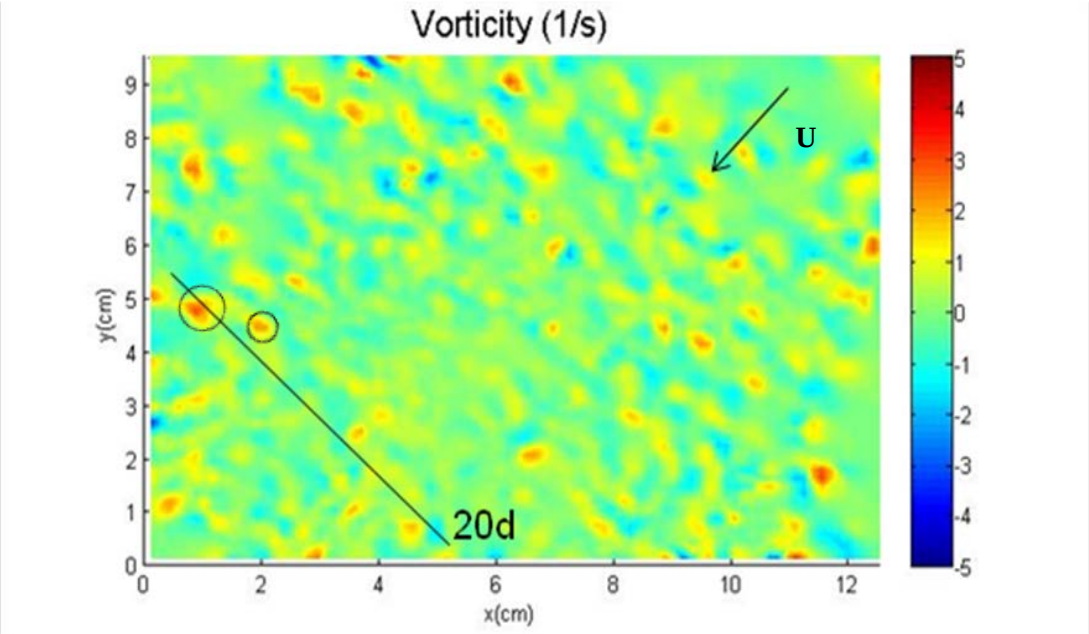

Figure 4.9: Vorticity map for the softstem bulrush patch with a reed density of 140 reeds per m^2. The arrow reveals the direction of the flow and the circles outline where eddies are merging 20 diameters downstream from the reeds.

Reed Density of 264 reeds/m^2

Figure 4.10: The image captured at this location was again downstream of the reeds and marked with the purple box. Softstem bulrush patch #2 has a reed density of 264 stems per m^2. The black arrow signifies the X direction and the white arrow the Y direction, relating to the axes on the vorticity map in Figure 4.11.

The strongest vorticity was found at 16 diameters from the colony for a reed density of 264 reeds/m^2, with an area of energy dissipation, creating lower vorticity levels, in areas closer to the bulrush. Figure 4.11 reveals the vorticity downstream from the softstem bulrush patch. The region 16 diameters downstream from the bulrush had the largest amount of vorticity in the vorticity map, or a peak vorticity ranging from 4 s^{-1} to -4 s^{-1}. This peak vorticity is much higher, over one and a half times, the peak vorticity of the 140 reeds/m^2 bulrush patch. Still, it is also at an upstream position when compared to the previous patch, which could influence this difference in peak vorticity. In the region, between 1 to 15 diameters downstream of the reeds, the vorticity range is much lower, 1.6 s^{-1} to -1.6 s^{-1}. Again, the eddy size remains relatively consistent at 0.64 cm, which is half of the average spacing of 1.28 cm, but here there is less room for the eddies to grow in size due to this being a more dense bulrush patch. Eddies of this size and with the average vorticity found in the vorticity map resulted in an eddy circulation from 0.5 cm^2/s to -0.5 cm^2/s. Similar to the previous reed density, an area of merging eddies occurs, which results in an increase in vorticity at 16 diameters downstream from the softstem bulrush patch. As the reed density of the patch increases, the region of merging eddies moves closer to the reeds, or the distance downstream decreases. This decrease is due to the higher circulation, or momentum, of the downstream eddies.

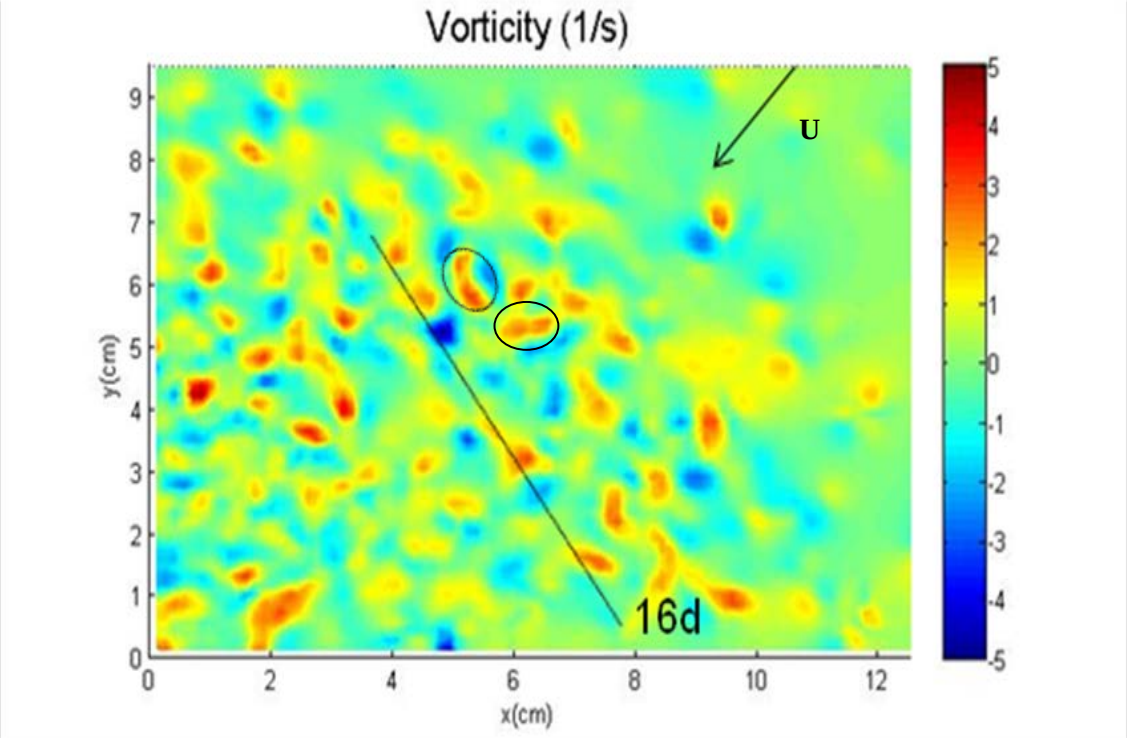

Figure 4.11: The flow through a bulrush patch of reed density of 264 reeds per m^2 is characterized in the vorticity map above. The arrow reveals the direction of the flow and the circles outline where eddies are merging 16 diameters downstream from the reeds.

Reed Density of 388 reeds/m^2

Figure 4.12: Softstem bulrush patch #3, the third of the examined colonies of bulrush, had a reed density of 388 stems per m^2. The image captured was downstream of the reeds, and at an 180^o angle to this picture. The image capture area is again marked with the purple box. The black arrow signifies the X direction and the white arrow the Y direction, relating to the axes on the vorticity map in Figure 4.13.

Figure 4.13 outlines the vorticity for a reed density of 388 reeds/m^2. The strongest vorticity was found 10 to 12 diameters downstream from the bulrush colony. These regions saw the largest amount of vorticity in the vorticity map, or a peak vorticity ranging from 10 s^{-1} to -10 s^{-1}. In the region preceding 10 diameters downstream from the patch of bulrush, the vorticity range is slightly less than half, 4.5 s^{-1} to -4.5 s^{-1}. This higher downstream vorticity is again due to the merging of eddies downstream in this region, which has also moved closer to the bulrush patch with this increase in reed density. The eddy size remains relatively consistent at 0.56 cm in diameter over the entire region, which is slightly smaller than half the average spacing of 1.28 cm in the bulrush patches and looks to be restricted in size due to the further increase in reed density. Eddies of this average size and vorticity resulted in an eddy circulation from 1.1 cm^2/s to -1.1 cm^2/s. Figure 4.14 reveals the comparison of the peak vorticity for the three softstem bulrush patches. An increase in vorticity is correlated with an increase in plant density. The peak vorticity levels for this bulrush patch are over twice those of the 264 reeds/m^2 patch, and four times those of the 140 reeds/m^2 colony. Again, the downstream distance for where the peak vorticity values are located has decreased, which may have influenced this increase in the peak vorticity.

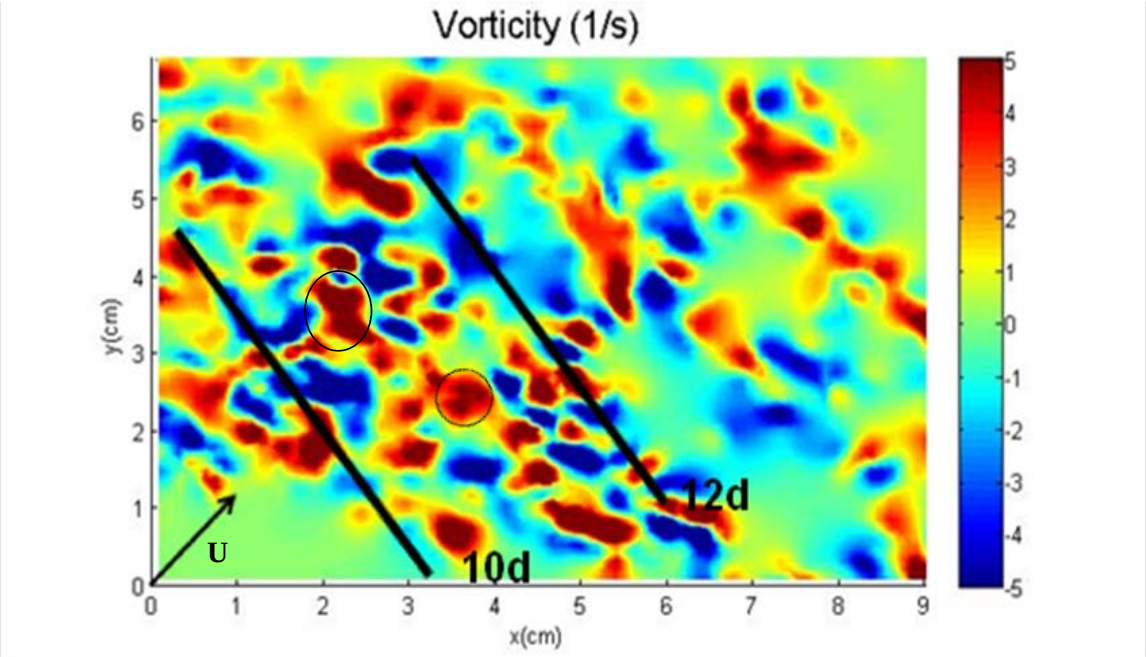

Figure 4.13: Vorticity map for the third softstem bulrush patch with a reed density of 388 reeds per m^2. The arrow reveals the direction of the flow and the circles outline where eddies are merging 10 to 12 diameters downstream from the reeds.

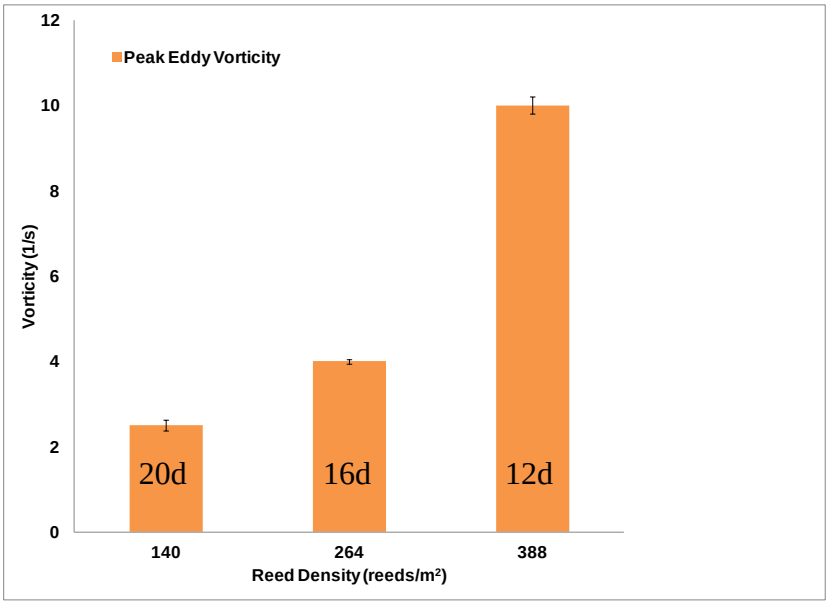

Figure 4.14: Peak vorticity for all three softstem bulrush patches. Each value was found at a decreasing downstream distance from the bulrush colonies (d stands for reed diameter, with the number of reed diameters downstream of the edge of the marsh being identified).

Table 4.1: Summary of Peak Vorticity, Eddy Diameter, Average Vorticity, and Circulation as the change in reed density occurs for the three bulrush colonies.

Reed Density (Reeds/m^2)	Peak Vorticity (1/s)	Eddy Diameter (cm)	Avg. Vorticity (1/s)	Circulation (cm^2/s)
140	2.5	0.70	0.7	0.3
264	4	0.64	1.6	0.5
388	10	0.56	4.5	1.1

Table 4.1 outlines the changes in peak and average eddy vorticity, eddy size and strength as the reed density changed in the three softstem bulrush patches examined. Here the data reveal the large increases in vorticity and circulation over the range of reed densities in the bulrush colonies. At the same time, the eddy size across the three bulrush colonies changes by 20%, reflecting the 20% change in reed spacing over the reed density range examined.

Figures 4.15, 4.16 and 4.17 reveal the changes in vorticity, eddy size and circulation as the reed density changes in the three softstem bulrush patches examined. The vorticity and eddy size was based on a downstream distance of 16 diameters from the colony. At 16 diameters downstream, the average positive eddy vorticity and size were measured to calculate the average positive eddy circulation for each set of image pairs collected. As mentioned earlier, this distance is representative of typical and well-established flow conditions. The error bars represent one standard deviation, based on repeated experiments.

The same method of vortex identification (described in the previous chapter) was utilized in the processing all of the field data. In Figure 4.15, the eddy diameter is examined as the reed density increases. This figure shows a 10% decrease in eddy size as the reed density increases from 140 reeds/m^2 to 264 reeds/m^2, and again a 10% decrease in eddy diameter from 264 reeds/m^2 to 388 reeds/m^2. Therefore, a 20% decrease in eddy

size occurs as the reed density to the highest reed density. In the results for the average eddy size for the three densities, the error is extremely small at 1.5%. Therefore, the influence of the error on the 20% decrease in eddy size as the reed density increases is minimal. Eddy size for all three densities is still very close to 0.64 cm. The average spacing ratio for the softstem bulrush is 2, which again allows for discrete vortex shedding downstream (Sumner et al., 1999), and results in the distance between the reeds being most frequently twice the reed diameter (Figure 4.1). This means that the average wake size is two times the reed diameter, with an eddy size equaling the reed diameter, or half of the wake diameter (Figure 4.16). Therefore, the size of the wake, and subsequent vortices, is determined by the reed spacing (Sumner et al., 1999; Lam and Cheung, 1988). Reed spacing does decrease slightly in higher density patches (Figure 4.1). Therefore, this change in eddy size reflects the change in reed spacing over the reed density range. Figure 4.16 shows how the change in reed density influences vorticity. There is an increase in vorticity of almost six times as the density increases from 140 reeds/m^2 to 388 reeds/m^2.

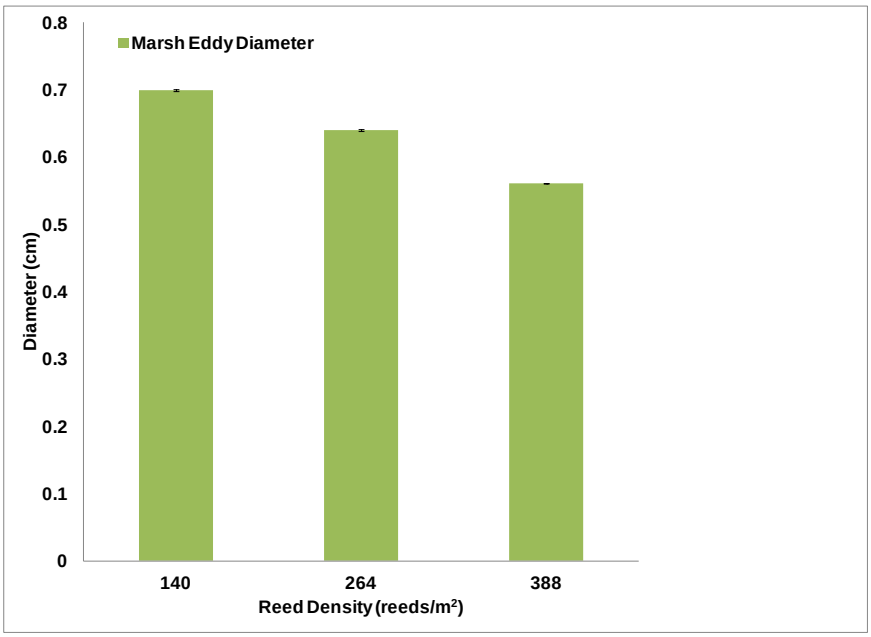

Figure 4.15: Eddy size as the reed density changes for the three bulrush colonies studied, taken at 16 diameters downstream from the bulrush patches.

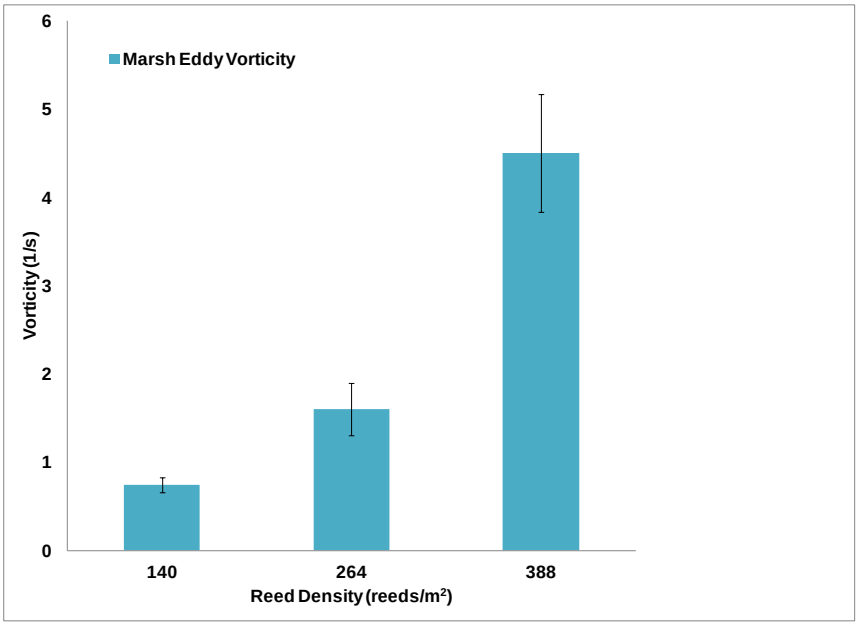

Figure 4.16: The change in positive vorticity with the change in stem density for the three softstem bulrush patches examined at 16 diameters downstream from the colonies.

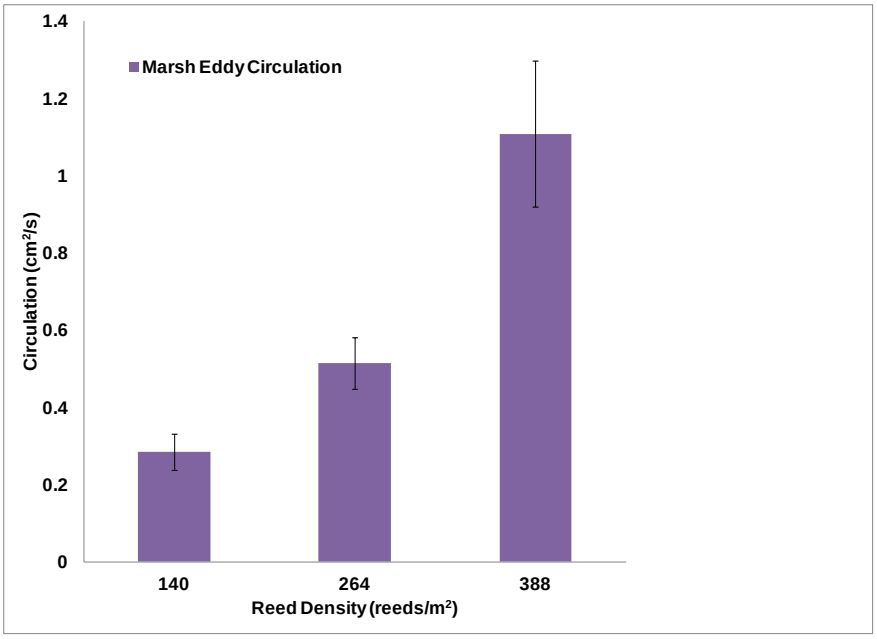

Figure 4.17: Resulting circulation, 16 diameters downstream from the bulrush colonies, calculated for each of the softstem bulrush patches examined and compared to the change in reed density for each patch.

Finally, Figure 4.17 shows the increase in marsh eddy circulation with the increase in reed density. This increase is more dramatic as the reed density changes from 264 reeds/m^2 to 388 reeds/m^2. The eddy circulation increases by 60% from a plant density of 140 reeds/m^2 to 264 reeds/m^2, and a twofold increase in eddy circulation occurs as the plant density is increased by 264 reeds/m^2 to 388 reeds/m^2.

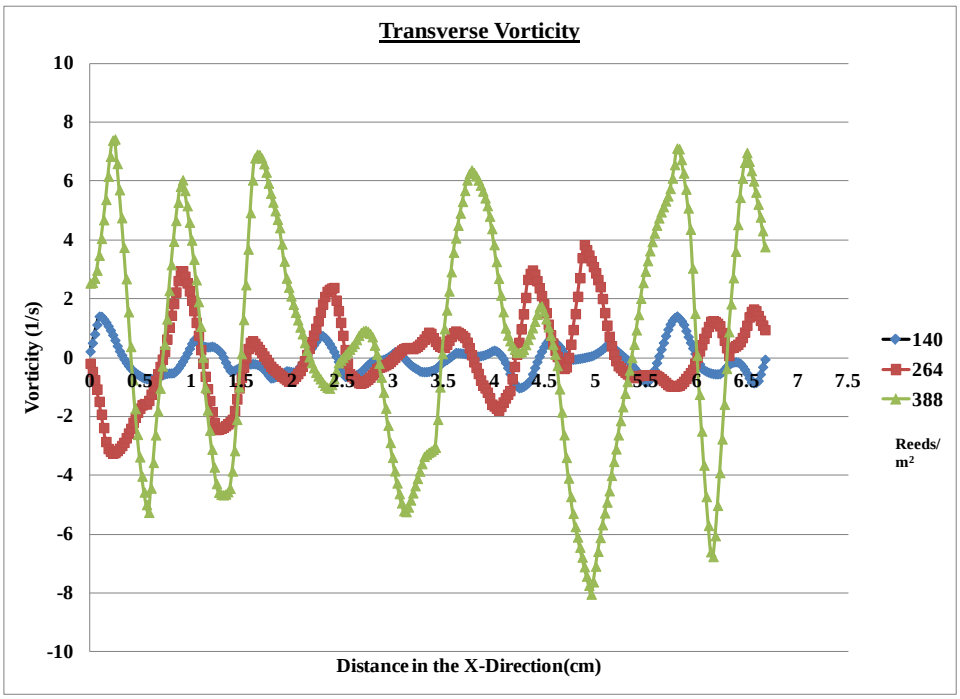

Figure 4.18: Vorticity line plots in the transverse direction, horizontally across the test region downstream from the bulrush colonies at 16 diameters downstream, i.e. for 264 reeds/m^2 this region is identified in Figure 4.11 with respect to the softstem bulrush patch in Figure 4.10.

Figure 4.18 shows the eddy vorticity as it changes transversely across the downstream test areas of the softstem bulrush patches. Each of the line plots outline vorticity at 16 diameters downstream from the bulrush colonies of different stem densities. There is evidence of a sinusoidal wave pattern at all densities. Positive vorticity represents the counterclockwise rotating eddies in the wake while the negative values reveal the other half of the wake, eddies rotating clockwise. The spacing between each alternating positive/negative vorticity region provides a means to evaluate the wake width independently from the results shown earlier (Figures 4.15 and 4.16). However the findings are similar, with an eddy size on the order of 0.5 to 0.8cm depending on stem density. Figure 4.18 clearly reflects the relatively constant eddy size and vorticity for

each specific reed density. There is some scatter in the data as this is in a field setting and the measurements are not trivial to obtain, but over 60% of the vorticity maxima and minima reach similar absolute values of vorticity, at densities of 140 reeds/m^2 and 264 reeds/m^2. The wakes are even more closely correlated at the higher density case of 388 reeds/m^2 with an 80% match for peak vorticity values. The higher scatter at lower densities stems from the increased patchiness in those cases.

The consistent size of the wake, and subsequent vortices, is determined by the spacing between the reeds (Lam and Cheung, 1988; Sumner et al., 1999). This regularity in the reed spacing could also influence the consistency of the eddy strength for each bulrush colony. While more analysis needs to be conducted, the initial examination of the softstem bulrush growth pattern across the bulrush patches reveals that a linear trajectory appears to dominate the growth structure in these bulrush colonies (Figure 4.2). A linear pattern is expected due to the linear rhizome root structure of the softstem bulrush. This pattern influences the spacing between the reeds as the bulrush plant forms its root system, creating a consistent distance between reeds in that linear trajectory. This results in eddies being formed that are of a similar size and strength downstream from the bulrush patches (Figure 4.18).

Chapter 5: Laboratory Experiments of Different Simulated Marsh Configurations

5.1 Experimental Procedure

To further understand the physical characterization of flow structures created in a marsh environment, laboratory experiments were designed to simulate marsh configurations under different conditions. Observations were made in the Engineering Laboratory Design Flow Visualization Water Tunnel (Figure 5.1). In this water tunnel the observation section is 60 cm wide and 250 cm in length and a variable speed pump allows the water to be recirculated at different velocities. All tests were conducted with a water depth of 54 cm. Flow measurements were performed with a two-dimensional PIV system described in Chapter 2. The laser sheet was situated at a depth of 29 cm. The laser sheet was 2 cm downstream from the rods with a width of 17.5 cm and a length of 13.5 cm, and a thickness of 2 mm. This allowed the laser sheet to be placed in the center of the water tunnel and avoided interference from the walls of the tunnel. The water in the recirculating water tunnel was seeded with neutrally buoyant hollow glass spheres (Dantec Dynamics), 10 μm in diameter, at a concentration of 1 ppm. These spheres were illuminated in the flow downstream from the rods using a dual-head 532-nm pulsed laser (New Wave Gemini 120 mJ). The pulse separation of the lasers was 4 ms for the (low-density and high-density) alternating configurations to be described below. Images of the

flow structure downstream of the marsh configuration were captured using a 10-bit, 1 mega pixel, 30 fps Uniq Vision (UP-1030-10) black and white CCD camera. 140 pairs of images were captured for each experimental run using the PixelFlow software (General Pixels, Inc.). This was the maximum number of pairs allowed to be saved by the software for each run, based on the size of the photographed area. Therefore, a compromise had to be made between the number of images and the size of the image area.

Images of the particles were converted into velocity vector fields using cross-correlation techniques, and based on the velocity vector field, vorticity was calculated. The image processing follows typical PIV operations of vector smoothing and filtering to reduce the number of bad vectors due to reflections or edge effects (Willert and Gharib, 1991). The identification of eddies involved using the method described by Drucker and Lauder (1999) where eddy centers were identified based on the local maximum and minimum of vorticity. Time averaged quantities were calculated using all the 140 pairs of images, and for each experiment, two sets of data were obtained.

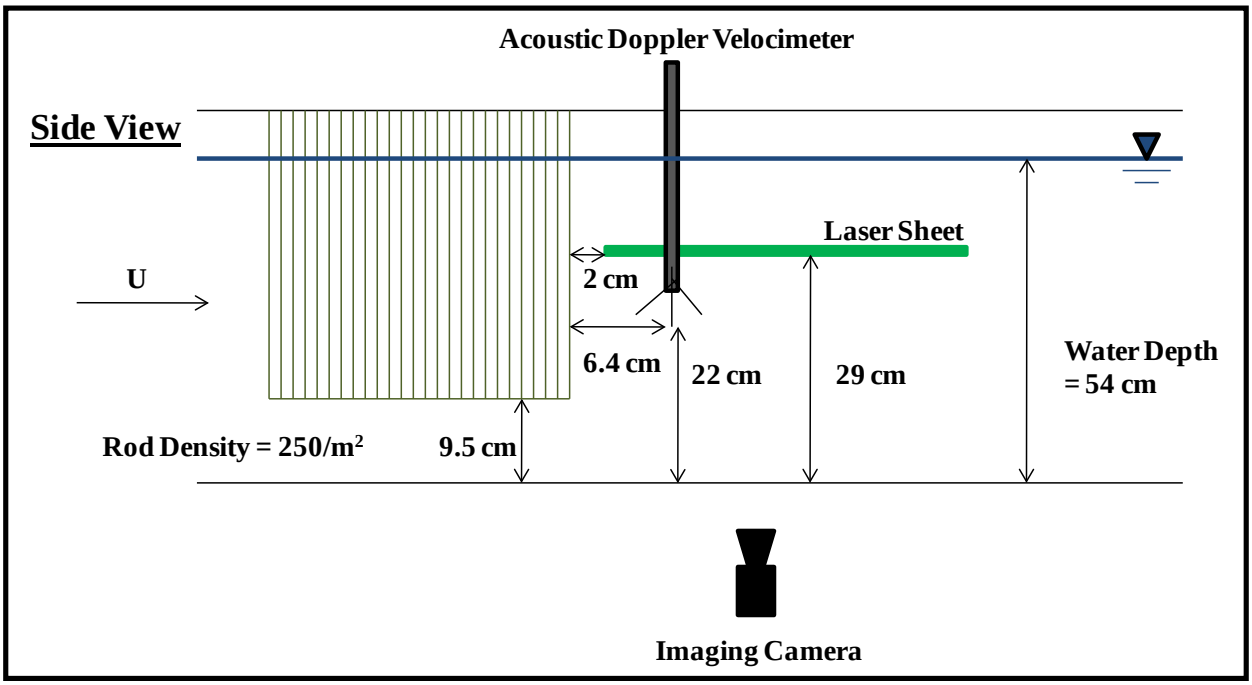

Figure 5.1: Experimental PIV and Acoustic Doppler Velocimetry (ADV) setup used for examining the turbulence downstream from the rod configuration. The horizontal laser sheet was viewed from the bottom of the recirculating flume by the imaging camera.

Plexiglas rods, with a diameter of 0.64 cm, were used to simulate the marsh environment. The rods were fixed into plates on the bottom and the top of the water tunnel, and arranged into a specified configuration; low-density alternating (Figures 5.2(a) and 5.3), high-density alternating (Figure 5.2(b)), or random (Figure 5.2(c)). The alternating configuration experiments started with a single row placed on the plates, with additional rows added up to a maximum of 10 rows. Rows of rods were added to the low-density and high-density configurations, to understand how the downstream flow structure changed with the addition of rows to the laboratory setup. The bottom plate, where the rods are fixed, served as a false bottom and was 9.5 cm from the actual bottom of the flume. The low-density alternating arrangement of rods had a density of 250

rods/m^2, and the high-density alternating arrangement of rods had a density of 400 rods/m^2. The random configuration (Figure 5.2(c)) of rods in the marsh setup was utilized to explore the effect of reed patchiness and clusters found in a natural environment. Here, the rods were arranged using MATLAB's (The Math Works, Inc.) random number generator, at densities of 50, 150, 250 and 400 rods/m^2. The rod densities for both the alternating and random experiments correspond to those found in natural environments (Augustin et al., 2009).

Depth averaged velocities at which the different configurations were examined were 10 cm/s and 15 cm/s. This resulted in Reynolds numbers of 700 and 1,100 respectively, based on rod diameter. These velocities are larger than typical average velocities in natural marshes, and are used to simulate extreme events such as storms. Water velocities of 2.5, 5, 10 and 15 cm/s were used for the random experiment, requiring laser pulse separations of 40, 25, 12 and 7 ms and corresponding to Reynolds numbers of 200, 400, 700 and 1,100, based on the rod diameter. The velocities that were used in the random configuration extended to lower velocities more representative of average velocities in a marsh, but also included extreme conditions. A typical average water velocity in a marsh is closer to 5 cm/s (Nepf, 1999). With climate change and the resulting predicted increase in extreme storm events, understanding the influence of higher velocity flow is essential when studying the interaction between biota and turbulence in a vegetated environment. Another intriguing aspect of marshes is their ability for formidable energy dissipation during storm events, as they providing shelter to a wide range of species. These experiments aim to characterize these flow conditions.

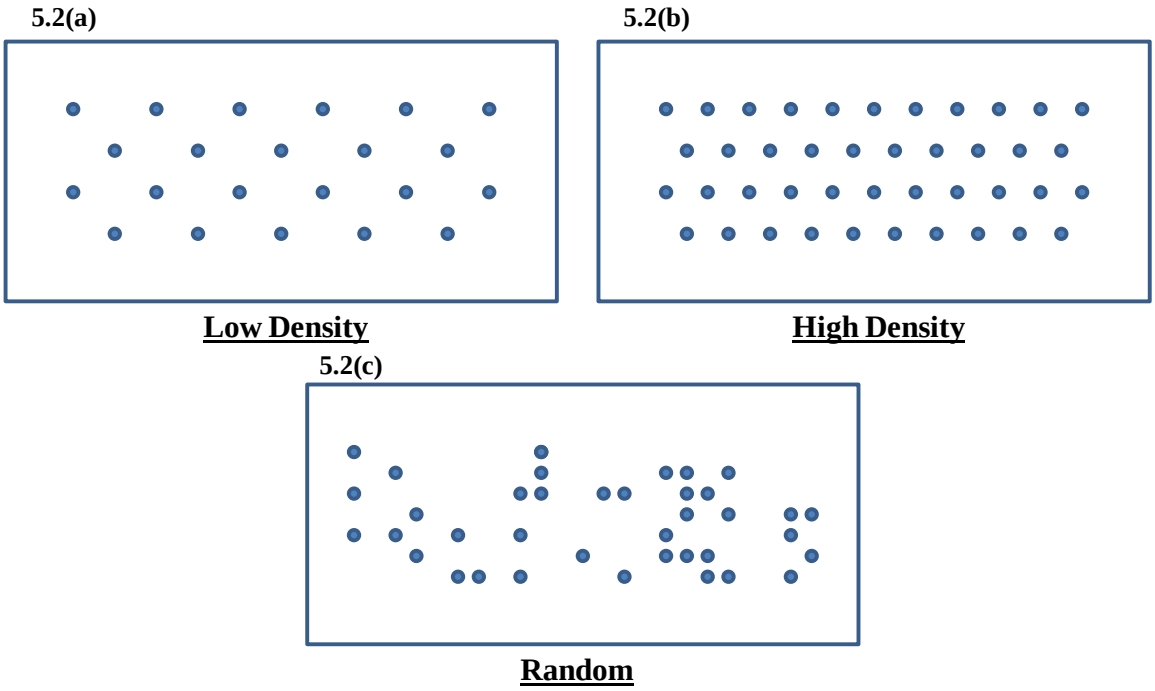

Figure 5.2: Sample rod setup for each configuration: Low-Density (250 rods/m^2) 5.2(a), High-Density (400 rods/m^2) 5.2(b) and Random (400 rods/m^2) 5.2(c).

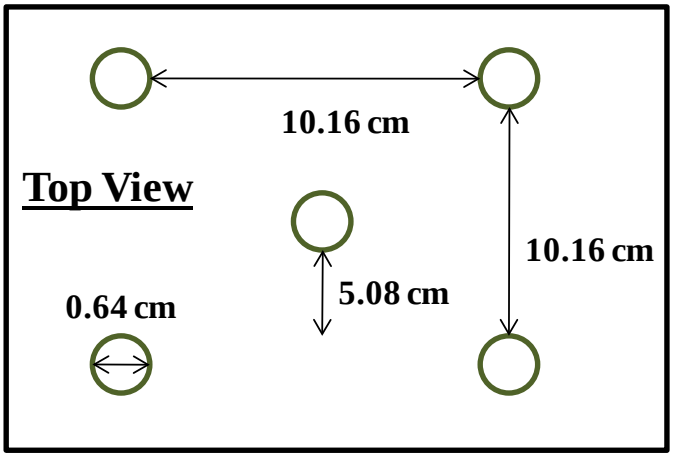

Figure 5.3: An example of the dimensions of the Low-Density rod configuration.

Three downstream locations were examined. These locations were based on the rod diameter (0.64 cm) and they were 16, 20 and 25 rod diameters downstream from the

marsh configuration. The locations were chosen as positions that characterize the wake as it is travelling downstream from the rods.

5.2 Flow Structure Results for Low-Density Marsh Configuration

In an effort to gain further understanding of the field measurements, laboratory experiments were conducted examining a low-density marsh configuration (250 rods/m^2) using an alternating pattern of Plexiglas rods. Figure 5.4 shows the typical flow structure captured in a vorticity map downstream from the experimental setup. Figures 5.6 and 5.7 compare the time averaged laboratory observations of eddy size in the wake downstream from the rods for three downstream locations: 16d, 20d and 25d, where d is the rod diameter. The flow characteristics were also examined at two flow velocities of 10 cm/s and 15 cm/s, or Reynolds numbers of 700 and 1100. In addition to this, rows of rods were added to the laboratory setup, to see how this influenced the downstream flow structure.

Based on the observations, eddy diameter increases one and a half times with an increase in rows up to four rows. The eddy diameter becomes constant once four rows were present. This was found for both Reynolds numbers of 700 and 1,100, and for all locations downstream of the rods. As additional rods are added, the flow becomes more uniform and the eddy size is almost constant. At the lower number of rows, i.e. two or three rows, some interesting dynamics are taking place. Most likely, eddies are merging creating larger vortices (e.g., in the case of three rows at 20d for Re=1,100) or reducing in size due to the vorticity of opposite signs cancelling each other out (e.g., in the case of

two rows at 25d for Re=1,100). These eddy interactions occur downstream from the original discrete vortex formation at the rods, which occurs for high spacing ratios (see Chapter 2). The spacing ratio for this particular configuration is 8 and falls in this category. This merging of eddies is due to the upstream wakes interfering with the downstream wakes in the alternating rod setup (Figure 5.5). The spacing ratio results in a distance of 5 cm between the rods. Therefore, a typical eddy size downstream of the rod array would be on the order of 2.5 cm, since the eddy diameter is about half of the wake width or half of the spacing between the rods (Figure 5.4). As confirmed in Figures 5.6 and 5.7, the average eddy size is around 2.5 cm, showing that rod spacing is the controlling parameter in determining typical eddy size in such a configuration. Also, it is important to note that there is no influence of Reynolds number on eddy size in these low-density experiments.

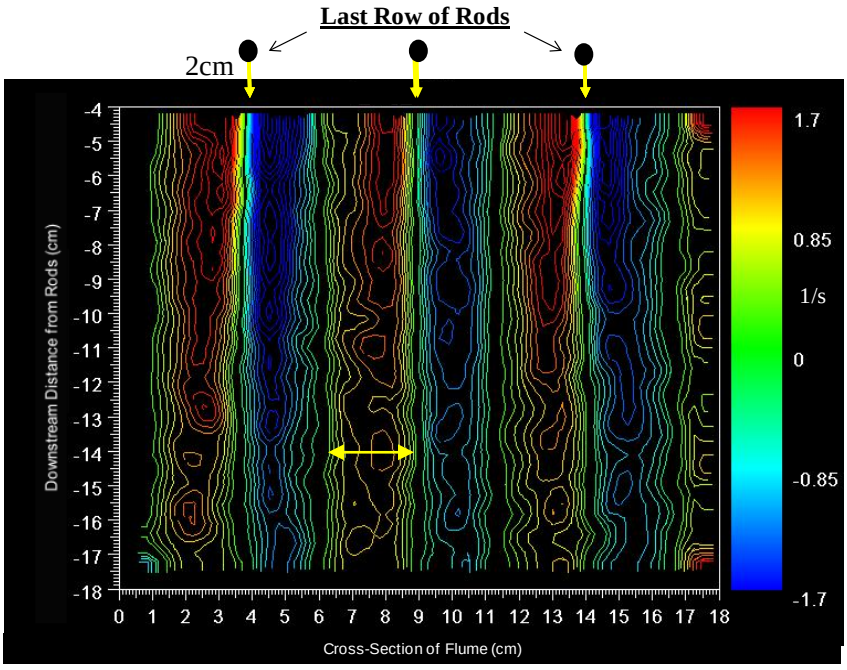

Figure 5.4: Example vorticity map for the low-density configuration at 10 rows of rods and a velocity of 10 cm/s. The eddy diameter is highlighted with a yellow arrow.

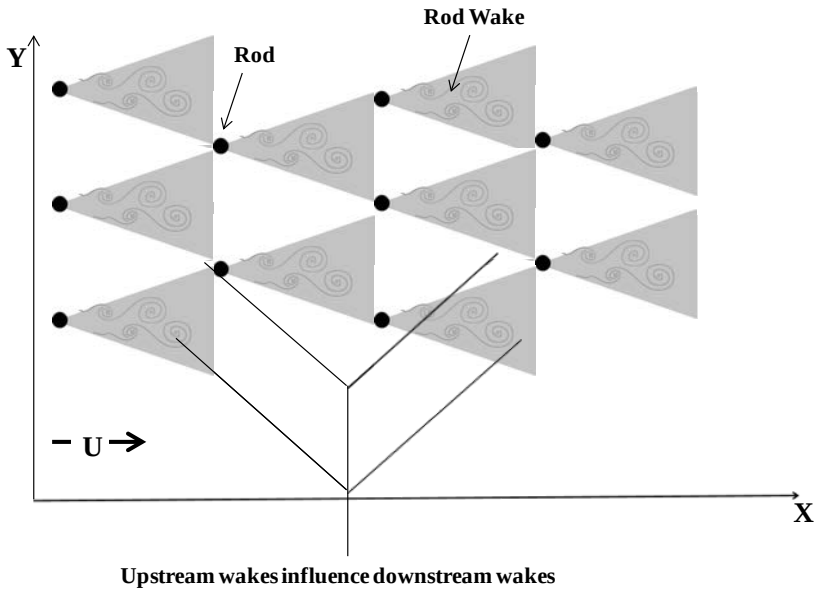

Figure 5.5: Top view of the low-density marsh configuration showing rods and wakes downstream from the rods. Here the influence the upstream wakes have on the downstream wakes can be seen from the wakes lining up in the alternating configuration, and can further observed in the vorticity maps below which show the combined wakes. Wakes are spreading at a 40º angle based on the observations from the laboratory experiments.

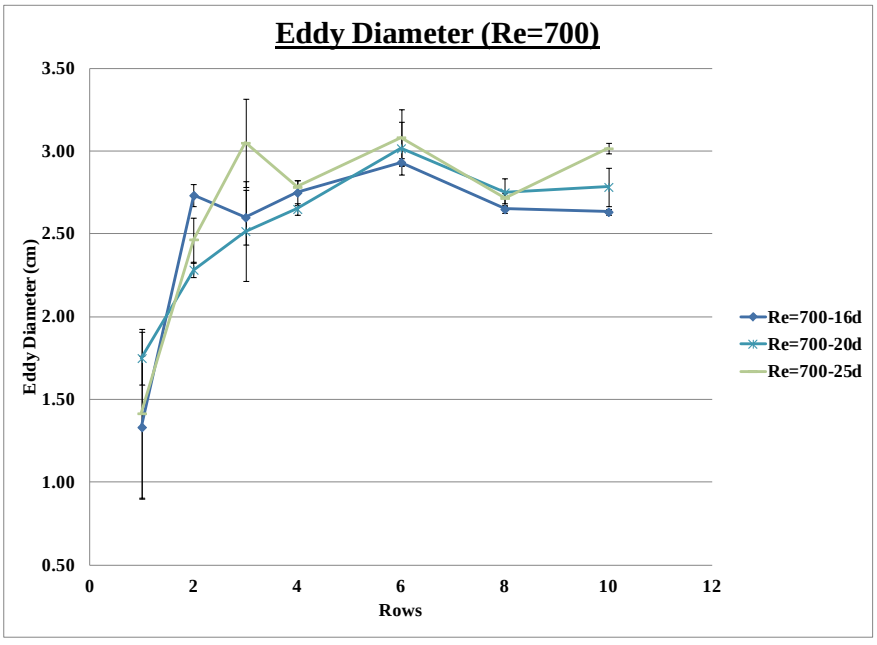

Figure 5.6: Eddy diameter for low-density configuration and Re = 700: Re = UD/ν. (Error bars are based on one standard deviation from the data point, and based on repeated experiments.)

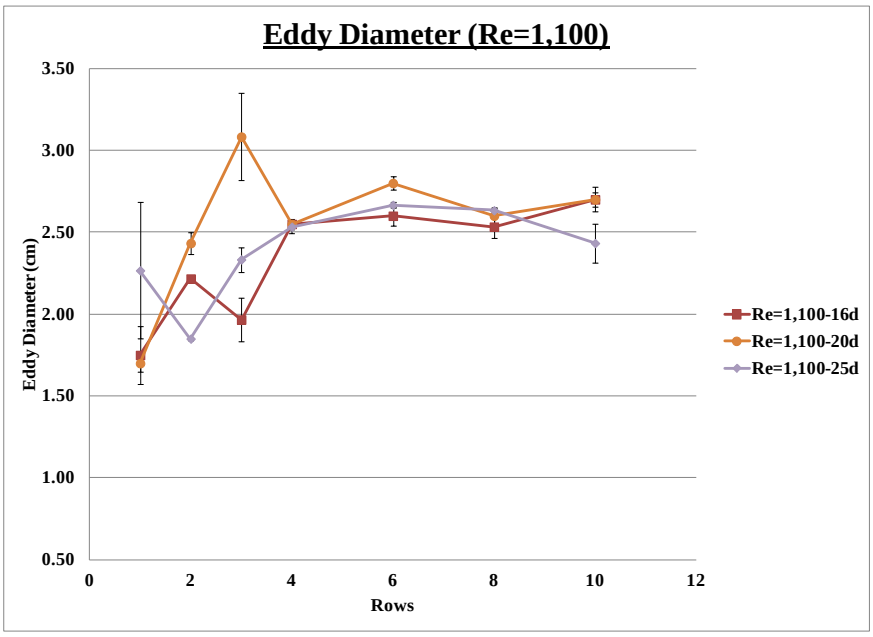

Figure 5.7: Eddy diameter for low-density configuration and Re = 1,100.

The eddy vorticity was measured in the same three locations in the downstream wake of the rods. Figures 5.8 and 5.9 show the observations of the time-averaged vorticity results for the low-density setup. The vorticity at a Reynolds number of 1,100 is, on average, one and a half times larger than the vorticity at a Reynolds number of 700. This increase is due to an increase in the velocity in the flume of the same order. Both figures reveal that the eddy vorticity doubles after each row when the first four rows are added to the rod configuration, with constant eddy vorticity being observed thereafter. The transition to homogeneous conditions is similar to what was found in the analysis of the eddy diameter. What is different in these observations from those of the eddy size is that there is a 30% decrease in the eddy vorticity as the downstream distance from the rods increases. Despite the size being maintained as the distance increases, the vorticity diminishes. This trend in vorticity is most likely due to the dissipation of energy as the

eddies move downstream, while the consistency of the eddy size is due to the eddy diameter being determined by the rod spacing.

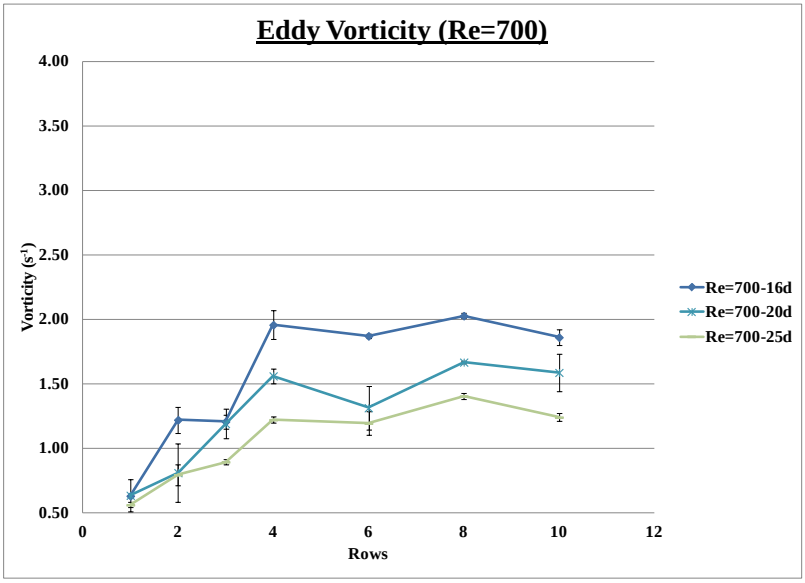

Figure 5.8: Eddy vorticity for low-density configuration and Re = 700.

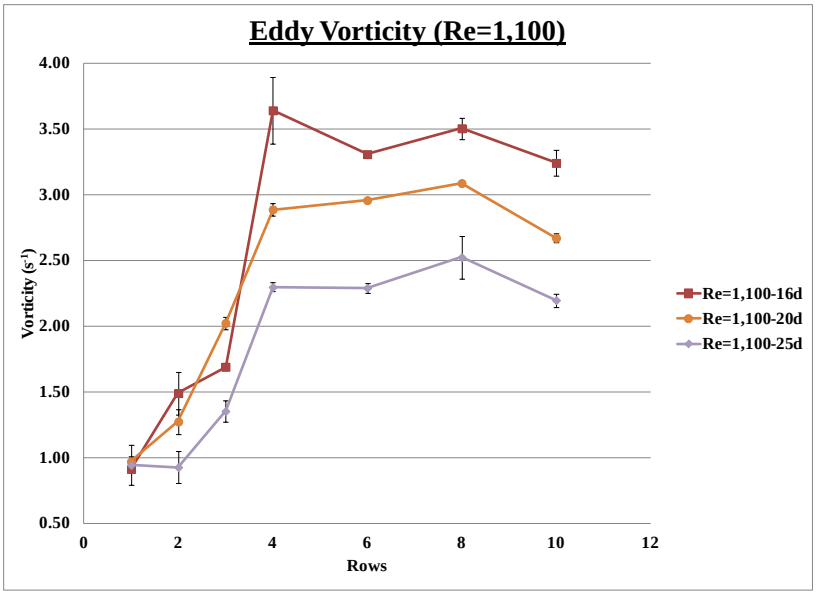

Figure 5.9: Eddy vorticity for low-density configuration and Re = 1,100.

The eddy circulation (Γ) calculated using equation 5.1, using vorticity (ω), the area of the eddy (A) and the diameter of the eddy (D), combines these results of the eddy diameter and the eddy vorticity.

$$\Gamma = \omega \cdot A = \omega \cdot \pi \left(\frac{D^2}{4} \right) \qquad (5.1)$$

Figures 5.10 and 5.11 show an increase in eddy circulation of at least six times between the one row and four row configurations at each Reynolds number. Once four rows are added, similar to the eddy diameter and vorticity results, a constant value of circulation is obtained. A large decrease of 30% is seen at a Reynolds number of 1,100 and 25d at two rows, again reflecting the eddy diameter behavior, with an error on the order of 15%. Since circulation is a function of eddy surface area, the effect of eddy diameter is more prominent in the results of eddy circulation, specifically before the transition to more uniform flow. A 30% decrease in circulation can be observed as the distance downstream of the rods is increased, revealing the energy dissipation that was seen in the vorticity results. The larger eddy circulation at a Reynolds number of 1,100 is again, on average, one and a half times larger than the circulation for the Reynolds number of 700.

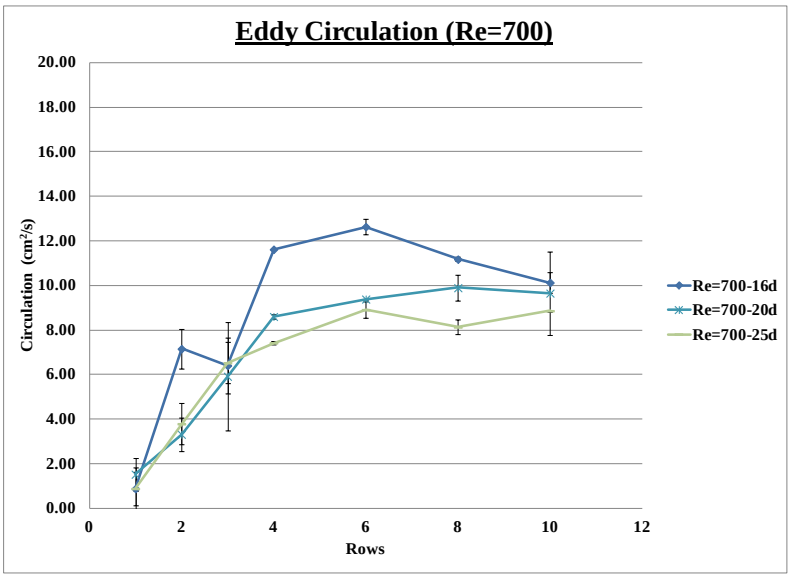

Figure 5.10: Eddy circulation for low-density configuration and Re = 700.

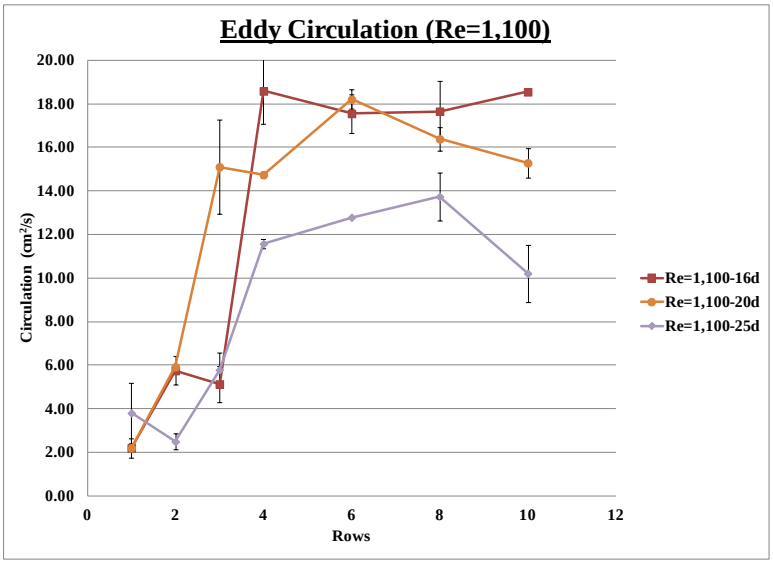

Figure 5.11: Eddy circulation for low-density configuration and Re = 1,100.

Figures 5.6 through 5.11 represent characteristics of eddies rotating counter clockwise within the wake. These eddies are defined to have positive vorticity (See Figure 2.2). Similar results were obtained for eddies in the wake rotating in the opposite

direction with negative vorticity. Both Figures 5.12 and 5.13 show the results for negative eddy circulation, based on negative vorticity. Similar trends between positive and negative circulation are observed, an increase in the absolute value of eddy circulation is seen with the addition of rows and constant circulation is again seen at four rows. The absolute value of the negative eddy circulation increases at an average rate of one and a half with the increase in the Reynolds number from 700 to 1,100. There is also a 30% dissipation of the absolute value of the negative circulation with increasing downstream distance, for both Reynolds numbers. At ten rows and a Reynolds number of 700, for a downstream distance of 16d, a 10 cm^2/s absolute value is obtained for both the positive and negative eddy circulation. This exemplifies the symmetry in the wake and how the eddies in the wake can be measured separately, but can share the same value.

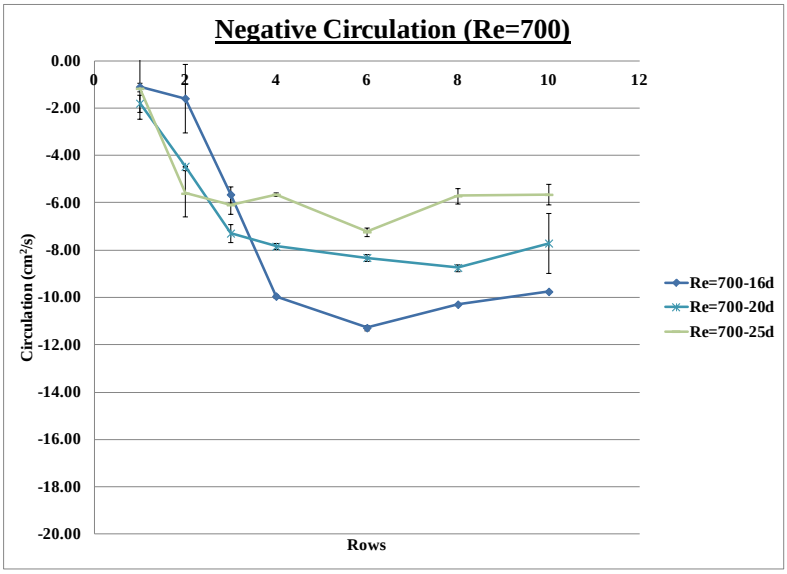

Figure 5.12: Negative eddy circulation for low-density configuration and Re = 700.

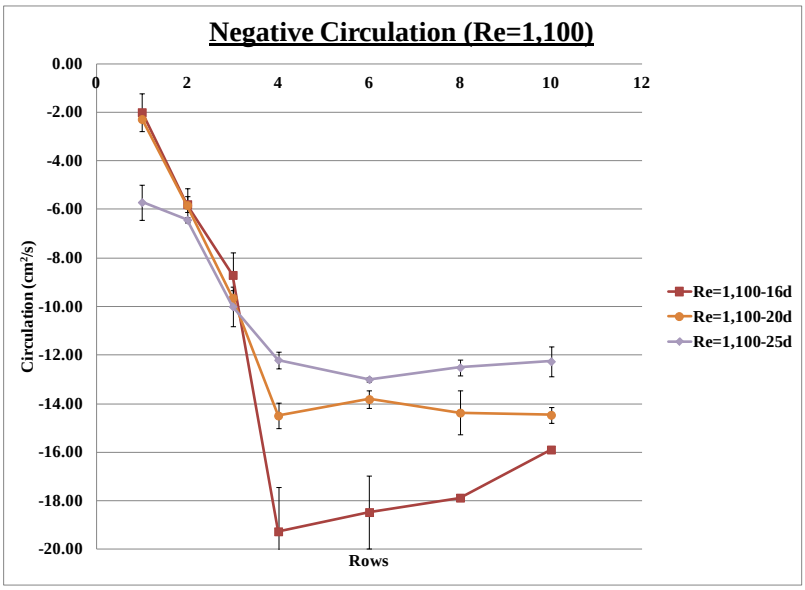

Figure 5.13: Negative eddy circulation for low-density configuration and Re = 1,100.

When there is only one row in the low-density marsh configuration, two strong wakes develop downstream from the rods as the water flows past the rods. The formation of the vortex pairs is due to the forcing of the fluid past the rods, as the inertia of the rod resists the motion of the fluid past the rod and the wake is generated. This fluid forcing imparts circulation into the flow around the rod. Eventually, fluid vorticity created by the rod is shed into the wake.

Figure 5.14(a) reveals the formation of two wakes from the first row of rods being added to the low-density alternating configuration. Figures 5.14(b), 5.14(c) outline the formation of three distinct wakes downstream from the rods, once four and ten rows of rods are added to the rod setup, respectively. The formation of distinct wakes of equal size is created by the pattern of the alternating rod configuration at more than 4 rows of Plexiglas rods. There is also a slight decrease in vorticity in the second wake, as can be

seen in Figure 5.15. This decrease in vorticity is most likely a consequence of the geometry, since the second row is further upstream, compared to the rows producing the other two wakes. Therefore, the wake from the second row has traveled a greater distance and experiences some dissipation of energy before it is captured in the vorticity map downstream. Still, Figure 5.15, examining the transverse vorticity, or the vorticity as it changes across the flume at 16 diameters downstream from the rods, clearly reveals the wake pattern and fairly constant value of vorticity independent of the number of rows added once four rows are in place. This consistency in vorticity in the transverse direction is reflected in the three similar wakes found in the vorticity maps in Figures 5.14(b) and 5.14(c).

Due to the space between the rods allowing room for the wakes to grow, the upstream wakes combine and grow to fill the gaps between the downstream rods. These gaps in the low-density laboratory setup are equal to 5 cm, with the average eddy size equaling half of the wake diameter, or 2.5 cm. The growth pattern of the wakes is due to the alternating arrangement of the rods, which is revealed in the wake pattern of consistent size and strength.

Overall, this regularity in the eddy diameter and vorticity across the observational area is similar to what was observed in the downstream flow structure in the field experimental results (Chapter 4). This is reflected in the similar sinusoidal pattern of the transverse vorticity plots, resulting in maximum and minimum vorticity values being of the same magnitude and the distances between these max and min values equal to the eddy size. Again, the influence of the upstream vortex shedding, on the downstream wake formation, through the merging of eddies and the creation of a wake pattern, is

similar to that observed by Kiya et al. (1980) and Zradavkovich and Pridden (1977) (Figure 5.5). The size of the wake, and subsequent vortices, is determined by the rod spacing and pattern as observed in both the field and laboratory experiments, as well as by Lam and Cheung (1988).

Another interesting aspect of the flow pattern is the transition region between wakes. In Figure 5.15, arrows identify regions between the wakes characterized by points of zero vorticity in the low-density marsh configuration. Figure 5.16 highlights these regions even more, the yellow arrows reveal the slower flow behind the rods, while the red arrows outline the faster flow past the rods. The velocity across the flume, 16 diameters downstream from the rods, is shown in Figure 5.17, which also outlines the transverse vorticity at the same location. The areas of zero vorticity now line up with the regions of maximum velocity. These regions are then observed at the transition between the faster flow past the rods and the slower flow behind the rods. In Figure 5.17, points of zero vorticity occur on the edge of the wakes, where there is a change in velocity in the transverse direction. This velocity gradient (du/dy, or the change in the longitudinal velocity in the transverse direction) calculated in the vicinity of the points of zero vorticity is constant and found to be on the order of 0.73/s, for each of the four regions identified by the arrows in Figure 5.15. Such regions are very interesting and significant with respect to biota behavior, as fish have been observed to have difficulty crossing regions with high velocity gradients in fish passage ways (Tarrade et al., 2008).

5.14(a)

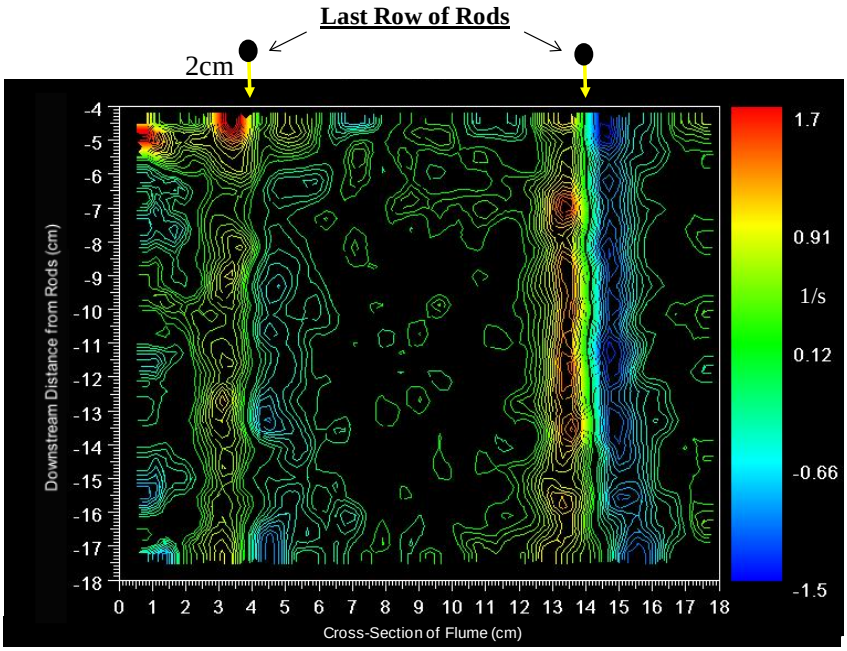
Last Row of Rods
2cm
Downstream Distance from Rods (cm)
-4 -5 -6 -7 -8 -9 -10 -11 -12 -13 -14 -15 -16 -17 -18
0 1 2 3 4 5 6 7 8 9 10 11 12 13 14 15 16 17 18
Cross-Section of Flume (cm)
1.7
0.91
1/s
0.12
-0.66
-1.5

5.14(b)

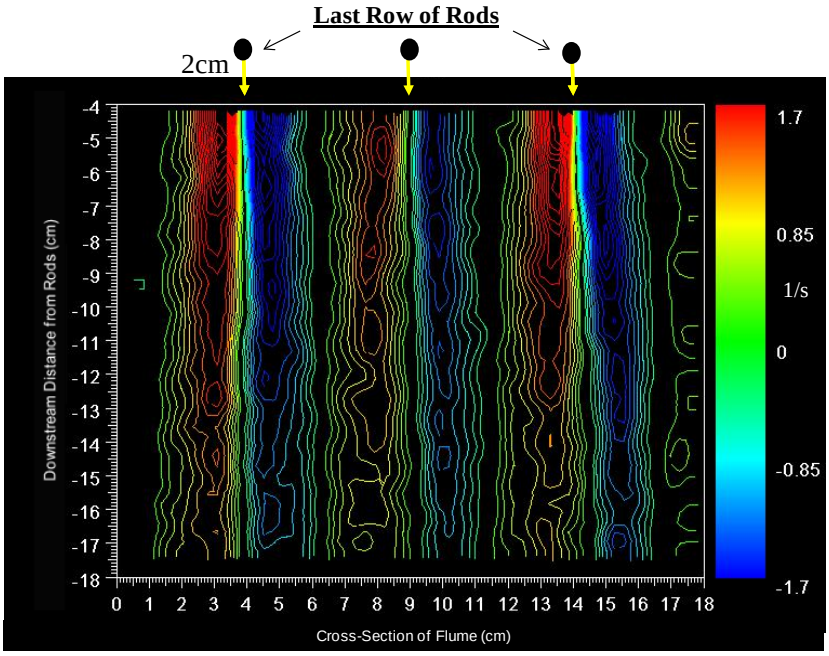
Last Row of Rods
2cm
Downstream Distance from Rods (cm)
-4 -5 -6 -7 -8 -9 -10 -11 -12 -13 -14 -15 -16 -17 -18
0 1 2 3 4 5 6 7 8 9 10 11 12 13 14 15 16 17 18
Cross-Section of Flume (cm)
1.7
0.85
1/s
0
-0.85
-1.7

5.14(c)

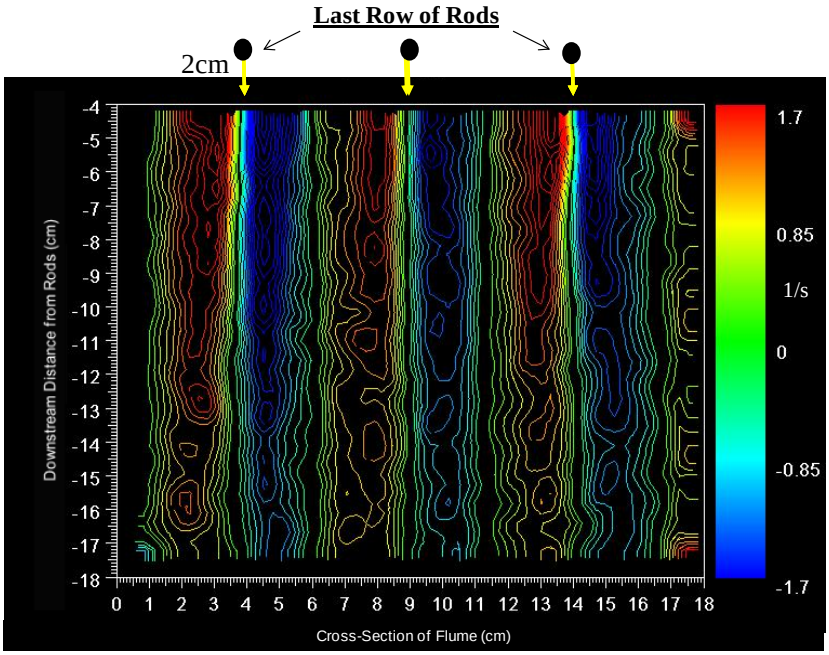

Figure 5.14: Vorticity maps for one row (a), four rows (b), and ten rows (c) of rods in to the low-density configuration (Figure 5.2(a)).

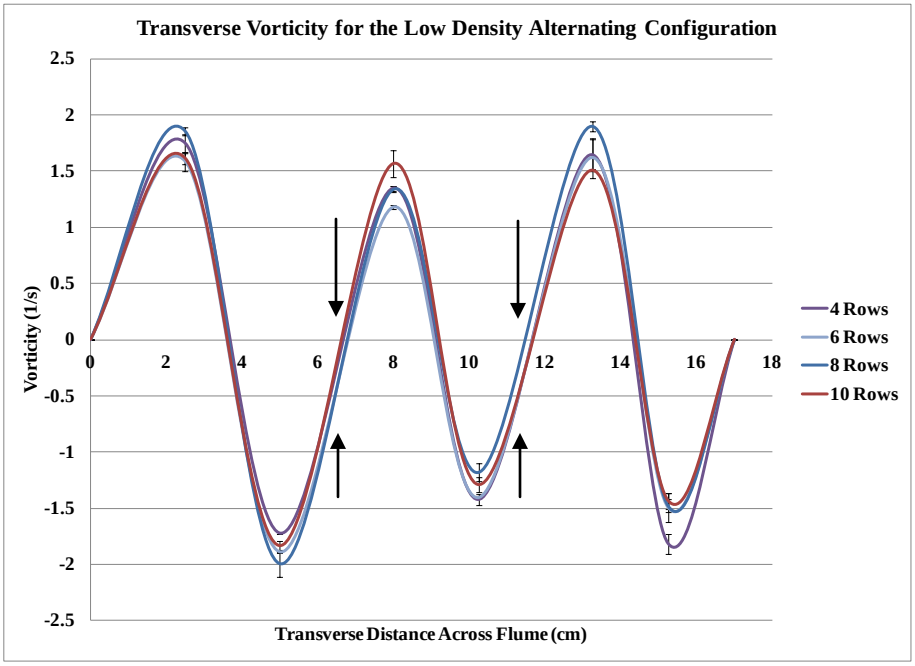

Figure 5.15: Vorticity measured across the flume in the transverse direction 16 diameters downstream from the low-density marsh configuration. The arrows identify the regions of zero vorticity.

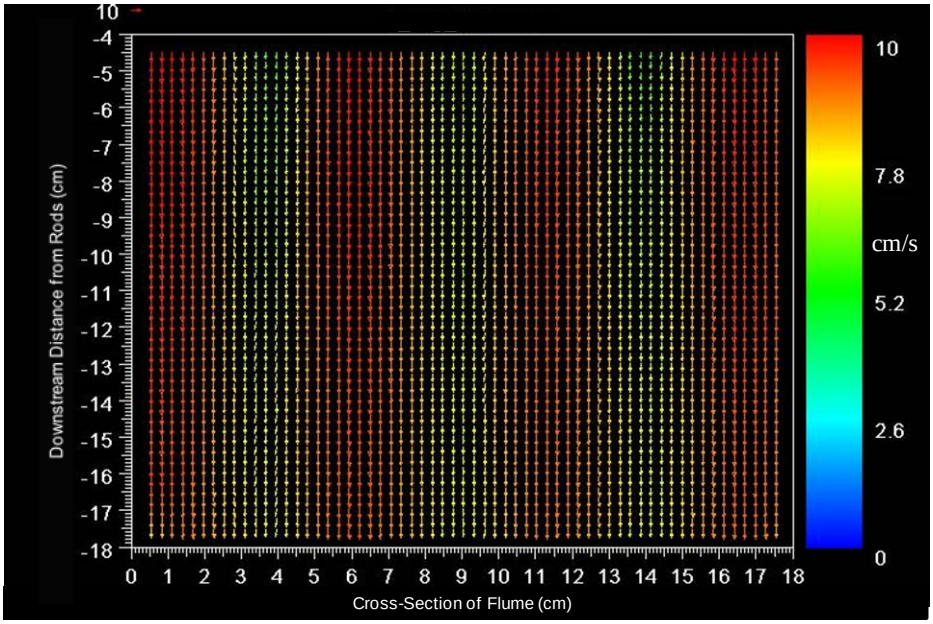

Figure 5.16: Velocity vector map for the velocity in the x-direction in cm/s for the low-density marsh configuration.

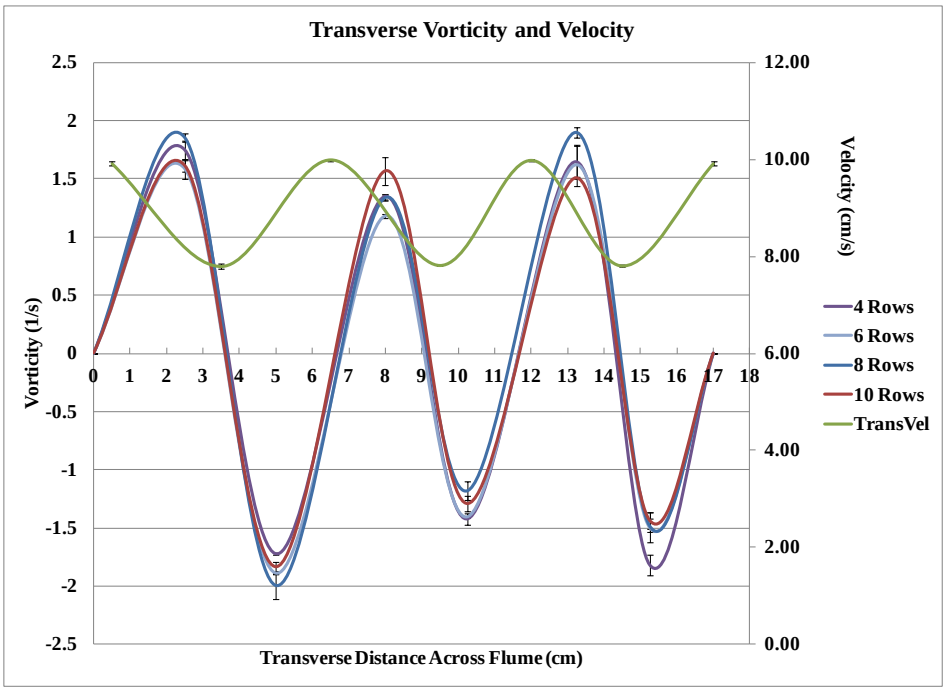

Figure 5.17: Transverse velocity profile in cm/s combined with the transverse velocity plot for the low-density marsh configuration at 16 diameters downstream from the rods.

5.3 Flow Structure Results for High-Density Marsh Configuration

The experiments described in Section 5.1 were repeated for a higher density configuration of 400 rods/m^2. Following the methods described earlier, time-averaged measurements of vorticity were used to calculate eddy size in the wake downstream from the rods for three downstream locations: 16d, 20d and 25d, and two Re numbers (Figure 5.18, Re = 700 and Figure 5.19, Re = 1,100). Again these three downstream distances are based on rod diameters and were the same locations analyzed for the low-density configuration. These observations showed a 30% decrease in eddy diameter between one row and two rows in the high-density marsh setup, with an error of 10%. Since there was a large number of rods in the flume, once two rows were achieved, the wake was significantly diminished in its width. Conditions became relatively constant at two rows for most (88%) of the observations, compared to four rows for the low-density configuration. In contrast to the low-density setup, where the eddy size did not change much as the distance downstream from the rods increased, the size of the eddies for the high-density configuration increased by 25% as a function of downstream distance. Also, the increase in Reynolds number had almost no effect on the eddy diameter in the high-density results. The transition from one row to two rows greatly affected the eddy size, increasing the number of rods in the flume reduced the size of the eddies significantly.

In the high-density case, the spacing between rods is halved compared to the low-density case, resulting in a spacing ratio of 4. As described in Chapter 2, such a high spacing ratio will determine eddy size. Initially, for the one row configuration the wake is defined by the spacing between the rods, which is 5cm; however, once the second row is in place, the spacing between the rods is cut in half (2.54 cm), creating a wake that is

producing eddies 1.27 cm in diameter, corresponding to approximately ½ the wake width. The eddy size grows as the wake progresses downstream, where the eddy diameter measurements are made. Within the 10% errors in measurements, adding more rows beyond two rows does not significantly change the eddy size.

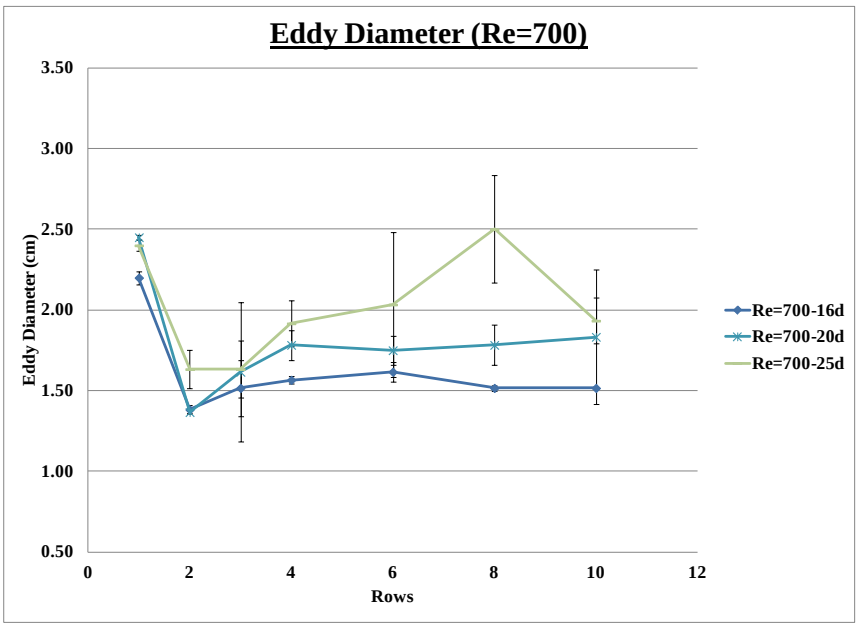

Figure 5.18: Eddy diameter for high-density configuration and Re = 700. (Error bars are based on one standard deviation from the data point, and based on repeated experiments.)

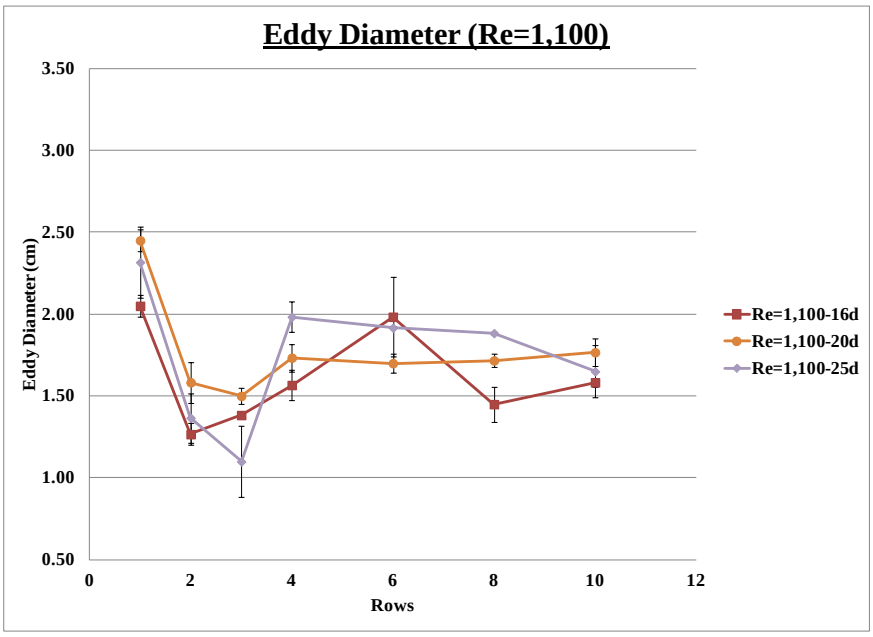

Figure 5.19: Eddy diameter for high-density configuration and Re = 1,100.

Figures 5.20 and 5.21 outline the observations of the vorticity results for this setup. Eddy vorticity was measured at three locations in the downstream wake of the rods. Similar to the low-density configuration, a 60% decrease in vorticity was seen as the downstream distance from the rods increased. This decrease in vorticity was due to the dissipation of energy downstream from the rods. Higher Re numbers generally result in higher vorticity; here, an average increase of 50% in vorticity was seen at a Reynolds number of 1,100 and at downstream locations of 16d and 20d, compared to the results at a Reynolds number of 700. At 25d, there was almost no change in vorticity between the two Reynolds numbers. For a given Reynolds number, vorticity increases when the number of rows is increased. At the downstream position of 16d, there is a 40% increase from one row to ten rows for Re of 1,100. Overall, in the case of the high-density

configuration, the low vorticity was due to the lack of room for the wakes to combine and grow from the high density of rods.

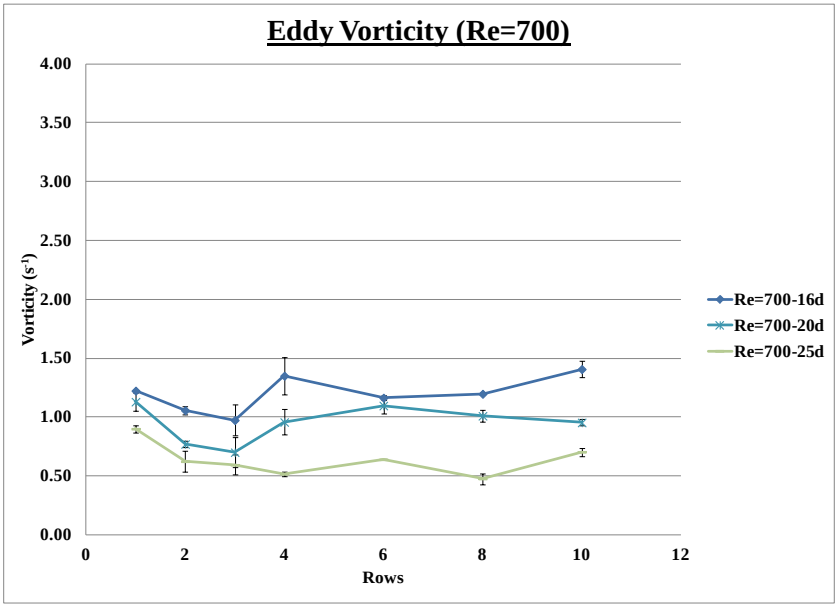

Figure 5.20: Eddy vorticity for high-density configuration and Re = 700.

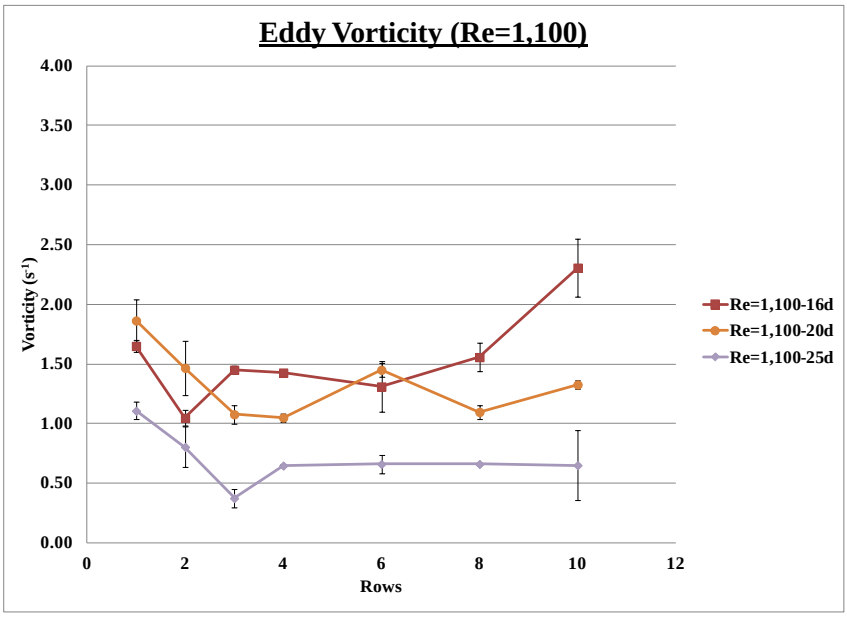

Figure 5.21: Eddy vorticity for high-density configuration and Re = 1,100.

The calculated eddy circulation combined the results of the eddy vorticity and eddy diameter. Figures 5.22 and 5.23 reveal a sharp 70% decrease in eddy circulation when two rows are added. Once two rows were added, constant circulation was obtained. This constant circulation was observed at a Reynolds number of 700, while the circulation at the Reynolds number of 1,100 was not observed to be as constant. At a Reynolds number of 1,100, for downstream distance of 20d and 25d, an average decrease in circulation of 50% was observed at three rows, showing a similar trend to the 700 Re number case; however, more fluctuations were observed in this case. An average increase in circulation of 50% was observed with an increase in the Reynolds number from 700 to 1,100 for 16d and 20d, while at the downstream location of 25d the circulation was constant. For both Reynolds numbers, a 20% decrease in eddy circulation was seen from 16d to 25d due to the dissipation of energy as the distance downstream was increased.

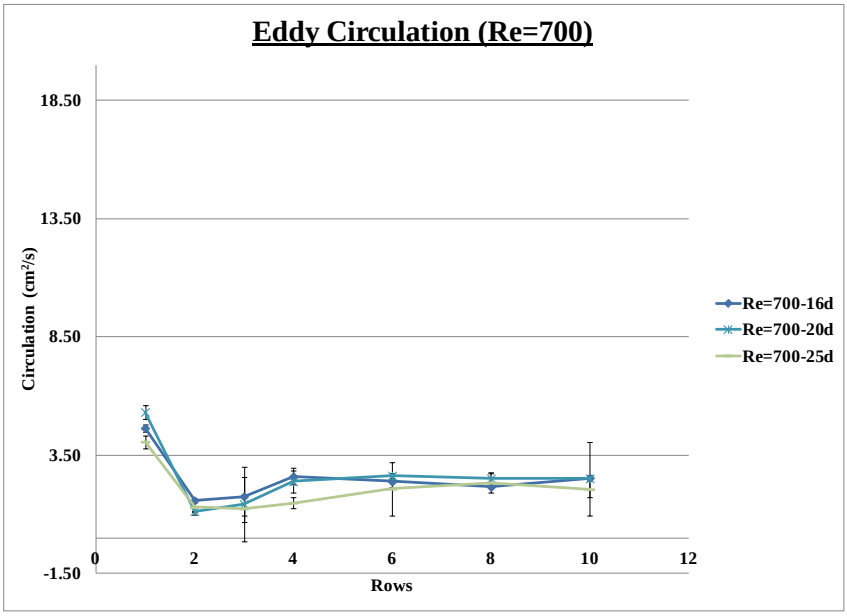

Figure 5.22: Eddy circulation for high-density configuration and Re = 700.

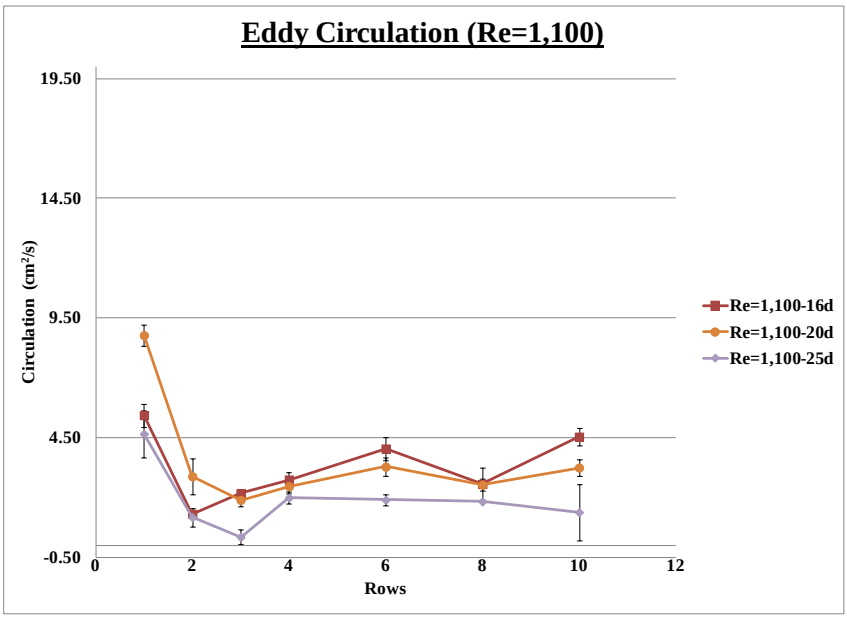

Figure 5.23: Eddy circulation for high-density configuration and Re = 1,100.

In summary, the results in the high-density configuration yielded a one and a half times lower vorticity at a Reynolds number of 700, and a three times smaller vorticity at a Reynolds number of 1,100, than the low-density results. In addition to the differences in vorticity for the two configurations, at high-density the eddy size is in general one and a half times smaller than the eddy size that was observed for the time averaged low-density configuration. The average high-density eddy circulation was then four times smaller than the average eddy circulation of the low-density marsh setup. These trends result from the large number of rods in the flume, spaced evenly in the alternating configuration, forming an obstruction to the flow. The water flow is so constricted through the high-density of rods and the alternating pattern of the rods, that little eddy development occurs, leading to smaller eddies with less vorticity.

The spacing ratio for the high-density alternating results was 4, which allowed for discrete vortex shedding downstream from the upstream rods. Therefore, the wakes were restricted by the gaps between rods after two rows are added. These gaps were equal to 2.54 cm, with the average eddy size equaling half of the wake diameter, or 1.27 cm. Once one row was added to the high-density marsh configuration, three strong wakes developed downstream from the rods. Figure 5.24(a) reveals the formation of the three wakes after the first row of rods is placed in this marsh setup. Figure 5.24(b) then reveals additional wakes being created due to the addition of a row of rods in the alternating high-density pattern, resulting in a total of 2 rows. Finally, Figure 5.24(c) shows the wake structure for 10 total rows, revealing how the downstream flow structure was again dominated by the formation of three distinct wakes downstream from the rods, with low vorticity (Figure 5.24(c)) and high velocity (Figure 5.26) in between the wakes.

The major difference in the flow structure in the high-density alternating configuration, when compared to the low-density alternating configuration, is the eddy size and strength. In the high-density alternating rod pattern, each eddy is smaller with less vorticity, than the low-density case. Also, once the second row is added then the formation of distinct wakes of equal size is created by the pattern of the alternating rod configuration. This pattern is strengthened with the addition of each of the rows, after two rows, reinforcing the size and strength of the vortices in the downstream flow structure. For the high-density alternating configuration, two rows set this pattern, while it took four rows for the low-density case. In the low-density alternating configuration, there is room for the wakes to combine and grow to fill the gaps between rods as four rows are added. In the high-density pattern, even though more rows were added, there

was no room for the wakes to combine and grow as they are placed in tandem positions. Therefore, the transition in eddy size and vorticity seen after four rows, in the low-density configuration, cannot be seen for the high-density case.

Another interesting observation of the high-density marsh configuration is the region of zero vorticity (identified by the arrows in Figure 5.25) found in between the wakes. The transition between these zero vorticity regions and the wake occurs through regions of shear reflected by a sharp change in velocity as the velocity is measured transversely across the flume, downstream from the Plexiglas rods. The areas of shear are also outlined in the velocity vector map (Figure 5.26) where the faster flow past the rods is shown with red arrows, while the slower flow behind the rods is shown with yellow arrows. Figure 5.27 shows measurements of velocity transversely across the flume, through the wakes formed downstream from the rods, and again this shear region can be observed with the areas of zero vorticity lining up with the regions of maximum velocity. The velocity gradient (du/dy, or the change in the longitudinal velocity in the transverse direction) along the edges of the regions of zero vorticity is measured to be 0.8/s for each of these four individual regions. These regions are much larger in size than the points of zero vorticity in the low-density configuration, and are characterized by a higher velocity gradient. The regions of zero vorticity, in the high-density case, could be due to smaller eddies with less vorticity that are produced by rows of rods further upstream. These eddies dissipate faster as they move downstream compared to eddies shed from consecutive rows. In this configuration, there is less of an ability to form larger, stronger eddies, similar to those seen in the low-density case. The constriction of spacing between the rods in the high-density setup controls not only the size and strength

of the eddies downstream, but also creates the patterns within the downstream flow structure made evident in the transverse vorticity and transverse velocity plots.

5.24(a)

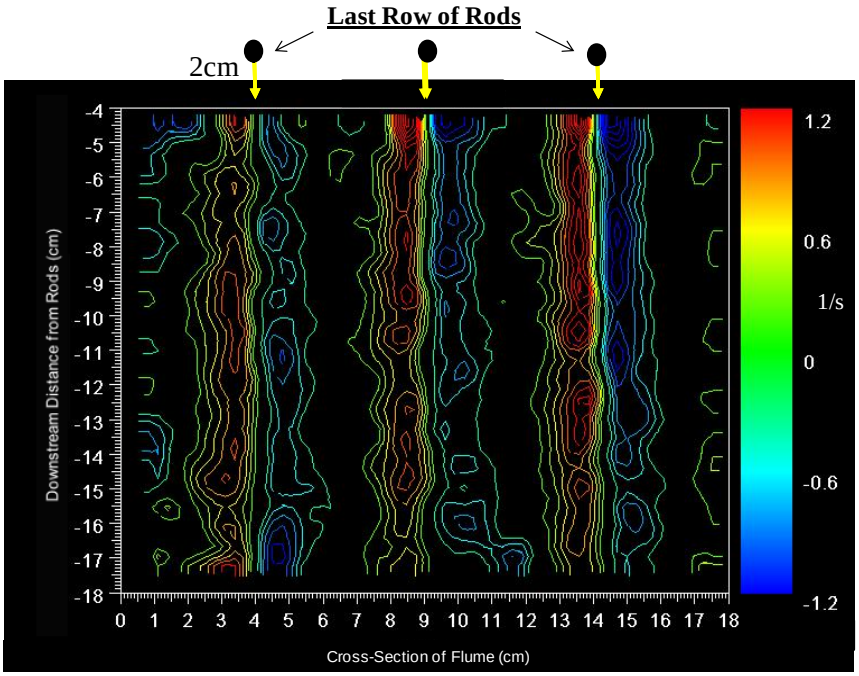

5.24(b)

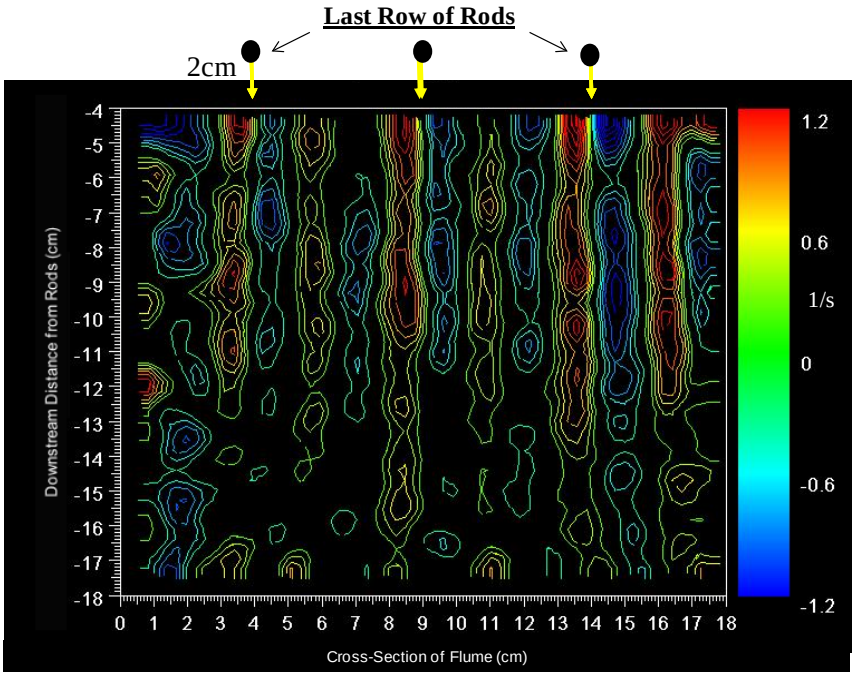

5.24(c)

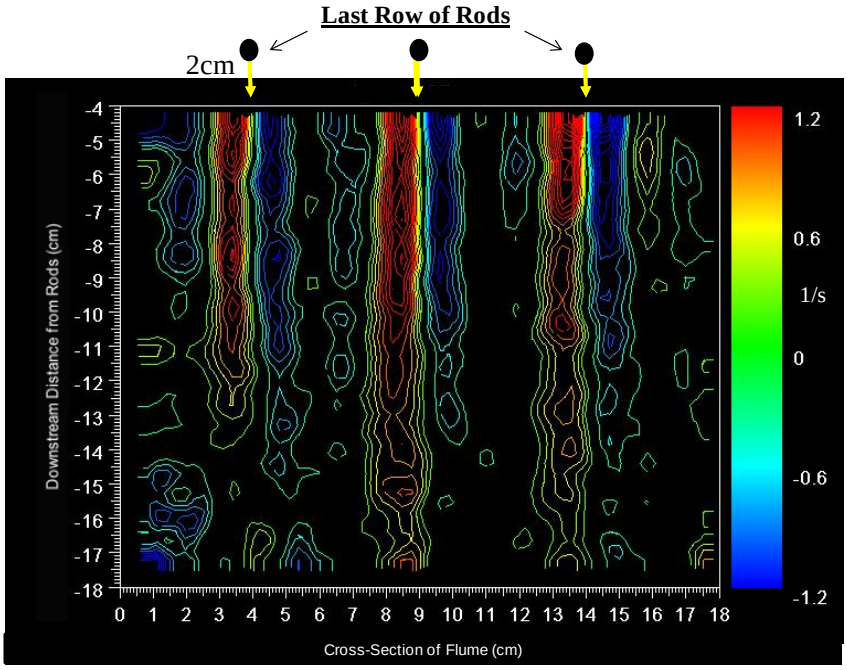

Figure 5.24: Vorticity maps for one row (a), two rows (b), and ten rows (c) of rods added to the high-density marsh configuration (Figure 5.2(b)).

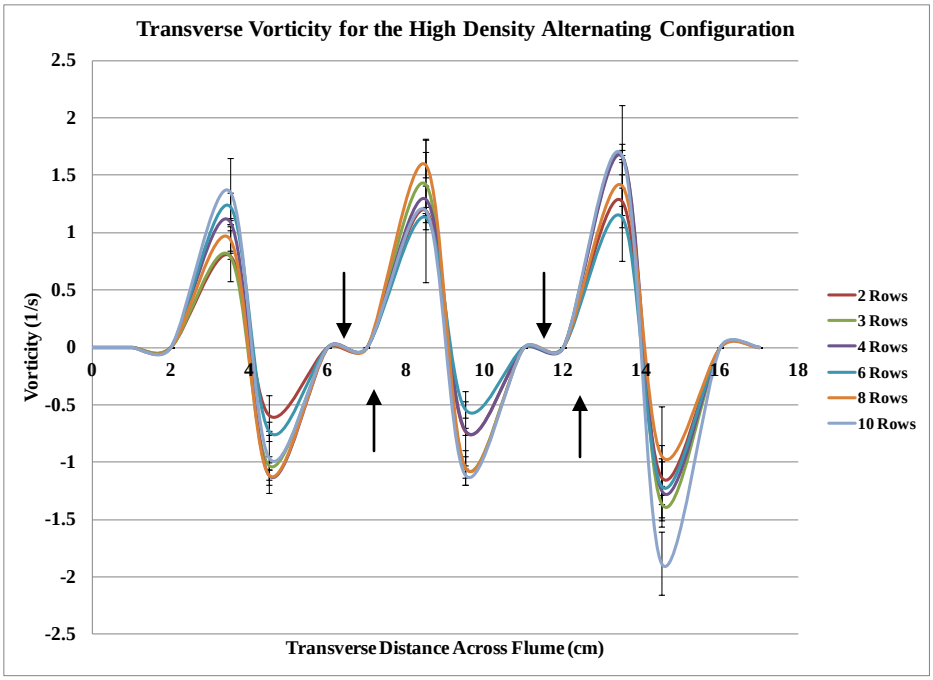

Figure 5.25: Vorticity measured across the flume in the transverse direction 16 diameters downstream from the high-density alternating marsh configuration. The arrows represent the regions of zero vorticity.

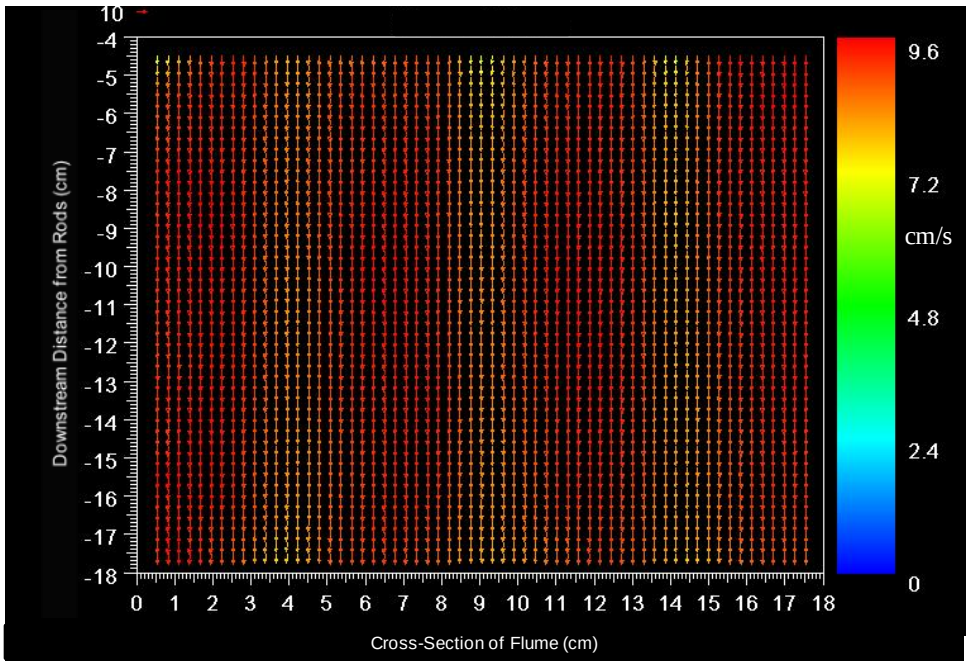

Figure 5.26: Velocity vector map for the velocity in the x-direction in cm/s for the high-density marsh configuration.

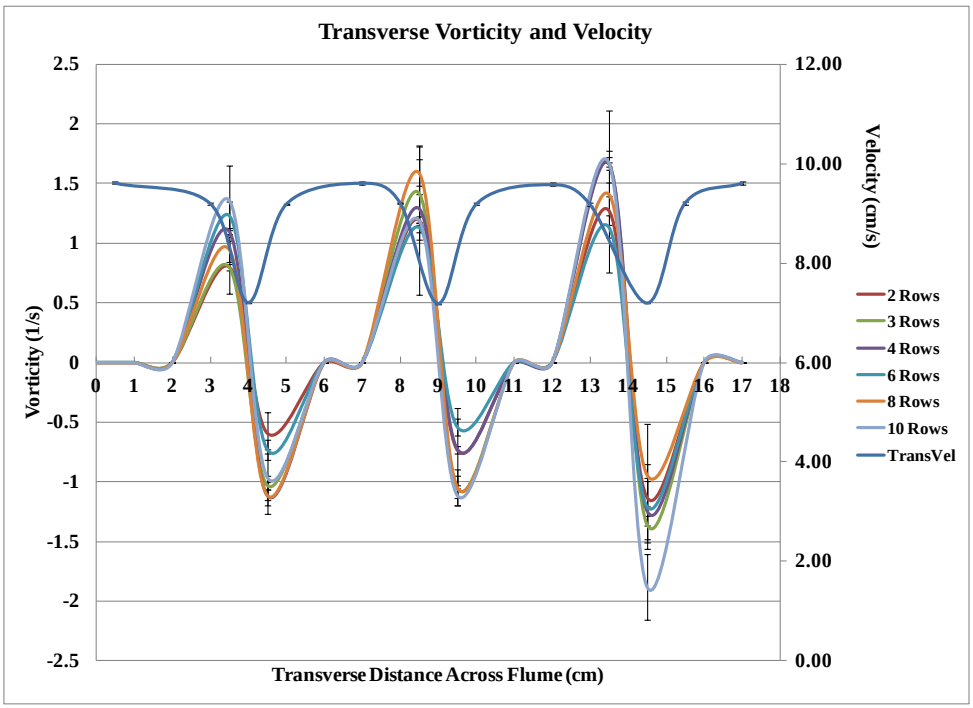

Figure 5.27: Transverse velocity profile in cm/s combined with the transverse velocity plot for the low-density marsh configuration at 16 diameters downstream from the rods.

5.4 Rod Spacing Results for the Random Configuration Experiments

As the results from the previous experiments discussed earlier show, the spacing of the rods in a laboratory marsh configuration is significant when determining the wake formation downstream (Spivack, 1946; Bearman and Wadcock, 1973; Zradavkovich and Pridden, 1977; Kiya et al., 1980; Williamson, 1985; Lam and Cheung, 1988; Le Gal et al., 1990; Sumner et al., 1999). The reed spacing not only influences the vortex formation, but also the merging of wakes as the fluid passes through the reeds (Kiya et al., 1980; Zradavkovich and Pridden, 1977). To examine in further detail the effect of the random reed placement in aquatic vegetation and how the growth pattern influences flow structure, an analysis of the rod spacing in a random marsh configuration was conducted.

Figure 6.8 shows the spacing ratio of the rods in the random setup as placed by MATLAB's (The Math Works, Inc.) random number generator, at densities of 50, 150, 250 and 400 rods/m^2. Logically, the spacing ratio decreases as the density increases and can be represented using an exponential curve fit equation, where SR is the spacing ratio and RD is the rod/reed density (Figure 5.28):

$$SR = 6.8161e^{-0.001RD} \qquad (5.2)$$

Based on this equation, for the random configuration, there is a 20% decrease in rod spacing from 50 rods/m^2 to 150 rods/m^2, and another 20% decrease from 150 rods/m^2 to 250 rods/m^2. At the same time, the increase in density from 250 rods/m^2 to 400 rods/m^2 produces only a 10% decrease in the spacing ratio. Therefore, the greater the density in the random rod configuration, the lesser the effect on rod spacing after a rod density of 250 rods/m^2 is reached.

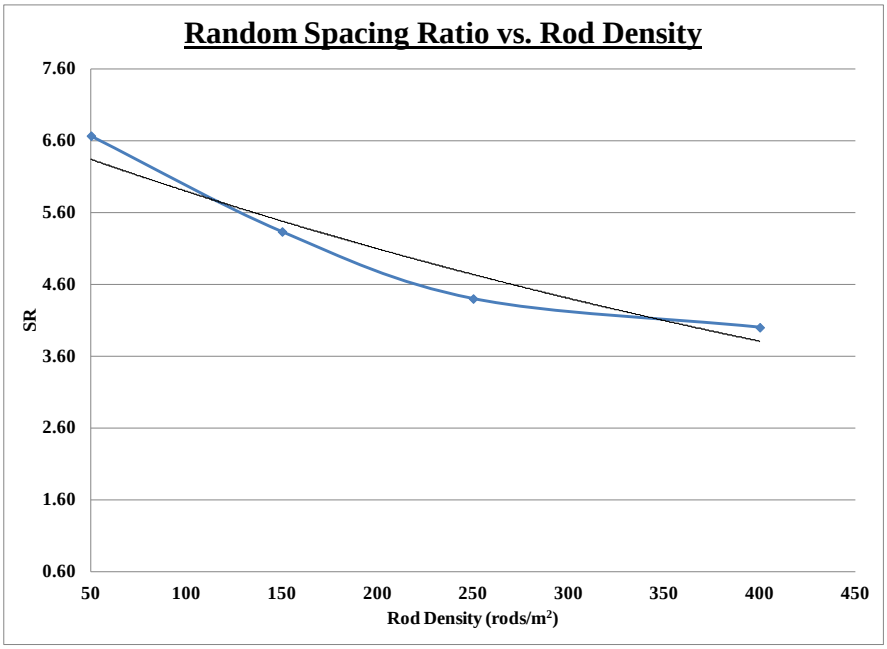

Figure 5.28: Spacing ratio for the random configuration, for the four different densities in the water tunnel experiments.

5.5 Random Configuration Experimental Results

Building on the growth pattern and spacing analysis of the random marsh configuration, vorticity maps and transverse vorticity were examined as the rod density and placement changed in the random rod experiments performed in the water tunnel. The spacing ratios for this random configuration were 4 to 6.7, which again allows for discrete vortex shedding downstream from the upstream rods. Therefore, the size of the wake, and subsequent vortices, was determined by the rod spacing and pattern. This influence of the rod spacing on the size of the wake was similar to the results of the alternating and field experiments. Further evidence of the influence of rod pattern on downstream flow characteristics can be found in comparing the vorticity maps of Figures 5.29 and 5.30, and the transverse vorticity plot in Figure 5.31. In Figure 5.30, a cluster of rods is found on the left and right sides of the downstream random rod configuration preceding the area where flow characteristics are measured. Eddy size and strength increase dramatically in both Figures 5.29 and 5.30, as well as in Figure 5.31, downstream from where these specific rod patches were placed in the water tunnel.

For the random configuration there is a lack of any pattern in eddy formation, with two wakes of larger eddy size and increased vorticity being formed on either side of the examined downstream region due to this combining of eddies downstream from the rod clusters. This result is in contrast to the consistent eddy size and strength that was found in both the field results, as well as the alternating configuration laboratory results. Due to the difficulty in being able to capture the effect of randomly placed rods on the downstream flow structure, and how to quantify the influence of the randomness or non-linearity on creating regions of patchiness within the rod configuration, further study of

these characteristics of the marsh needs to be conducted. Still, the effect of the lack of pattern in the random rod setup results in more variability in the size and strength of the eddies in the downstream flow than what was found in previous laboratory and field experiments (Figures 5.29 and 5.30).

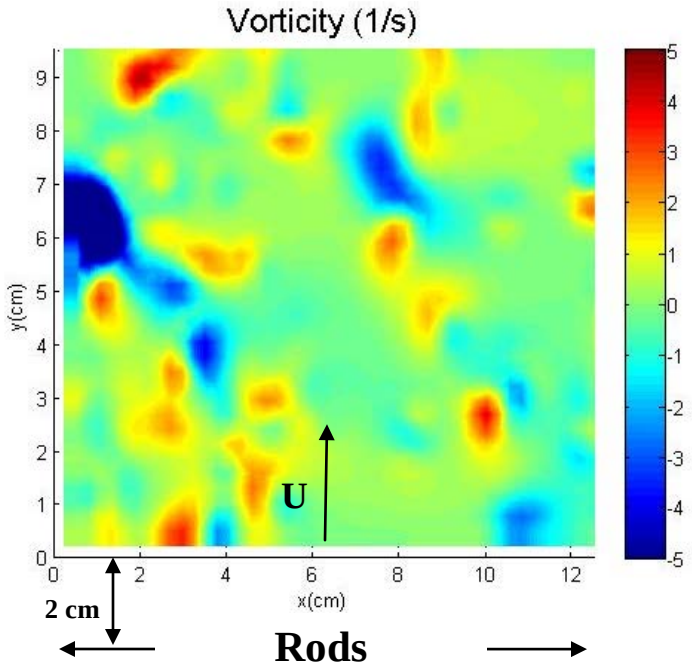

Figure 5.29: Vorticity maps of the random configuration for 50 rods/m^2. Red represents positive vorticity and blue represents negative vorticity. The arrows represent the last row of the random array.

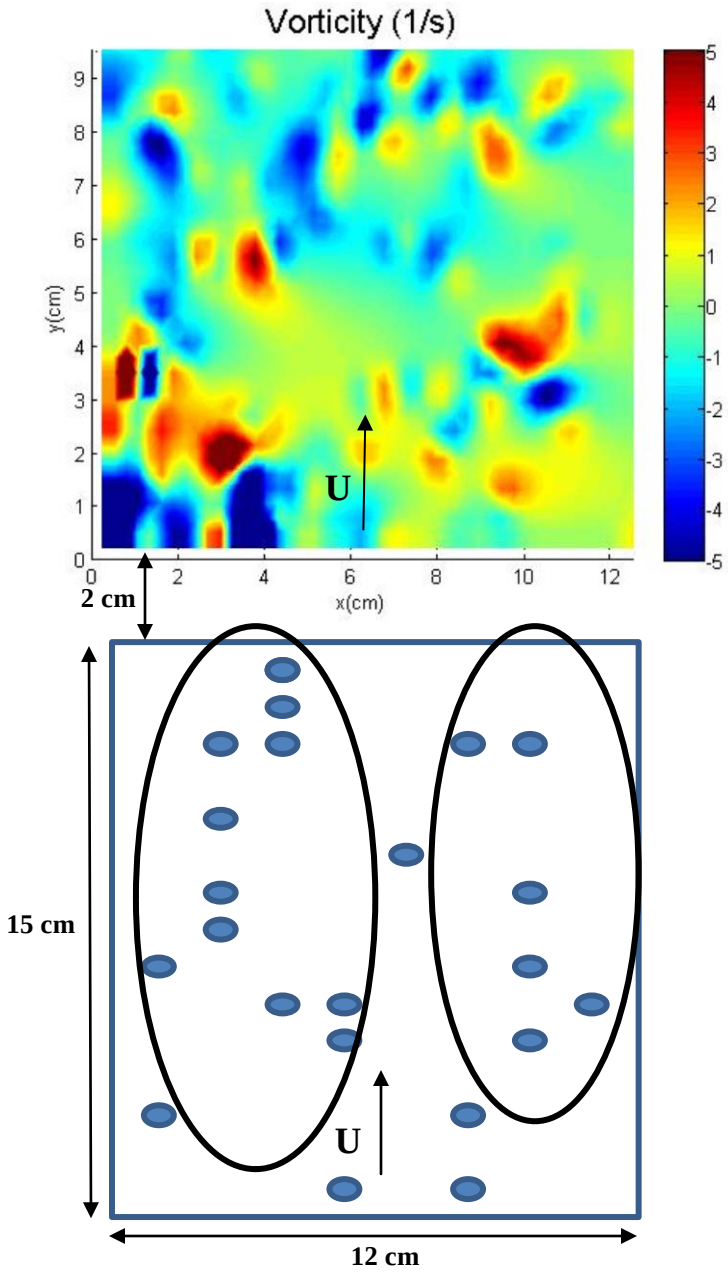

Figure 5.30: The pattern of rod placement for the random configuration of 400 rods/m^2 is represented in the bottom image. This image highlights the patches of rods placed upstream from the vorticity map above. These rods were placed in the more center region of the rod configuration, where the PIV data were taken and the transverse vorticity was examined. The top image is the resulting vorticity map based on the bottom rod placement at a rod density of 400 rods/m^2.

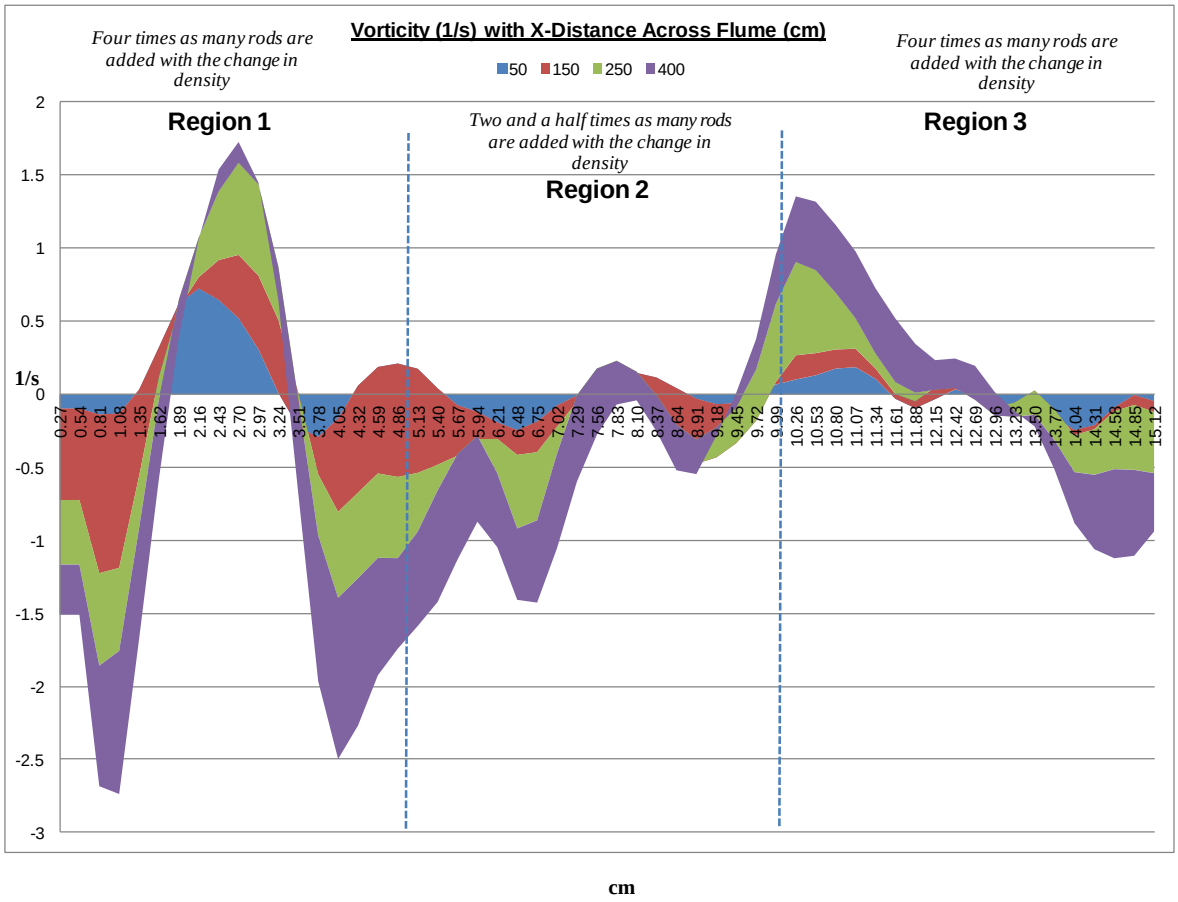

Figure 5.31: Horizontal change in vorticity, or transverse vorticity, across the flume as the rod density is changed in the random experimental rod setup.

Figure 5.31 shows vorticity in different regions across the flume, downstream of the rods, based on the change in rod density. The vorticity map downstream was divided into three equidistant sections, and each section has been explored to discover how different rod densities influence the change in downstream transverse vorticity. The two regions that had four times as many rods added as the density increased from 50 rods/m^2 to 400 rods/m^2, revealed a seven to eight times higher positive vorticity than the middle region. The middle region only had 2.5 times as many rods added to the random marsh setup as the density increased. In this region there was a larger negative vorticity than the

third area on its right. Still, this larger negative vorticity was due to the large wake forming in region one (Figure 5.31) that spread into this middle region. The actual full wake in the middle region had a negative vorticity that was only 40% of the negative vorticity in the third area, or 20% of the negative vorticity in the first region. Again, this variability in the transverse vorticity of the random configuration was unlike what was found in previous experiments.

In addition to looking at the rod spacing and transverse vorticity, average vorticity, eddy diameter and circulation were examined to understand the influence the random pattern of reed/rod placement on the downstream flow structure. The laboratory observations for the random configuration involved taking a sample of ten pairs of PIV images in the downstream wakes from the rods. Since there was no pattern to the placement of the rods, as they were randomly placed using the MATLAB code described earlier, looking at smaller samples of pairs of images, and the vorticity maps they produced, yielded more information than observing the time averaged results of all 140 pairs of images. The random configuration of rods in the water tunnel creates patchiness in the pattern with areas of high-density mixed with low-density regions. If the results were averaged over a large number of pairs of images, too much information would be lost in the processing. These results are an initial look at the effect of a random marsh configuration on the downstream turbulence.

Figures 5.32, 5.33 and 5.34 show the changes in average eddy vorticity, eddy diameter and eddy circulation as rod density is increased from 50 rods/m^2 to 400 rods/m^2, for a location of 16 diameters downstream from the rods and a Reynolds number range of 200 to 1,100. Outlined in Figure 5.32 is the change in eddy size, as a function of Re and

rod densities. For all Reynolds numbers: 200, 400, 700 and 1,100, a decrease in eddy diameter, within the measurements of error of 20%, occurs with an increase in density, reflecting the change in spacing over this rod density range. Overall, the eddy size is determined by the rod spacing in the random configuration, resulting in a change in eddy size that reflects the change in spacing that occurs when the rod density increases. This change in rod spacing is at most 30%, from the lowest rod density to the highest rod density, and is shown in Figure 5.28.

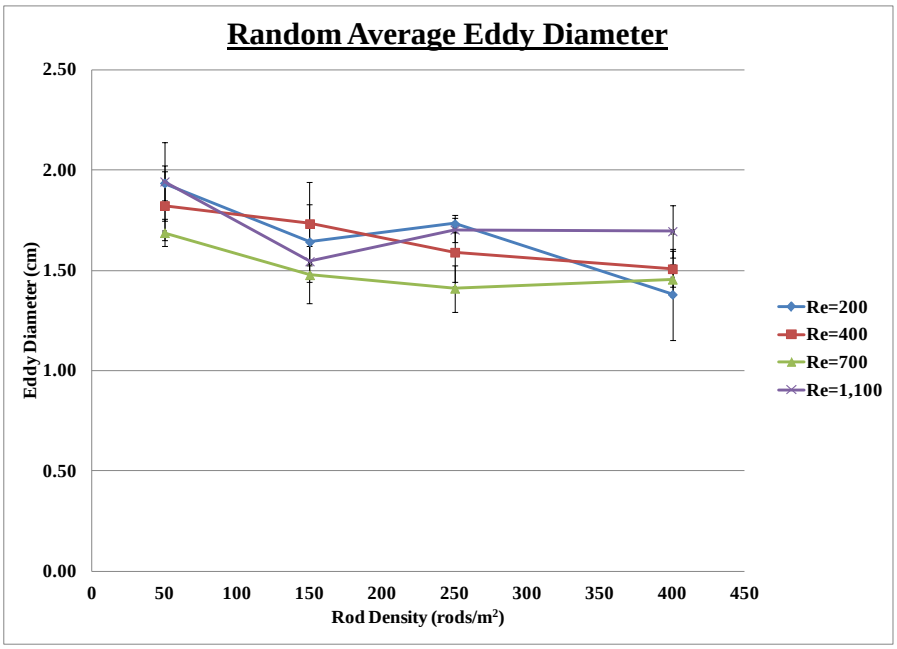

Figure 5.32: Average eddy diameter for the random configuration of Plexiglas rods, for Reynolds numbers from 200 to 1,100 and as rod density is increased.

Observations of vorticity produced by the random configuration can be found in Figure 5.33. A higher vorticity is reached at a higher Reynolds number for all rod densities. At low Reynolds numbers, i.e. 200 and 400, there is no significant change in eddy vorticity as the density of the random configuration increases. There is also no

significant change in eddy vorticity at higher Reynolds number, i.e. 700 and 1,100, when the density is increased from 50 rods/m^2 to 250 rods/m^2. The eddy vorticity was found to increase by 40% for Reynolds numbers of 700 and 1,100, when the density increased from 250 rods/m^2 to 400 rods/m^2.

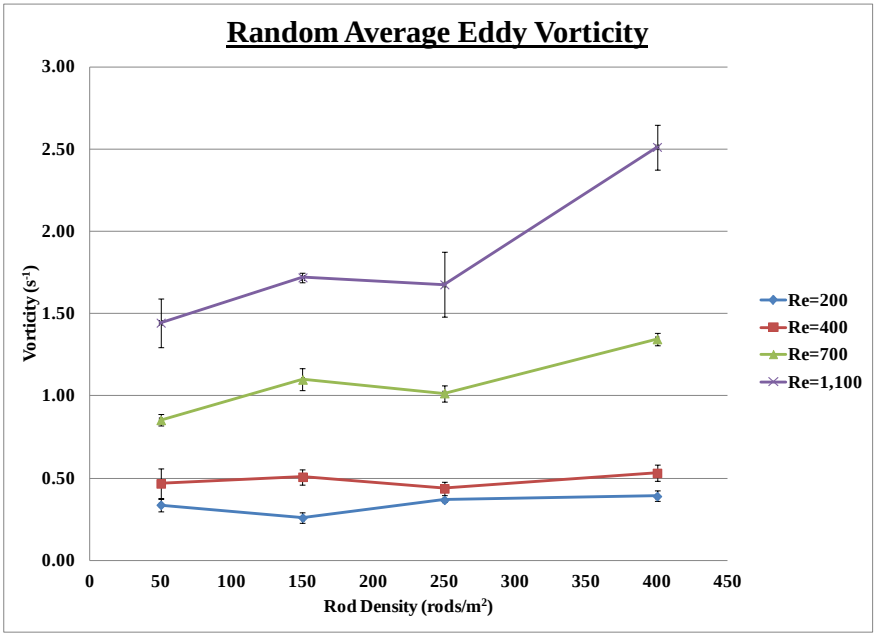

Figure 5.33: Average eddy vorticity for the random configuration with an increase in Reynolds number and as rod density is increased from 50 rods/m^2 to 400 rods/m^2. (Error bars are based on one standard deviation from the data point, and based on repeated experiments.)

Over the varying rod densities, the eddy vorticity at a Reynolds number of 400 is 67% more than the vorticity at a Reynolds number of 200 and doubles when the Re is increased 400 to 700. Finally, as the Reynolds number changes from 700 to 1,100, there is a 50% increase in the vorticity from 50 rods/m^2 to 250 rods/m^2, but a 92% increase at 400 rods/m^2. The vorticity increases in proportion to the increase in the velocity or Reynolds number, for all rod densities.

The results for eddy diameter and eddy vorticity are combined in the calculation of eddy circulation. Figure 5.34 reveals the change in eddy circulation, for the random rod setup, as a function of both density and Reynolds number. There is no significant change in eddy circulation as the density is increased from 50 rods/m^2 to 250 rods/m^2 and the Reynolds numbers increased from 200 to 1,100. Both of the higher Reynolds numbers of 700 and 1,100 produce a 50% increase in eddy circulation, as the density is increased from 250 rods/m^2 to 400 rods/m^2. Again, with only a 50% increase in the velocity from a Reynolds number of 700 to 1,100, the circulation increases by a factor of two for the larger Reynolds number of 1,100 over the entire range of varying rod densities.

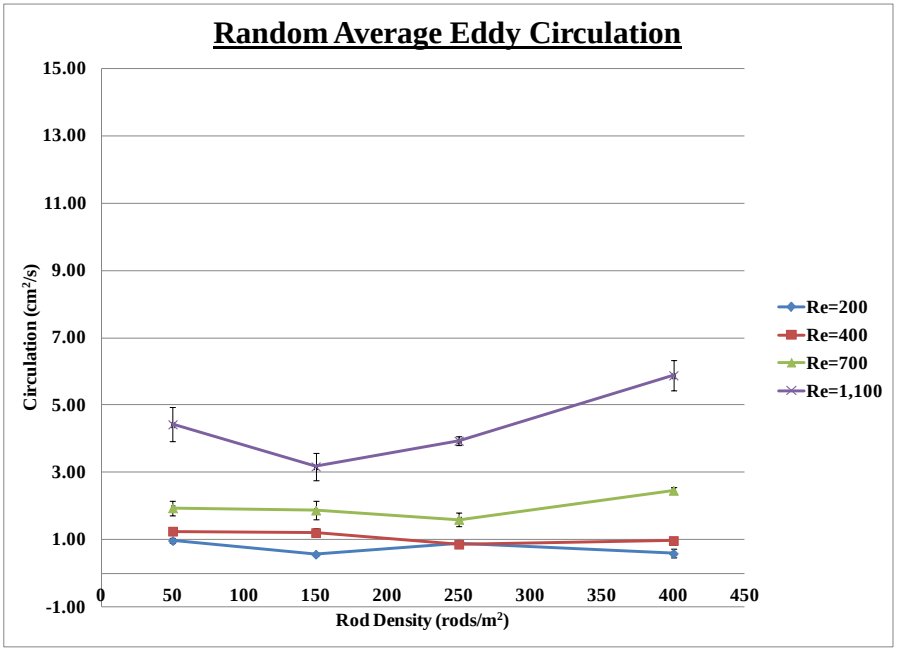

Figure 5.34: Average eddy circulation for the random setup, over the range of four Reynolds numbers and as rod density is increased.

In Chapter 4, field experiments looking at flow structure downstream from a natural marsh environment with a reed density of 140 reeds/m^2 resulted in twice as much average vorticity as the random configuration, at the same density and downstream distance. This difference in vorticity is mostly likely due to the difference in pattern, from the natural bulrush growth pattern, to the entirely random generated pattern which resulted in a significant amount of patchiness. For a reed density of 264 reeds/m^2 in the field experiments, when compared to the random experiments of a similar density, three times as much average vorticity was found in the eddies downstream from the natural marsh environment, and for a reed density of 388 reeds/m^2, ten times as much average vorticity was found in the field results when compared to those from the random laboratory experiments. Also, for all of the reed densities examined in the field experiments, the eddy size was smaller, around 0.6 cm or less than half of the random results, due to the decrease in spacing between the reeds in the softstem bulrush patches.

Unlike the cases of low and high-density alternating configurations, where the patterns are even and predictable, the random configuration creates patchiness in the pattern with areas of a high-density of rods mixed with regions containing a low-density of rods. The lower vorticity results in the random case are most probably an artifact of the method used to obtain average vorticity. Vorticity values are averaged over the area covered by the laser sheet which contains areas of high and low vorticity. This current method of measuring average eddy characteristics is not optimal to fully resolve the smaller scale impact of patchiness on vorticity dynamics. More statistical analysis of the size and strength of the eddies being produced, their frequency and location, would allow the subtle changes in rod pattern to be captured in the downstream flow characteristics.

5.6 Alternating and Random Configuration Comparison

A comparison of average eddy diameter, vorticity, and circulation was made between the random, low-density and high-density alternating marsh configuration results from the previously discussed experiments (Figure 5.2). The comparison of the random and alternating marsh configurations is based on a sample of ten pairs of PIV images, similar to the base analysis of the random rod setup. The results in Figure 5.35 reveal that there is only a slight decrease in the eddy diameter with the increase in rod density from 250 rods/m^2 to 400 rods/m^2 for the random configuration. This similarity in eddy size is due to the comparable rod spacing for these two rod densities. For the alternating configuration, the eddy diameter is halved, due to the decrease in rod spacing by 50%. Since the rod spacing is similar for the high-density random and alternating configurations, there is not much of a difference in the average eddy size. There is also no distinct pattern in the change in eddy diameter as the Reynolds number is changed. This lack of pattern, over the range of Reynolds numbers, is due to the size of the eddies being determined by the spacing ratio, or distance between the rods in each of the specified configurations. Overall, the pattern of the arrangement of the rods did not influence the average eddy size as much as the average spacing between the rods. Therefore, the influence of pattern was negligible compared to the influence of the rod spacing in determining eddy diameter.

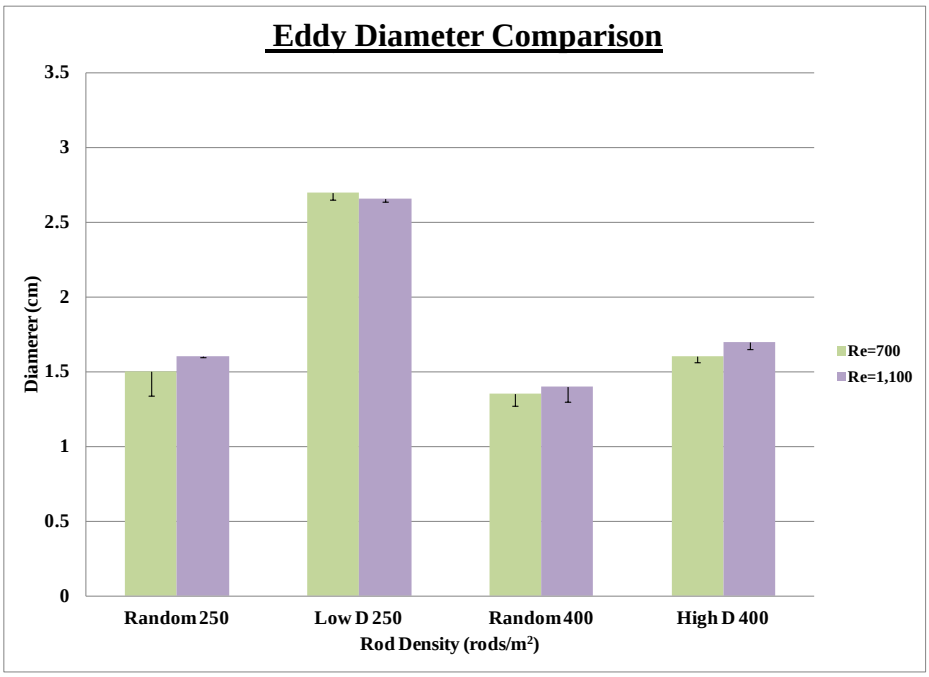

Figure 5.35: Eddy diameter comparison between the random, low-density and high-density rod configurations.

The same comparison was conducted for average eddy vorticity for each of these rod configurations. Figure 5.36 reveals that an average 13% increase in vorticity is observed at higher densities, for the random configurations, at both Reynolds numbers. This small increase in vorticity is due to the higher level of patchiness in the higher density pattern, where eddies are merging. This is similar to the increase in vorticity with reed density that was found in the field results, even though the field results saw a much larger increase. In contrast to this, there is a 15% decrease in vorticity for the alternating configuration as the rod density is increased. Again, this small decrease in eddy vorticity for the alternating configuration is due to the large number of rods in the flume, spaced evenly in this rod setup, forming an obstruction to the flow. The water flow is restrained due to the high-density of rods, and the alternating pattern of the rods creates smaller

eddies with less vorticity. Here, the pattern of the placement of the rods has a strong influence on the vorticity. The strictly alternating pattern limits the growth of the eddies for the high-density configuration, therefore, the vorticity is reduced with the addition of more rods in the flume. Finally, the values of average vorticity for the random setup are consistently lower than the values of the alternating setup, even though they increase with rod density. This is due to the averaging of the random results losing the larger wakes that can be formed by the patchiness in the rods, which create larger eddies with higher vorticity.

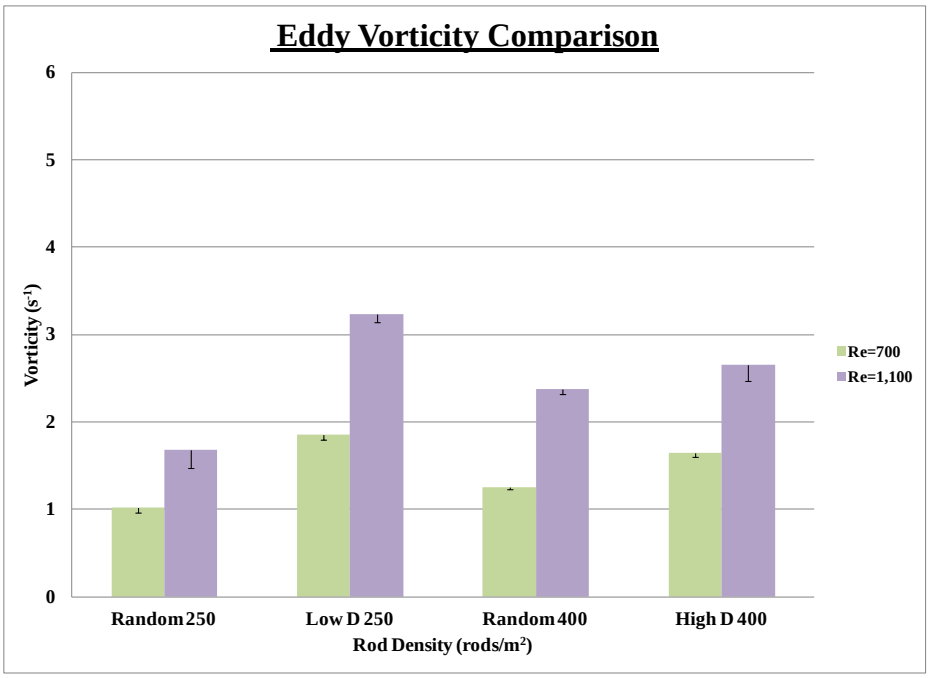

Figure 5.36: Eddy vorticity comparison between the random, low-density and high-density configurations.

Figure 5.37, compares the results of the eddy circulation for each rod setup. Similar to the results for eddy vorticity, a lower eddy circulation is seen in the random configurations, as opposed to the alternating configurations. This difference is dramatic for the lower density results. The eddy circulation for the low-density alternating configuration is six times that for the lower density random configuration. For the high-density, the alternating configuration is 1.5 times the value for the random configuration. Unlike in the low-density alternating configuration, where there is room for the wakes to combine and grow to fill the gaps, in the high-density and random configurations the average spacing is smaller, leading to a smaller, weaker eddy. This decrease in eddy size and strength, based on the type of configuration, is significant. Cotel et al. (2006) showed that fish tend to choose areas of lower turbulence for their habitats in trout streams. Therefore, the effect the configuration, whether random or alternating, has on altering the size and strength of the eddy that a fish in these environments would interact with is notable.

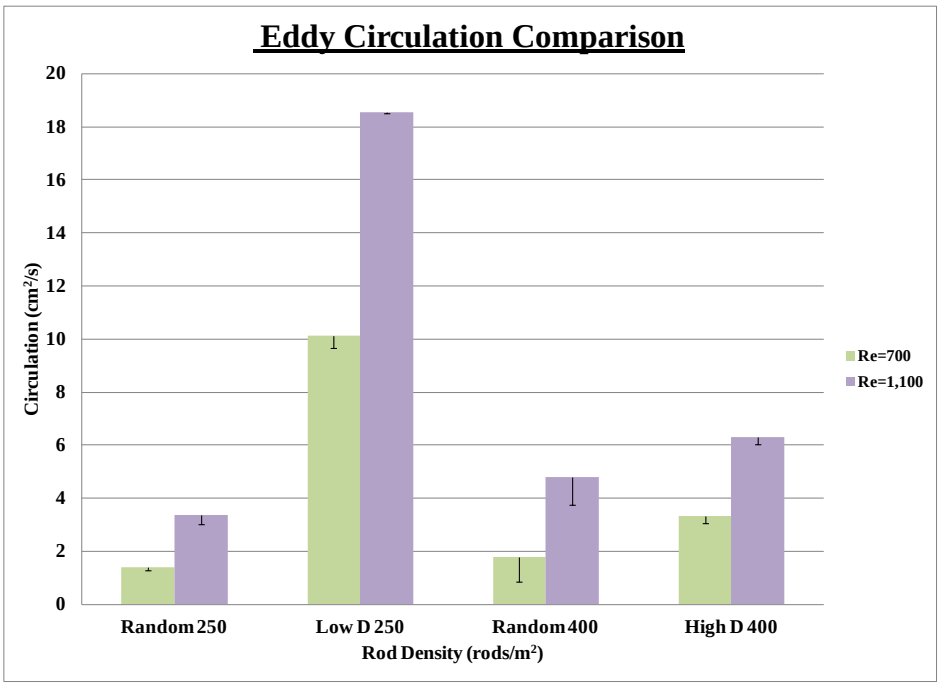

Figure 5.37: Eddy circulation comparison between the random, low-density and high-density configurations.

5.7 Flexibility Experiments

Structural complexity of vegetation growth pattern in aquatic environments has mostly been studied to reveal how stem density and pattern influences fish predators and their prey (Lewis and Helms, 1964; Laur and Ebeling, 1983; Savino and Stein, 1989), in the context of looking at the biological influences of growth characteristics. In contrast to this, Jarvela (2002) examined both the placement pattern and the flexibility of emergent plants, using grasses, sedges and willows in a water tunnel. This study was conducted in the context of frictional flow characteristics, as opposed to the biological influences of these parameters. Jarvela (2002) examined how these growth characteristics influence frictional losses and found that the pattern did not have as much

influence on frictional loss, as the flexibility of the vegetation. In this case, the flexibility created less frictional losses.

Nepf et al. (1997) observed that the wake size downstream from flexible stems can be altered by the motion the plant stems create due to their flexibility. In this study, turbulent diffusivity was examined with both rigid and flexible marsh grasses. Nepf et al. (1997) found that as the stem population increases the individual wakes, created downstream from each stem, begin to overlap. This trend was observed for stem densities from 200 to 2000 stems/m^2. The rigid vegetation model produced a stronger turbulent wake, than the flexible model, per stem. This study revealed that the flexible model had less turbulent diffusivity when both models were examined under comparable conditions. However, beyond looking at drag and frictional losses, very little work has been done to describe the flow structure and strength based on the biological influence of growth pattern and flexibility.

Now that growth pattern and spacing results have been examined for a random configuration of rods, an analysis of flexibility and its effect on the flow structure downstream is the next step in understanding the effect aquatic vegetation has on flow turbulence. The motivation for this study is to understand how flexibility of natural bulrush marshes impacts the flow field as well as eddy size and strength. The first experiments conducted in this area involve examining the stress and strain of softstem bulrush, in an effort to find materials that will simulate this flexibility in the laboratory environment.

Figure 5.38(a) and Figure 5.38(b) are photos of the deflection experiment involving a reed of natural softstem bulrush. These images show the reed before and after the application of the weight to the stem. The deflection of the reed occurs once the weight is added.

$$d_{reed} = \frac{WL^3}{E_{reed} \cdot I} \tag{5.3}$$

Where d_{reed} is the reed deflection, W the weight that is added to the end of the reed, E_{reed} the modulus of elasticity of the reed, L the reed length, and I the moment of inertia (Chu et al., 1993). Once deflection occur it is measured by a ruler and used to calculate the stress and strain values presented in Figure 5.39, using equations 5.3, 5.4, and 5.5. In solving for the stress (σ) and strain (ε) figures, equation 5.4 is used to find the modulus of elasticity of the reed (E_{reed}).

$$E_{reed} = \frac{\sigma}{\varepsilon} \tag{5.4}$$

$$\sigma = \frac{F}{A_{reed}} \tag{5.5}$$

The stress on the reed is found by taking the force of the weight at the end of the reed (F) and dividing it by the area of the reed (A_{reed}) (Equation 5.5). Finally, once the modulus of elasticity of the reed is calculated, the strain can be found using the previously calculated stress value. Outlined in Figure 5.39 are the values from the stress and strain calculations for the natural softstem bulrush. The Young's Modulus values obtained

from the deflection experiment are in MPa, similar to the Young's Modulus of stem material in plants (Gibson, 2012).

5.38(a)

5.38(b)

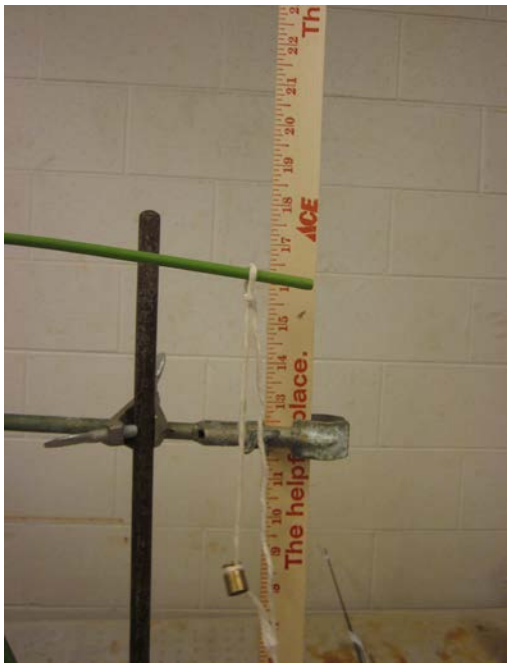

Figure 5.38: Images from the deflection measurements made of a reed of softstem bulrush. 5.38(a) before the weight is applied and 5.38(b) after the application of the weight to the reed.

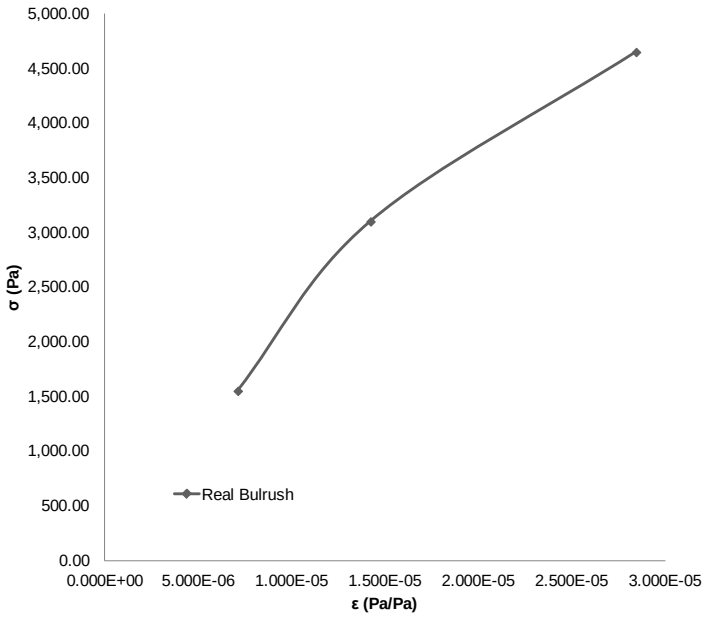

Figure 5.39: Stress and strain curve for softstem bulrush.

The second set of experiments, involved examining the stress and strain of flexible rod materials, to find a representative material for simulating the flexibility of softstem bulrush in the laboratory environment. The stress and strain experiments required measuring the deflection of three types of metal rods, each with more flexibility than the Plexiglas material used previously. Weight was added to the end of three types of metal rods: brass, threaded steel and weld steel, and the vertical deflection was measured to calculate the Young's Modulus. These materials were chosen due to their representation of three different levels of material strength and their availability in a quantity and size that met the requirements for insertion into the 0.64 cm in diameter plastic tubing that created a rod diameter for the flexible rods that could be compared to the other experiments. These rods were then placed into the low-density marsh configuration of 250 rods/m^2.

Figure 5.40 shows the results of the deflection measurements that were used to calculate the stress and strain for each rod. These measurements were dependent on how much weight was applied to the end of the rod. The Young's Modulus values obtained from the metal rod deflection experiment are in the range of each of the rod materials (MacGregor et al., 1978). Figure 5.40 reveals the outcome of the stress and strain calculations for each of the different metals inserted into the flexible tubing. The metal rods do not reflect a bulrush material, but can show the effect of flexibility on flow characteristics. The Young's Modulus for bulrush was calculated to be in MPa, while the Young's Modulus for the metal spines were in GPa.

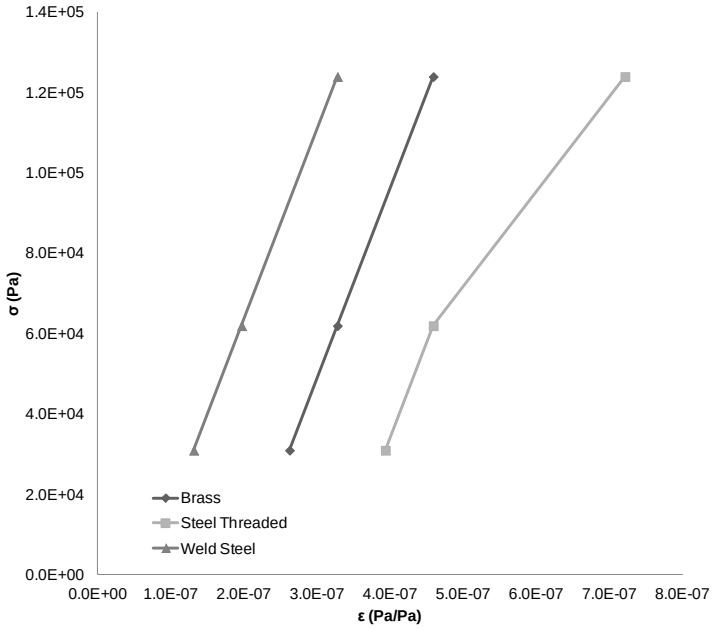

Figure 5.40: The stress and strain curve for the metal rods inserted in the plastic tubing in the flexible rod experiment. The presence of the plastic tubing did not influence the stress and strain for each of these materials when they were used in the laboratory experiments.

5.10 Flexibility Flow Structure Experimental Results

The motivation for investigating flexible rods was to analyze the effect of the flexibility within the marsh configuration on vorticity, eddy size and circulation. The setup for the study of the flexible rods was a low-density, alternating marsh configuration of 250 rods/m^2 (Figure 5.41), with a spacing ratio of 8. The rods were fixed at the top and bottom of the flume, similar to previous laboratory setups. This time only one location downstream of the rod setup was examined, 16 diameters downstream. Only one downstream location was chosen, since this is an initial look at the influence of flexibility, and the location closest to the rods was selected to avoid significant energy dissipation further downstream.

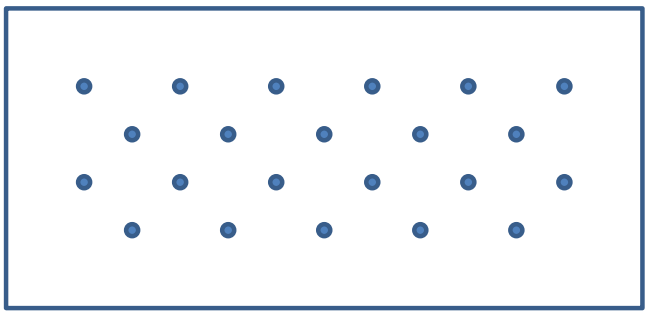

Flexible

Figure 5.41: Rod setup (250 rods/m^2) for the experiments using flexible rods.

Figure 5.42 shows a consistent size of the eddies, despite the addition of rows. Overall, the size of eddies was determined by the spacing of the flexible rods in the low-density, alternating configuration in the flume, since the spacing ratio of 8 results in discrete vortex formation (Lam and Cheung, 1988). The more flexible rods tended to have a larger eddy diameter at both Reynolds numbers. Still, the difference in eddy size only seems to change by 20% between the most flexible rods, and least flexible of rods.

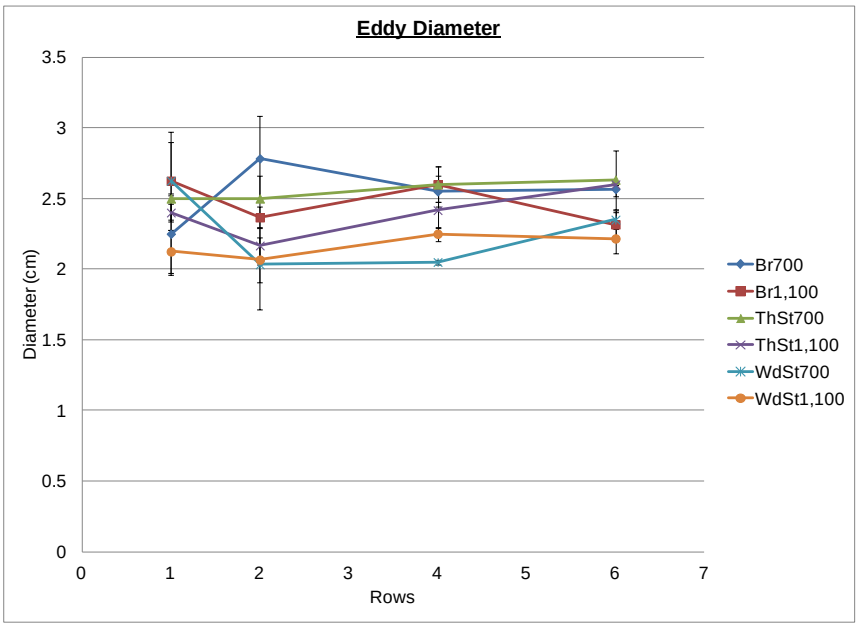

Figure 5.42: Different metal rods influence the eddy size as rows are added to the low-density alternating configuration at two different Reynolds numbers.

In Figure 5.43, the eddy vorticity reflects little variation for the higher Reynolds numbers, as rows one through four are added. From four to six rows, at the higher Reynolds number, the vorticity increases by 30% for the flexible rods. At the same time, the eddy vorticity decreases by 20% for the brass and weld steel rods at lower Reynolds numbers when one row is added. There is an increase of 30% for the brass rods and 55% for the weld steel rods for the lower Reynolds numbers from two rows to four rows. After four rows, the vorticity for the brass rod stays constant, at the lower Reynolds number, while the eddy vorticity of the weld steel only increases by 21% as the rows are increased from four to six. The steel threaded rods had no significant change in eddy vorticity at a lower Reynolds number of 700. Overall, the most flexible rods had a 15% higher vorticity than the least flexible rods. This occurred at both Reynolds numbers, as well as during the addition of each of the row of rods until six rows are reached. Here the

lower Reynolds number saw a convergence in eddy vorticity for all three metals. The eddy vorticity is higher at a higher Reynolds number for all of the different rod materials.

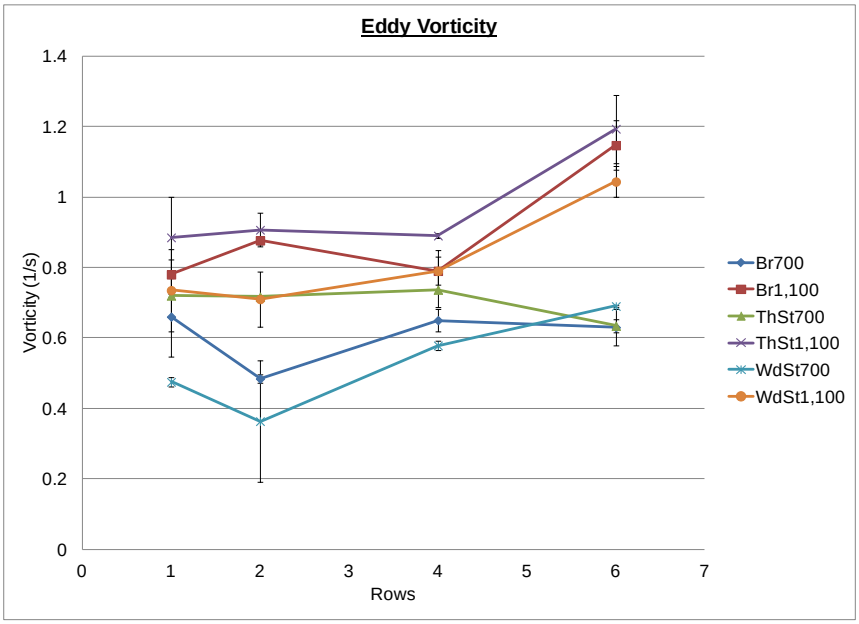

Figure 5.43: Eddy vorticity for the flexible rods with metal spines made of brass, threaded steel and weld steel. Vorticity is measured at two Reynolds numbers, as rows are added to a low-density alternating configuration.

In Figure 5.44, eddy circulation is higher at higher Reynolds numbers. The threaded steel rods and the brass rods kept a constant eddy circulation until the addition of the sixth row at a high Reynolds number where the threaded steel rods had an increase in eddy circulation of 52%, and the brass rod had an increase of 14%. The weld steel rods, the least flexible, had the lowest eddy circulation. Still, these rods had an increase in eddy circulation of 60% at a Reynolds number of 1,100 between the addition of the second row and the sixth row, resulting in an eddy circulation near 4 cm^2/s at six rows. For the weld steel rods at a Reynolds number of 700, there is a decrease in circulation from one to two rows of 50%, and then an increase in circulation from two to six rows of

one and a half times the eddy circulation found at two rows. Finally, there is no significant change in the eddy circulation of the brass and threaded steel rods at lower Reynolds numbers.

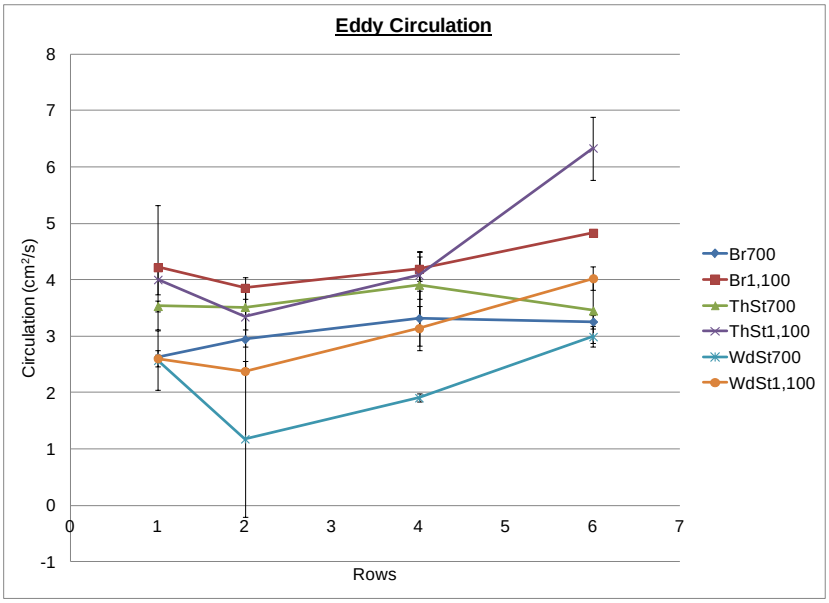

Figure 5.44: Eddy circulation for the flexible rods, at two Reynolds numbers, as rows are added to the low-density alternating configuration.

Overall, the trend in vorticity and circulation is not similar to the results found for the Plexiglas rod, low-density alternating marsh configuration. Vorticity for the flexible rod configuration was reduced by the flexibility of the rod materials in the water tunnel. This reduction in turbulence is similar to the effects of flexibility on the surrounding flow based on previous studies (Nepf et al., 1997; Jarvela, 2002). The more flexible material may be causing vibrations which are changing the rate of vortex shedding, which would then alter the Strouhal number, or the frequency at which vortices are shed. This could also influence whether the wake formation at the rod is discrete, and there could be cancellation of vortices due to side-by-side wake interactions. These experimental results

provide intermediate data to start quantifying the effect of flexibility on the flow structure of aquatic vegetation, but more research needs to be done in this area.

In Figures 5.45, 5.46 and 5.47, a comparison is drawn between the random, low-density alternating and flexible marsh configurations. Figure 5.45 reveals the effect of the flexible marsh configuration when comparing the results for the eddy diameter. The flexible and alternating marsh setups have an eddy size that is 40% larger than the random rod setup, due to the identical rod spacing in the alternating and flexible configurations, which is larger than the rod spacing of the random configuration. There is again no distinct pattern in the change in eddy diameter as the Reynolds number is changed because of the dependence of eddy size on the configuration of the rods. This consistency in eddy size over the change in Reynolds number, due to eddy diameter being determined by the rod spacing, was also observed by Sumner et al. (1999).

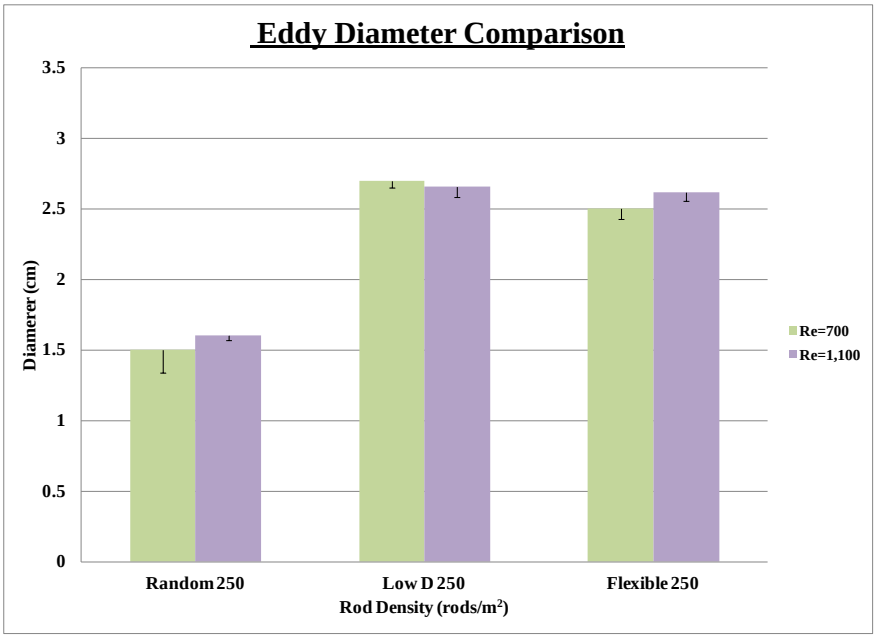

Figure 5.45: Eddy diameter comparison between the random, low-density alternating and flexible marsh experiments.

The same comparison was conducted for eddy vorticity in each of these configurations. Figure 5.46 reveals that the vorticity decreases for the flexible setup, when compared to the other configurations. At both Reynolds numbers, the vorticity for the flexible configuration decreases by an average of 30% from the random configuration. The decrease in vorticity is significantly higher when comparing the flexible setup to the low-density configuration. For both Reynolds numbers, the vorticity in the flexible case decreases by 60% when compared to the low-density configuration. Since the low-density alternating and flexible experiments had the same rod configurations, it follows that the difference in vorticity is due to the difference in the rigidity of the rods used in each of the experiments. Again, the flexibility of the rods could be changing the rate at which eddies are shed from the rod, which would again influence whether the wake formation at the rod is discrete. This change in the rate at which eddies are shed could result in a cancellation of vortices due to side-by-side wake interactions, and create an overall reduction in vorticity.

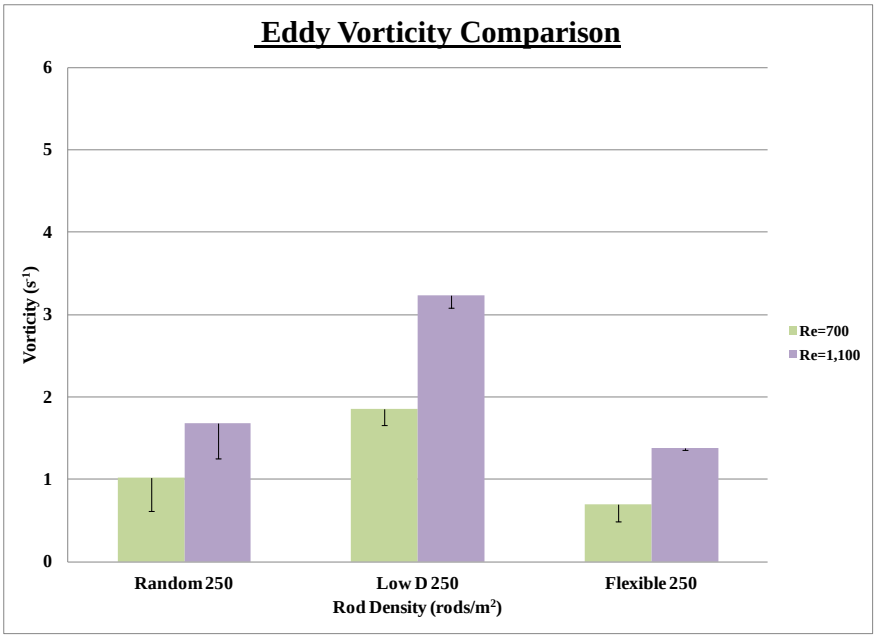

Figure 5.46: Eddy vorticity comparison between the random, low-density alternating and flexible marsh experiments.

Figure 5.47, compares the results of the eddy circulation for each marsh experiment. When comparing the eddy circulation for the flexible marsh configuration with the random marsh configuration, at both Reynolds numbers, the eddy circulation decreased by 55% for the random marsh setup results. This decrease is due to the smaller eddies in the random configuration, which are created by the smaller spacing between rods. Across the same Reynolds number range, the flexible marsh configuration circulation decreased by 65% with respect to the low-density alternating configuration. These results are completely due to the decrease in vorticity, since the rod spacing was identical for the flexible and low-density alternating rod configurations. Again, Nepf et al. (1997) and Jarvela (2002) found a similar reduction in turbulence when studying the effects of flexibility on fluid flow. This reduction in turbulence results in a weaker wake

being created, which again could be due to wake interactions due to the use of more flexible materials.

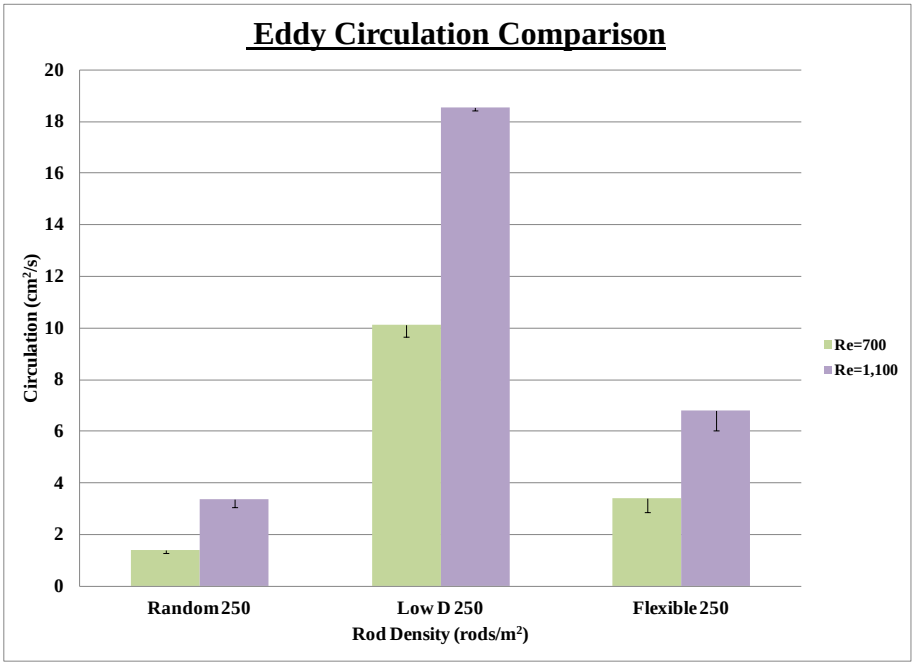

Figure 5.47: Eddy circulation comparison between the random, low-density alternating and flexible marsh experiments.

Chapter 6: Conclusions

6.1 Field and Laboratory Experiments

Three softstem bulrush patches with different reed densities were observed in the Huron River, Ann Arbor, MI. Particle Image Velocimetry was used to acquire flow data directly in the field environment; this is the first time such data were acquired within a natural marsh. In each of the softstem bulrush patches there was an increase in vorticity as a function of reed density. Also, as the density of the bulrush patch increased, the location of merging eddies decreased in downstream distance from the reeds.

Wakes, defined as entrained flow that is formed by the shedding of eddies from the reeds in the bulrush patches, formed downstream from the reeds, and upstream wakes merged with downstream wakes within the bulrush. As the density of the reeds in the bulrush colonies increased, so did the vorticity of the eddies merging within the downstream region. In each of the bulrush colonies, the merging of the eddies translated into an increase in vorticity, with an overall increase in circulation. The size of the eddies was determined by the spacing of the bulrush reeds. This spacing of the reeds created an average spacing ratio of 2, with an eddy size that was half the distance between the reeds, or the size of one reed diameter. Finally, the transverse vorticity plot revealed a sinusoidal pattern for each reed density, reflecting the consistency of the eddy size and strength.

Based on the observations analyzing the flow structure downstream from modeled aquatic vegetation in the laboratory, the configuration of the stems or rods is important. Whether that configuration is random in pattern, or represents an alternating pattern, it influences the eddy size and strength that a fish would interact with in these environments. For all configurations, eddy size was characterized by rod spacing. The influence of the spacing ratio, or distance between rods, greatly affected the size of the eddies in each of the laboratory experiments. The size of the eddies was determined by the spacing ratio, i.e. half of the distance between the rods, in all cases. In addition to this, for both densities, the alternating setup produced more vorticity and more circulation than the random marsh setup.

Observations of the changes in eddy characteristics with the change in Reynolds number revealed that the Reynolds number did not have an influence on the eddy size, since that was determined by the rod spacing, but did have an influence on vorticity and thus circulation. As the Reynolds number increased, so did the eddy vorticity and eddy circulation. In the field, an increase in vorticity was also observed, as the reed density increased. This trend is in contrast to the decrease in vorticity, with the increase in rod density, for the alternating configuration. Instead, a similar relationship between vorticity and density is found in the results for the random experiments. Therefore, this trend in the field observations could be due to the existence of non-linearity, and patchiness, in the reed growth pattern. This patchiness contrasts to the alternating experiments' control of the flow in the laboratory, through the restricted structure of the rods as the density was increased, restricting the growth of eddies or any increase in vorticity.

The influence of the alternating rod pattern on creating an eddy of consistent size and strength was also observed in the vorticity maps shown for each rod configuration. Interesting shear dynamics were discovered in the wake patterns of the alternating configurations, and velocity gradients on the edge of the wake were found. These velocity gradients were due to pattern in the placement of the rods producing low velocity regions downstream from the rods where the wake was formed, separated by the high velocity regions in between the rods. This pattern in the rod placement also produced a pattern in the downstream flow structure, resulting in eddies that had similar vorticity and size. This eddy consistency was in contrast to the random configuration, where the merging of wakes downstream from the clusters of Plexiglas rods lead to inconsistencies in eddy structure and circulation.

Analysis of the reed/rod spacing, in the marsh configurations, also revealed an influence of growth patterns on the transverse vorticity within the marsh environment. This effect could only be seen once the transverse vorticity was analyzed, and in the alternating experiments it produced a consistent eddy size and strength. The transverse vorticity that was produced shared similarities to the transverse vorticity from the field experiments. This could be used in the design and development of artificial marsh environments, in an effort to produce an eddy of consistent size and strength for the fish to interact with. This design of an artificial marsh would have to also take into consideration the current guidelines for plant placement (EPA, 2005).

Further analysis of the influence of the experiments conducted on the biota of the natural environment reveals that the size of the eddies produced in the laboratory and field results were under a few centimeters. Therefore, they would cause instabilities for

fish of a similar size swimming in the marsh environment (Tritico, 2009; Tritico and Cotel, 2010). These would be young fish, based on the size of the eddies, and due to marsh environments serving as breeding grounds for fish, could deter fish from using an area as their nursery if the swimming environment was not conducive for the development of young fish.

Another influence on the interaction between the development of artificial marsh environments, based on this research and the ability for local biota to thrive in a marsh installation, is the effect of the fluctuating water levels caused by the extreme weather of a warming environment. The major influence of global warming on water bodies involves the fluctuation of water levels producing either shallow/low velocity flow, or shallow/high velocity flow, due to changing weather events and the sedimentation in water bodies (Leopold, 1994). This change in flow pattern could result in additional frictional losses as processes linked to boundary layer dynamics would become dominant. This would create additional vorticity that could interact with shed vorticity from the marsh vegetation.

The influence of higher velocities was examined in the alternating and random configuration experiments. In the alternating experiments a larger, stronger eddy was produced, but the eddy was of a predictable size and strength due to the rod pattern. This is in contrast to the larger, stronger eddies that were created in a random setup, which did not represent the average eddy being created and were unpredictable in their occurrence. Overall, the eddy size and strength could be predicted even under extreme circumstances if the pattern of reed placement, and the density of reeds in the bulrush patch, are consciously controlled in the construction of an artificial marsh.

Finally, the examination of rod flexibility and its effect on the flow structure downstream from aquatic vegetation revealed a significant decrease in vorticity once a more flexible material was used for the alternating marsh configuration. Even though the rod material was only slightly more flexible then the previously utilized Plexiglas rods, the effect this flexibility had on the vorticity was significant in its reduction of turbulence downstream from the array.

6.2 Future Research

Building on the work that has already been performed, examining the effects of plant density in a marsh, as well as the arrangement of plants, more variables in the design of an artificial marsh should be assessed. From the previous laboratory experiments, the effect of the density of rods in the flume was seen to be highly dependent on the arrangement of the rods. Rod spacing controlled the dynamics in each of the laboratory experiments, as well as in the field. It was revealed that rod spacing and pattern influence not just the pattern in transverse vorticity, but also the amount of vorticity in the downstream eddies, due to upstream wakes combining with downstream wakes. Although, this increased vorticity could be dampened if the rods are made of a more flexible material, since the preliminary experiments examining flexibility found a decrease in vorticity when less rigid rod materials were used.

Based on the initial look at random rod placement and flexibility, more research needs to be conducted in these areas. Examining the effect of clusters of rods, or patchiness, on the downstream flow structure is important. This can be achieved with a

sample set of patterns that can be defined as either linear or non-linear, and using a numerical code that allows a rod configuration to be broken up into segments, with each segment analyzed for evidence of non-linearity. In addition to this, further work studying the influence of flexibility on the downstream flow structure would require examining a rod-like material that more closely resembles the flexibility of actual softstem bulrush.

Possible future directions also involve examining biota in marsh environments and how a marsh contributes to fish choosing these environments for their habitat. Laboratory experiments could also be conducted to understand the response of fish swimming downstream of artificial marsh configurations in the water tunnel. Use of PIV, as well as video of the response of the fish, would provide insight into whether rod density or flow pattern are influencing fish response in these differing environments. Additionally, these tools could be used in a natural marsh to observe how the flow structure of the aquatic vegetation influences the ability of fish to swim, obtain nutrition and make these environments their habitat.

Finally, since there are marshes in coastal areas, it is significant to look at how waves will affect turbulence created by marsh environments. Waves increase both velocity and vorticity within the marsh, thereby increasing the turbulence (Cotel et al., 2008). Waves also add complexity, due to the introduction of new time and length scales, such as wavelength, period and amplitude, and understanding the effect of waves is important in their applicability to not just shorelines, but also to wakes created from boats and storm surges.

APPENDIX

Further examination of the comparison of ADV and PIV equipment was conducted on the low-density alternating marsh configuration. Point measurements of turbulence were made downstream from the low-density laboratory setup, using both techniques, to measure TI and TKE. PIV data were used to calculate the velocity fluctuations 6.4 cm downstream from the rods and in the center of the flume (Figure 5.1), corresponding to the placement of the ADV in the laboratory flume. The observations in Figure A1 for a Reynolds number of 700 found a five-fold increase in TI as rods are added to the marsh setup, with constant results after the addition of four rows. This trend is similar, although larger in magnitude, to what was observed for eddy diameter and eddy vorticity in Figures 5.7 through 5.10, due to the growth in the wakes from the additional rows of rods. For a Reynolds number of 1,100, the observations were similar with an increase in TI by a factor of four between rows three and four. Another difference at this Reynolds number is the 30% decrease that occurs in TI after four rows. There also appears to be a 30% decrease in TI at three rows for both Reynolds numbers, where the values differ by only 10%. Again, these variations that occur at three rows, as well as the difference between the two Reynolds numbers, could be due to the cancellation of eddies downstream from the rod configuration, where the velocity fluctuations were measured.

Overall, a 20% lower TI was found at a higher Reynolds number, an artifact of the definition of turbulence intensity, since turbulent fluctuations are normalized by the average velocity. Again at three rows, the combined wakes in alternating rows could be interfering with the initial wake that is produced upstream from the point measured. These peripheral, combined wakes can create vortex interference, or eddies merging or cancelling each other out, in the region of the centered wake, upstream from where the velocity measurements were taken. Other issues at three rows could be due to the location of the point measurements, and the inability for one point to be able to reflect the overall trends in the two-dimensional flow.

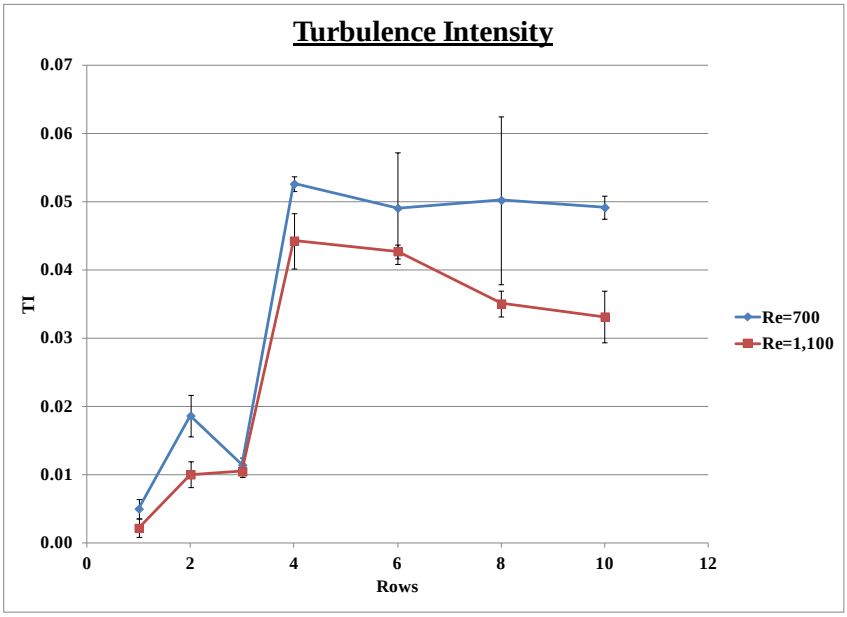

Figure A1: Turbulence intensity for low-density configuration.

Higher Reynolds numbers lead to lower TI values, due to TI being defined as the ratio of the standard deviation of the velocity fluctuations divided by the average velocity. The velocity and velocity fluctuations were measured in both the x

(longitudinal) and y (transverse) direction. Therefore, to better understand the dynamics of these flows, the measured velocity fluctuations should be examined on their own to see if they increase with an increase in Reynolds number. Figure A2 reveals that the velocity fluctuations are one and a half times higher for a higher Reynolds number. Also, a 30% decrease in the velocity fluctuations is again revealed for a Reynolds number of 1,100 from the fourth row to the tenth row. Still, this figure shows there is a 20% dip in velocity fluctuations at three rows for a Reynolds number of 700, but no dip in at a Reynolds number of 1,100. Also, at a Reynolds number of 700, large error bars on the order of 20% can be found.

Overall, there is a clear transition in the flow after four rows are established, with a much higher value of velocity fluctuations (four times the third row value) after four rows for both Reynolds numbers. This increase in turbulent fluctuations is representative of the structure of the flow at these configurations, i.e. large number of rows, a larger number of eddies are present producing higher velocity fluctuations. Also, at four rows, two tandem rows of rods are now positioned in the low-density configuration (Figure 5.6). From these tandem rows of rods, two wakes combine to create consistent turbulence patterns. This consistency in wake patterns was shown to exist when two wakes combine from two rods that were in close proximity with one another, by Williamson (1985).

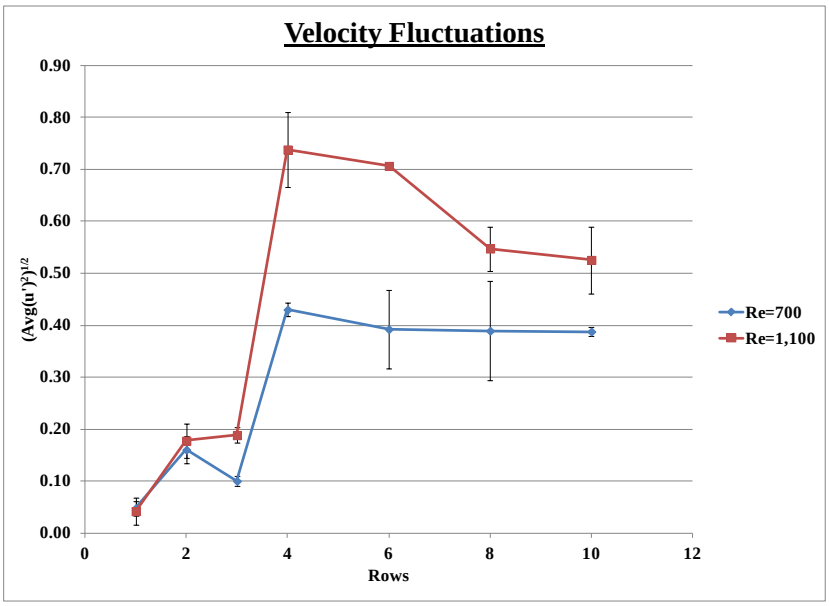

Figure A2: Velocity fluctuations for low-density configuration.

Figure A3 outlines the turbulent kinetic energy results for the same position, 6.4 cm downstream from the rods and in the center of the flume, based on the PIV data. Again, a one and half times higher TKE value is observed at a Reynolds number of 1,100, when compared to the value at a Reynolds number of 700. At a Reynolds number of 700, the TKE increases by 80% from one row to two rows and 15% from two rows to three rows. After that the TKE decreases by 35% at four rows and remains constant until ten rows. For a Reynolds number of 1,100, the TKE more than double from one row to two rows and decreases by 20% at three rows, remaining constant thereafter. The effect of an increase in TKE values for the first couple of rows, with a constant level being achieved after four rows, agrees with the pattern that has been observed in the eddy quantification and TI results. TKE is again calculated using the point measurement of the velocity fluctuations in two directions when using PIV data: x (longitudinal) and y

(transverse). These measurements are also only taken at one point and information that was previously found from looking at the structure of the eddy may be lost in just examining the turbulence at one point downstream from the rods.

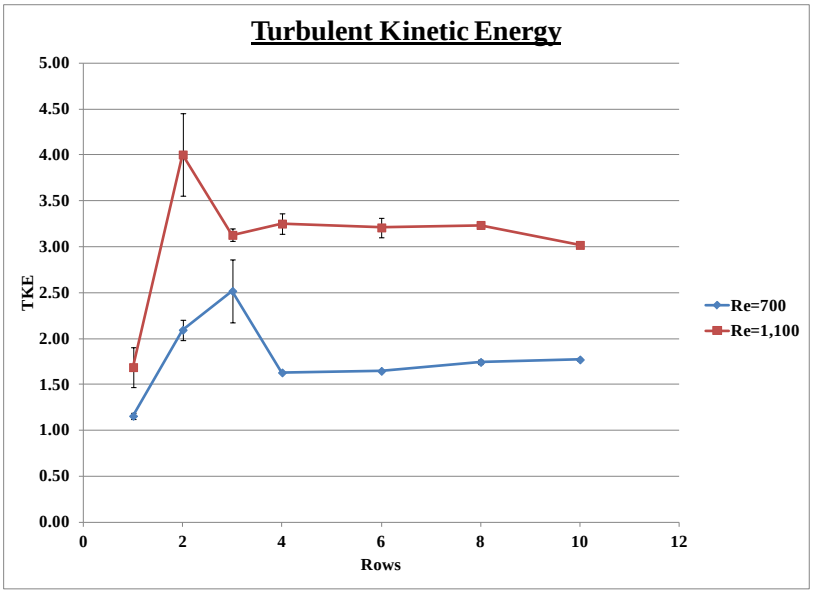

Figure A3: Turbulent Kinetic Energy for low-density configuration.

Acoustic Doppler Velocimeter (ADV) measurements were taken at the same location described above, with a sampling frequency of 50 Hz. The observations made by the PIV and ADV are compared in Figures A4 and A5. The TKE results from the PIV data have a peak at three rows, with a dip at four rows, while the results from the ADV has a peak at four rows and dip at six rows. The peak for both of them is close to a value of 2.5, while the dip is near 1.6. The TKE levels, measured by the PIV, stay constant after four rows, but the ADV levels have an increase by 25% at eight rows. Overall, the ADV determined values for TKE (Figure A4) follow the same trend and are of the same

order of magnitude as the PIV results, however there is a shift in the location of the peak value.

The comparison of the TI results for both the PIV and ADV data did not show the same similar trend. The ADV results steadily increase by 75% overall, while the PIV data show an increase by a factor of four at four rows, constant value until six rows and then a decrease by 20% from six rows to ten rows. Also, at the first row, the results for the ADV data are almost ten times larger than what is observed for the PIV data. Differences in the results from the ADV and the PIV data could be due to the placement of the ADV in an eddy-dominated flow. Since our average eddy size is on the order of 2.5 cm, a small error in the measurement location between ADV and PIV (on the order of 1 cm or so) would provide different results, i.e. the point of comparison could be located in the center of an eddy versus on the edge. This reveals the limitations of comparing results from instruments that involve different turbulence measurement techniques. Another difference in the two pieces of equipment is the way velocity is measured and the amount of velocity fluctuations that are recorded. The PIV is capturing the spatial changes in the velocity as opposed to the temporal changes that the ADV measures. For this reason, the ADV may be measuring more of the fluctuations in velocity that the PIV misses when looking only at one point. Due to TI being calculated as the standard deviation of velocity divided by the average velocity, the more fluctuations in the velocity, the larger the TI values. This may explain the differences in the results in Figure A5.

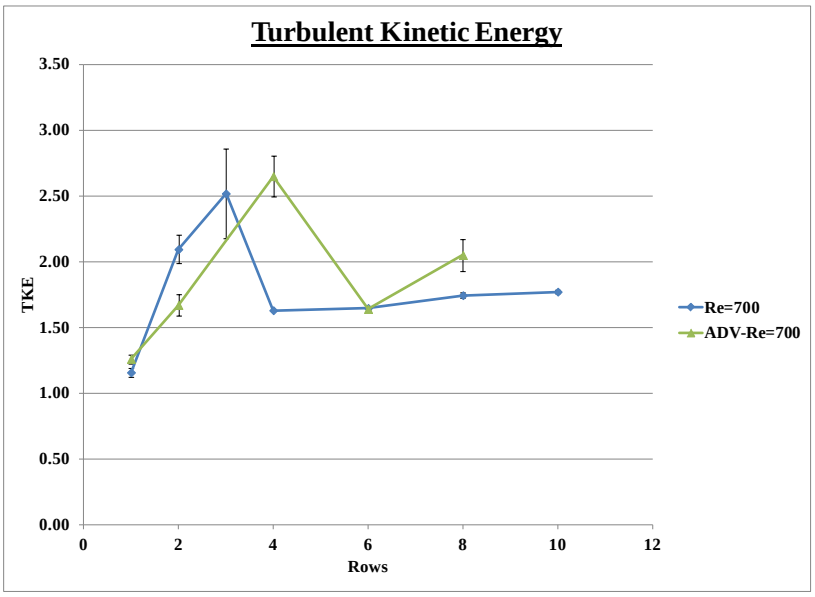

Figure A4: ADV and PIV comparison for turbulent kinetic energy for low-density configuration.

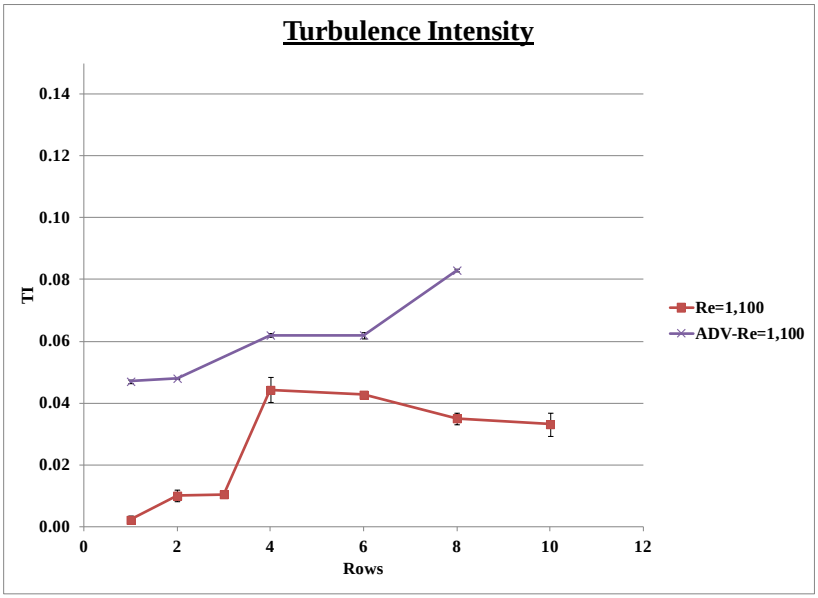

Figure A5: ADV and PIV comparison for turbulence intensity for low-density configuration.

REFERENCES

Abdelrhman, M.A. (2003). "Effect of eelgrass Zostera marina canopies on flow and transport." *Marine Ecology Progress Series*, 248, 67-83.

Anderson, J. D. (1991). "Fundamental of Aerodynamics, 2nd Edition." *McGraw-Hill, Inc*., New York, NY.

Anderson, S. M. and Charters, A. C. (1982). "A fluid dynamics study of seawater flow through Galadium nudifrons." *Limnology and Oceanography,* 27, 399-412.

Augustin, L.N., Irish, J.L. and Lynett, P. (2009). "Laboratory and numerical studies of wave damping by emergent and near-emergent wetland vegetation." *Coastal Engineering*, 56, 332-340.

Ayaz, F. and Pedley, T.J. (1999). "Flow through and particle interception by an infinite array of closely-spaced circular cylinders." *European Journal of Mechanics - B/Fluids*, 18(2), 173-196.

Bearman, P. W. and Wadcock, A. J. (1973). "The interaction between a pair of circular cylinders normal to a stream." *Journal of Fluid Mechanics*, 61, 499-511.

Bertuccioli, L., Roth, G. I., Katz, J. and Osborn, T. R. (1999). "A submersible particle image velocimetry system for turbulence measurements in the bottom boundary layer." *Journal of Atmospheric and Oceanic Technology*, 16, 1635-1646.

Cada, G. F. and Odeh, M. (2001). "Turbulence at Hydroelectric Power Plants and its Potential Effects on Fish." *Report to Bonneville Power Administration*, Contract No. 2000AI26531, Project No. 200005700: 1-37.

Chu, W., Mehregany, M. and Mullen, R. L. (1993). "Analysis of tip deflection and force of a bimetallic cantilever microactuator." *Journal of Micromechanics and Microengineering*, 3(1), 4-7.

Cimbala, J. M., Hassan, M. N. and Roshko, A. (1988). "Large structure in the far wakes of two-dimensional bluff bodies." *Journal of Fluid Mechanics*, 190, 265-298.

Cotel, A., Meadows, L. and Webb, P.W. (2008). "The Effect of Unsteady Flow on the Shoreline of Les Cheneaux Islands." *Inaugural International Conference of the Engineering Mechanics Institute*, Minneapolis, MN.

Cotel, A. J. and Webb, P. W. (2011). "The Challenge of Understanding and Quantifying Fish Responses to Turbulence-Dominated Physical Environments*" The Institute of Mathematics and its Applications (IMA) Conference Proceedings*, University of Minnesota, Minneapolis, MN (in review).

Cotel, A. J., Webb, P. W. and Tritico, H. M. (2006). "Do Brown Trout Choose Locations With Reduced Turbulence?" *Transactions of the American Fisheries Society*, 135, 610-619.

Crites, R., Reed, S. C. and Middlebrooks, E. J. (2006). "Natural Wastewater Treatment Systems." *Taylor & Francis Group*, Boca Raton, Fl.

Cui, J. and Neary, V.S. (2008). "LES study of turbulent flows with submerged vegetation." Journal of Hydraulic Research, 46(3), 307-316.

Cwikiel, W. (1998). "Living With Michigan's Wetlands: A Landowner's Guide." *Tip of the Mitt Watershed Council*, (Third Printing), Conway, MI.

Dabiri, J. O., Colin, S. P., Costello, J. H. and Gharib, M. (2005) "Flow patterns generated by oblate medusan jellyfish: field measurements and laboratory analyses." *The Journal of Experimental Biology*, 208, 1257-1265.

Davis, F. W. and Goetz, S. (1990) "Modeling vegetation pattern using digital terrain data." *Landscape Ecology*, 4(1), 69-80.

Drucker, E. G. and Lauder, G. V. (1999). "Locomotor Forces on a Swimming Fish: Three-Dimensional Vortex Wake Dynamics Quantified Using Digital Particle Image Velocimetry." *Journal of Experimental Biology*, 202, 2393-2412.

Environmental Protection Agency (EPA) (2005) "An Introduction and User's Guide to Wetland Restoration, Creation, and Enhancement." *Interagency Workgroup on Wetland Restoration*.

Epps, B. P. and Techet, A. H. (2007). "Impulse generated during unsteady maneuvering of swimming fish." *Experiments in Fluids*, 43(5), 691-700

General Pixels. (2000). "PixelFlow 2.1: Installation and User's Guide."

Gerrard, J. H. (1966). "The mechanics of the formation region of vortices behind bluff bodies." *Journal of Fluid Mechanics*, 25(2), 401-413.

Ghisalberti, M. and Nepf, H.M. (2002). "Mixing layers and coherent structures in vegetated aquatic flows." *Journal of Geophysical Research*, 107, NO. C2.

Gibson, L. J. (2012). "The hierarchical structure and mechanics of plant materials." *Journal of Royal Society Interface*, pub. online, 1-19.

Guard, J.B. (1995). "Wetland Plants of Oregon & Washington." *Lone Pine Publishing*, Redmond, WA.

Jarvela, J. (2002). "Flow resistance of flexible and stiff vegetation: a flume study with natural plants." *Journal of Hydrology*, 269, 44-54.

Jeong, J. and Hussain, F. (1995). "On the identification of a vortex." *Journal of Fluid Mechanics*, 285, 69-94.

Kiya, M., Arie, M., Tamura, H. and Mori, H. (1980). "Vortex shedding from two circular cylinders in staggered arrangement." *ASME Journal of Fluids Engineering*, 102, 166-173.

Kolmogorov, A. N. (1941). "Local Structure of Turbulence in Incompressible Viscous Fluid for Very Large Reynolds Numbers." *Reprinted in Proceedings: Mathematical and Physical Sciences*, 434(1890), 9-13 (1991).

Lam, K. and Cheung, W. C. (1988). "Phenomena of vortex shedding and flow interference of three cylinders in different equilateral arrangements." *Journal of Fluid Mechanics*, 196, 1-26.

Laur, D. R. and Ebeling, A. W. (1983). "Predator-prey relationships in surfperches." *Environmental Biology of Fishes*, 8 (3-4), 217-229.

Le Gal, P., Chauve, M. P., Lima R. and Rezende, J. (1990). "Coupled wakes behind two circular cylinders." *Physical Review A*, 41, 4566-4569.

Leonard, L. and Luther, M. (1995). "Flow hydrodynamics in tidal marsh canopies." *Limnology and Oceanography*, 40, 1474-1484.

Leopold, L. B. (1994) "A View of the River." *Harvard University Press*, Cambridge, MA.

Lewis, W. M. and Helms, D. R. (1964). "Vulnerability of Forage Organisms to Largemouth Bass." *Transactions of the American Fisheries Society*, 93(3), 315-318.

Liao, J. C. (2007). "A review of fish swimming mechanics and behavior in altered flows." *Philosophical Transactions of the Royal Society B*, 362(1487), 1973-1993.

Lin, J.-C., Towfighi, J. and Rockwell, D. (1995). "Instantaneous Structure of Near-Wake of a Cylinder: On the Effect of Reynolds Number." *Journal of Fluids and Structures*, 9, 409-418.

Linden, P. F. and Turner, J. S. (2001) "The formation of 'optimal' vortex rings, and the efficiency of propulsion devices." *Journal of Fluid Mechanics*, 427, 61-72.

Lopez, R.O.T. and Cowen, E.A. (2009). "Effects of Aquatic Vegetation Density on Low Speed Flows." *7th ISE & 8th HIC*, Chile.

Lupandin, A. I. (2005). "Effect of Flow Turbulence on Swimming Speed of Fish." *Biology Bulletin*, 32(5), 461-466.

MacGregor, C. W., Symonds, J., Vidosic, J. P., Hawkins, H. V., Thomson, W. T. and Dodge D. D. (1978) "Strength of materials." *Mark's Standard Handbook for Mechanical Engineers (Edited by Baumeister, T., Avallone, E. A. and Baumeister, T. III)*; p. 5. McGraw Hill, New York.

Mueller, D. S., Abad, J. D., Garcia, C. M., Gartner, J. W., Garcia, M. H. and Oberg, K. A. (2007). "Errors in Acoustic Doppler Profiler Velocity Measurements Caused by Flow Disturbance." *Journal of Hydraulic Engineering*, 133(12), 1411-1420.

Nepf, H.M. (1999). "Drag, turbulence, and diffusion in flow through emergent vegetation." *Water Resources Research*, 35(2), 479-489.

Nepf, H. M., Sullivan, J. A. and Zavistoski, R. A. (1997) "A Model for Diffusion Within Emergent Vegetation." *Limnology and Oceanography*, 42 (8), 1735-1745.

Nikora, V. I., Aberle, J., Biggs, B. J. F., Jowett, I. G. and Sykes, J. R. E. (2003). "Effects of fish size, time-to-fatigue and turbulence on swimming performance: a case study of Galaxias maculatus." *Journal of Fish Biology*, 63, 1365-1382.

Nimmo-Smith, W. A. M., Atsavapranee, P., Katz, J. and Osborn, T. R. (2002). "PIV Measurements in the bottom boundary layer of the coastal ocean." *Experiments in Fluids*, 33, 962-971.

Odeh, M., Noreika, J.F., Haro, A., Maynard, A., Castro-Santos, T. and Cada, G.F. (2002) "Evaluation of the effects of turbulence on the behavior of migratory fish." *Final Report to the Bonneville Power Administration*, Contract 00000022, Project 200005700, Portland, Oregon.

Palmer, M.A. (1988). "Epibenthic Predators and Marine Meiofauna: Separating Predation, Disturbance, and Hydrodynamic Effects." *Ecology*, 69(4), 1251-1259.

Pavlov, D.S., Lupandin, A.I. and Skorobogatov, M.A. (2000). "The effects of flow turbulence on the behavior and distribution of fish." *Journal of Ichthyology*, 40, (Supplement2), S232-S261

Peterson, C.H., Luettich Jr., R.A., Micheli, F. and Skilleter, G.A. (2004). "Attenuation of water flow inside seagrass canopies of differing structure." *Marine Ecology Progress Series*, 268, 81-92.

Roshko, A. (1993). "Perspectives on bluff body aerodynamics." *Journal of Wind Engineering and Industrial Aerodynamics*, 49, 79-100.

Rosman, J.H., Koseff, J.R., Monismith, S.G. and Grover, J. (2007). "A field investigation into the effects of a kelp forest (*Macrocystis pyrifera*) on coastal hydrodynamics and transport." *Journal of Geophysical Research*, 112, C02016.

Runkel, S. T. and Roosa, D. M. (1999). "Wildflowers & Other Plants of Iowa Wetlands." *Iowa State University Press*, Ames, IA.

Savino, J. F. and Stein, R. A. (1989). "Behavioural interactions between fish predators and their prey: effects of plant density." *Animal Behaviour*, 37 (2), 311-321.

Smith, D. L., Brannon, E. L., Shafii, B. and Odeh, M. (2006). "Use of the Average and Fluctuating Velocity Components for Estimation of Volitional Rainbow Trout Density." *Transactions of the American Fisheries Society*, 135(2), 431-441.

Sontek. (1997). "ADV Operation Manual Firmware Version 4.0."

Spivack, H. M. (1946). "Vortex frequency and flow pattern in the wake of two parallel cylinders at varied spacing normal to an air stream." *Journal of the Aeronautical Sciences*, 13, 289-297.

Stone, B.M. and Shen, H.T. (2002). "Hydraulic Resistance of Flow in Channels with Cylindrical Roughness." *Journal of Hydraulic Engineering*, 128(5), 500-506.

Sumner, D., Wong, S. S. T., Price, S. J. and Paidoussis, M. P. (1999). "Fluid Behaviour of Side-By-Side Circular Cylinders in Steady Cross-Flow." *Journal of Fluids and Structures*, 13, 309-338.

Tanino, Y. and Nepf, H.M. (2008). "Laboratory Investigation of Mean Drag in a Random Array of Rigid, Emergent Cylinders." *Journal of Hydraulic Engineering*, 134(1), 34-41.

Tarrade, L., Texier, A., David, L. and Larinier, M. (2008). "Topologies and measurements of turbulent flow in vertical slot fishways." *Hydrobiologia*, 609, 177-188.

Tennekes, H. and Lumley, J. L. (1972). "A First Course in Turbulence." *The MIT Press*, Cambridge, MA.

Tiner, R. W., Jr. (1987). "A Field Guide to Coastal Wetland Plants of the Northeastern United States." *University of Massachusetts Press*, Amherst, MA.

Tritico, H. M. (2009). "The effects of turbulence on habitat selection and swimming kinematics of fishes." *Dissertation submitted in partial fulfillment of the*

requirements for the degree of doctor of philosophy. University of Michigan, Ann Arbor.

Tritico, H. M., Cotel, A. J. and Clark, J. (2007). "Development, Testing, and Demonstration of a Portable Submersible Miniature Particle Image Velocimetry Device." *Measurement Science and Technology*, 18, 2555-2562.

Tritico, H. M. and Cotel, A. J. (2010). "The effects of turbulent eddies on the stability and critical swimming speed of creek chub (*Semotilus atromaculatus*)" *Journal of Experimental Biology*, 213, 2284-2293.

Velasco, D., Bateman, A. and Medina, V. (2008). "A new integrated, hydro-mechanical model applied to flexible vegetation in riverbeds." *Journal of Hydraulic Research*, 46(5), 579-597.

Von Karman, T. (1937). "On the statistical theory of turbulence." *Proceedings of the National Academy of Sciences of the United States of America*, 23(2), 98-105.

Willert, C. E. and Gharib, M. (1991). "Digital particle image velocimetry." *Experiments in Fluids*, 10, 181-93.

Williamson, C. H. K. (1985). "Evolution of a single wake behind a pair of bluff bodies." *Journal of Fluid Mechanics*, 159, 1-18.

Williamson, C. H. K. (1996). "Vortex Dynamics in the Cylinder Wake." *Annual Review of Fluid Mechanics*, 28, 477-539.

Zdravkovich, M. M. and Pridden, D. L. (1977) "Interference between two circular cylinders; series of unexpected discontinuities." *Journal of Industrial Aerodynamics*, 2, 255-270.